Summer 2007

Modeling Habitat and Environmental Factors Affecting Mosquito Abundance in Chesapeake, Virginia

Alan Scott Bellows
Old Dominion University

MODELING HABITAT AND ENVIRONMENTAL FACTORS

AFFECTING MOSQUITO ABUNDANCE IN CHESAPEAKE, VIRGINIA

by

Alan Scott Bellows
M.S. Biology 1999, Virginia Commonwealth University
B.S. Biology 1996, Christopher Newport University

A Dissertation Submitted to the Faculty of
Old Dominion University in Partial Fulfillment of the
Requirement for the Degree of

DOCTOR OF PHILOSOPHY

ECOLOGICAL SCIENCES

OLD DOMINION UNIVERSITY
August 2007

Approved by:

_____
Robert K. Rose
(Co-Director of Committee)

_____
Thomas R. Allen, Jr.
(Co-Director of Committee)

_____
Alan H. Savitzky (Member)

ABSTRACT

MODELING HABITAT AND ENVIRONMENTAL FACTORS AFFECTING MOSQUITO ABUNDANCE IN CHESAPEAKE, VIRGINIA

Alan Scott Bellows
Old Dominion University, 2007
Co-Directors: Dr. Robert K. Rose
Dr. Thomas R. Allen, Jr.

The models I present in this dissertation were designed to enable mosquito control agencies in the mid-Atlantic region that oversee large jurisdictions to rapidly track the spatial and temporal distributions of mosquito species, especially those species known to be vectors of eastern equine encephalitis and West Nile virus. I was able to keep these models streamlined, user-friendly, and not cost-prohibitive using empirically based digital data to analyze mosquito-abundance patterns in real landscapes.

This research is presented in three major chapters: II) a series of semi-static habitat suitability indices (HSI) grounded on well-documented associations between mosquito abundance and environmental variables, III) a dynamic model for predicting both spatial and temporal mosquito abundance based on a topographic soil moisture index and recent weather patterns, and IV) a set of protocols laid out to aid mosquito control agencies for the use of these models.

The HSIs (Chapter II) were based on relationships of mosquitoes to digital surrogates of soil moisture and vegetation characteristics. These models grouped mosquitoes species derived from similarities in habitat requirements, life-cycle type, and vector competence. Quantification of relationships was determined using multiple linear

regression models.

As in Chapter II, relationships between mosquito abundance and environmental factors in Chapter III were quantified using regression models. However, because this model was, in part, a function of changes in weather patterns, it enables the prediction of both 'where' and 'when' mosquito outbreaks are likely to occur. This model is distinctive among similar studies in the literature because of my use of NOAA's NEXRAD Doppler radar (3-hr precipitation accumulation data) to quantify the spatial and temporal distributions in precipitation accumulation.

Chapter IV is unique among the chapters in this dissertation because in lieu of presenting new research, it summarizes the preprocessing steps and analyses used in the HSIs and the dynamic, weather-based, model generated in Chapters II and III. The purpose of this chapter is to provide the reader and potential users with the necessary protocols for modeling the spatial and temporal abundances and distributions of mosquitoes, with emphasis on *Culiseta melanura*, in a real-world landscape of the mid-Atlantic region. This chapter also provides enhancements that could easily be incorporated into an environmentally sensitive integrated pest management program.

This dissertation is dedicated to Eileen, my wife and best friend.

ACKNOWLEDGMENTS

I would like to acknowledge many people for helping me during my doctoral work. Most importantly, I thank my wife, Eileen, and our two sons, Caleb and Liam. Without their understanding and support, this work would not have been possible. Aside from my family, I would like to especially thank my Directors, Robert Rose and Thomas Allen, Jr., for their time and commitment. Throughout my doctoral work they encouraged me to develop independent thinking and research skills. This was particularly true for Robert Rose, who managed to steer me straight in so many ways beyond academia. I am also very grateful to my other committee members and wish to thank Alan Savitzky, William Resetarits, and Bradley Shellito. I also thank the Department of Biological Sciences and the Department of Political Science and Geography at Old Dominion University for their support. I extend many thanks to the many colleagues and friends I have met and worked with along the way, especially my GIS lab mate George McLeod. I thank David Kriz (National Soil Conservation Service), Bruce Harrison (North Carolina Department of Environment and Natural Resources), and Evan Stewart (Meteorologist, WVEC television) for their technical advice, and all the folks at the Chesapeake Mosquito Control Commission including: Gene Payne (Director), Louis DeMarco (Operations Director), and Melissa Cushing (GIS Analyst). This research was partially funded by the Virginia Space Grant Consortium Graduate Research Fellowship, NASA, and Virginia Access and Magic. Finally, I owe a special note of gratitude to Barbara Savitzky, who was the first to recognize my potential as a researcher and scientist.

TABLE OF CONTENTS

Page

LIST OF TABLES

Table Page

LIST OF FIGURES

Figure Page

Figure Page

CHAPTER I

GENERAL INTRODUCTION

Introduction

Geographic information system (GIS) technology has grown from relative obscurity to a worldwide industry (Bernhardsen, 2002). Before the relatively widespread availability of GIS, global positioning systems (GPS), and remotely sensed techniques and data, modeling spatial and temporal heterogeneity was often difficult, if not impossible. This difficulty was primarily associated with a general inability to manage, store, and analyze the huge banks of data needed to model complex real-world patterns and processes (Johnson, 1993). But now, applications for GIS are as diverse as the broad range of data that can be applied to this technology; this is reflected in recent literature. A burgeoning source of such information, GIS, GPS, and digital satellite remote sensing provide promising data and analytical tools for applied and multi-disciplinary studies.

The use of digital satellite data in GIS is becoming a valuable approach in the field of epidemiology for the study of vector ecology in disease transmission (Clarke et al., 1996; Kitron, 1998). Recent advances in earth-observing sensors have made possible the generation of a wide range of spatially explicit environmental and biophysical data relevant to the study of disease vector ecology (Goetz et al., 2000). Surveillance, monitoring, and subsequent health policies associated with the study of vector-borne emerging infectious diseases (EID), such as hantavirus (Glass et al., 2000), Lyme disease

---

This manuscript has been prepared in compliance with the journal Landscape Ecology

(Dister et al., 1997), Sin Nombre virus (Boone et al., 2000), and malaria (Srivastava et al, 2001) are becoming more streamlined and functional through the integration of spatial, ecological, and epidemiological data (Clarke et al., 1996). A common thread in many such studies is an attempt to lower disease transmission rates by interrupting the epidemiological cycle.

Two arthropod-borne viruses (a.k.a., arboviruses) that are currently of particular concern in the eastern United States are West Nile virus ([WNV] Wonham et al., 2004) and eastern equine encephalitis ([EEE] Hassan, et al. 2003). Primary vectors for both viruses are mosquitoes, and can be broadly cast into two non-mutually exclusive groups: enzootic (reservoir) and epizootic (bridge) vectors. Both viruses remain enzootic in avian reservoir hosts via bird-feeding (ornithophilic) reservoir vectors and become sporadically epizootic in wildlife, livestock, and human hosts via opportunistically feeding bridge vectors (Mclean et al., 2001; Hassan et al., 2003; Tate et al., 2005). These epizootic hosts, especially mammals, are generally considered "dead-end" hosts because they do not develop viremias high enough for transmission back to biting mosquitoes (Hassan et al., 2003).

The most recent major North American EID (Beasley et al., 2003), WNV, is a form of Japanese encephalitis (swelling of the brain) belonging to the taxonomic family Flaviviridae: *Flavivirus*. WNV was first isolated in 1937, from a woman in the West Nile province of Uganda. Human and equine outbreaks were restricted to the eastern hemisphere until 1999, when the first North American human case was reported in New York City (Devine, 2003). This outbreak began the largest documented arboviral epidemic recorded for the western hemisphere, and the largest worldwide for WNV

(Makar and Stowell, 2004). Since the 1999 outbreak, WNV has spread across North America and south to Central America and resulted in ≈17,000 human cases, including ≈670 deaths (Kilpatrick et al., 2005). Primary reservoir vectors of WNV are ornithophilic mosquitoes of the genus *Culex* (Turell et al., 2005), but the virus has been recovered from 43 mosquito species from 11 genera (Dauphin et al., 2004) and eight genera of ticks (Higgs et al., 2004). Since the New York case, WNV has been detected in dead birds of 138 North American species. Potential bridge vectors of WNV include opportunistic feeders such as *Aedes albopictus* and *Culex salinarius* (Turell et al., 2005).

EEE and two other closely related equine encephalitides, western (WEE) and Venezuelan (VEE) equine encephalitis, belong to the family Togaviridae: *Alphavirus*. EEE was first isolated in North America in 1933 during concurrent human outbreaks in Delaware, New Jersey and Virginia and currently persists in the eastern North America, the Caribbean, and South and Central America (Weaver et al., 1999). In North America, EEE tends to be more prevalent in summer and autumn, and foci are generally associated with freshwater swamps, the preferred habitat of the primary reservoir vector, *Culiseta melanura* (Weaver et al., 1999). Predominant reservoir hosts are gregarious passerine bird species that often roost *en masse* in swamp habitats (Komar et al., 1999). As with WNV, crows and jays are particularly susceptible to EEE (Hassan et al., 2003) and often serve as indicators of viral activity. Once enzootic transmission is established, the virus becomes available to epizootic bridge vectors such as *Coquillettidia perturbans* and *Aedes vexans*, which readily feed on mammals as well as birds (Hassan et al., 2003). As its name suggests, equine epizootics are the most commonly documented and infections

usually kill horses. Since 1964, there have been ≈200 confirmed human cases of EEE (Calisher, 2004) with a 30% mortality rate (CDC, 1992).

Persistence and transmission dynamics of arboviruses are functions of many factors, including vector competence, and the susceptibility, proximity, and mobility of vertebrate hosts (Hassan et al., 2003). Additionally, transmission generally coincides spatially with environmental conditions conducive to vectors breeding within habitats frequented by host species (Kitron, 1998; Kaya et al., 2004). Like many other mosquito-borne viruses, there is no human vaccine available for EEE (Calisher, 2004) or WNV (Li, 2004) and the most effective preventative measure is mosquito control, i.e., regulation of mosquito populations.

My models are based on the collective influence of spatially explicit habitat characteristics. These types of influences drive the spatial distributions of organisms, but were largely ignored before the publication of Levins' (1969) metapopulation theory. Notable exceptions are Huffaker (1958) and Andrewartha and Birch (1954). More recently, the role of spatial structure has emerged as a pivotal influence on the spatial and temporal distributions and abundances of organisms (e.g., Lindenmayer and Lacy, 1995; Lindenmayer and Possingham, 1996; Bender et al., 2003; Tischendorf et al., 2003) and has become a major motivation for much current research, including mine. Traditional models tended to oversimplify the mechanics of population regulation, and thus generally provide limited insight into real-world situations (Hanski 1994). In most cases, spatially influential factors were only implicitly addressed (Levins, 1969; Lande, 1987; Keeling, 2002). Population- and community-level studies generally do not explicitly incorporate the influence of spatial factors because hierarchical theory traditionally introduces

environmental factors only at the ecosystem and landscape levels of ecology. Distributional dynamics becomes even more convoluted if spatial heterogeneity of landscape characteristics is considered. Thus, spatially explicit landscape components, important and often continuous in variation, must be considered if ecologically integrated pest management techniques, such as those to control arthropod vectors, are to be effective.

The central purpose of this research was to create a series of complementary GIS-based models (Chapters II and III) capable of: 1) identifying potential mosquito habitat and 2) determining which of these are most likely to be active based on recent weather patterns. Chapter IV summarizes the necessary protocols for modeling the spatial and temporal distributions and abundance of mosquitoes, with emphasis on *Cs. melanura*, the primary reservoir vector of EEE, in a real-world coastal landscapes of the mid-Atlantic region (MAR).

This study was conducted with the cooperation of the Chesapeake Mosquito Control Commission (CMCC), Chesapeake, Virginia. The spatial extent is the entire city of Chesapeake, Virginia. The city, located on Virginia's Coastal Plain physiographic region, has a total area of 91,427 ha and has a growing 2004 human population of 214,725—up 20.8% from 1990. Chesapeake was selected for study because 1) the structure of the landscape represents a diverse mosaic of land use, 2) the CMCC is a well established and nationally respected mosquito control agency that strives to stay on the cusp of technology, and 3) of the known occurrence and relative distributions, within the city, of ~40 (~30 in 2004) mosquito species listed as potential vectors of WNV by the

Center for Disease Control (CDC). Among these species are the major reservoir and bridge vectors of EEE.

Suitable habitat for a broad range of mosquito species, including tidal and freshwater creeks and the Great Dismal Swamp with its canals and forested wetlands, lies embedded in the landscape mosaic. In addition, an extensive ditch network that allows for agriculture, and more recently, suburban development, drains much of southern Chesapeake. Thus, the close proximity of good mosquito habitat threaded within and among high densities of humans creates a landscape conducive to the transmission of WNV and other mosquito-borne diseases.

Each of the following three chapters (Chapters II-IV) will be separately submitted for publication in peer-reviewed journals, and thus, each is written as a stand-alone manuscript formatted as per the requirements of the journal. This introduction was designed and written as a general chapter overview with relevant sections appearing in the respective chapters that follow. It is also important to note that final analyses associated with Chapter III are dependent on the results of Chapter II. Because of this, readers should be aware that some sections of this dissertation and this general introduction, especially in methods, will be repeated in more than one chapter, and potentially in all three (Chapters II-IV). Chapter V will serve as a general summary of the research herein, and will not be submitted for publication.

Chapter II Overview

The primary objective of this chapter is to construct a set of predictive, spatially explicit, and scale-dependent habitat suitability indices (HSI models) based on the

"Hutchinsonian-niche concept" (Hutchinson, 1957). These models are based largely on remotely sensed (e.g., satellite imagery, land use/cover, soil surveys) data formatted for use in a GIS. Model results are predictive, and used to identify areas within the landscape in which mosquito species are most likely to occur. This approach requires the development of a baseline habitat classification model capable of identifying, categorizing, and ranking suitable habitat based on relationships between mosquito captures (Chesapeake, Virginia: 2004) and selected habitat attributes at mosquito trapping sites. This chapter will lay the groundwork for Chapter III.

Many life-history aspects that influence the distributions of populations (e.g., competition, physiological and behavioral niche tolerances) are controlled by landscape-level gradients, e.g., moisture (Kaya, et al., 2004; Bellows et al., 2001). Thus, digital surrogates are needed because direct measurement of habitat attributes is not practicable at the landscape-level. As such, selection of attributes for inclusion in these models is based on the ability to accurately represent, in digital format, the critical niche dimensions of mosquitoes.

The influence of environmental factors on landscape- or ecosystem-level patterns, processes, and functions is scale-dependent (Turner, 1989). Levin (1992) suggests that difficulties associated with the unification of population biology and ecosystems science can be attributed to problems of pattern and scale. Variation in the spatial heterogeneity among the environmental attributes used in this HSI is inherent, as is the variation in scale dependence among factors from an organism's point of view (Wiens, 1976). Therefore, the conception of a parsimonious set of measurable habitat attributes (variables) designed to collectively assess habitat suitability must incorporate issues of

scale, i.e., the spatial scale for each attribute to which a species, or group of species, most strongly responds. These issues are integrated into these HSI models via preliminary statistical comparisons of mosquito capture data and each habitat variable at different spatial scales, thereby isolating the most suitable scale for each variable for explaining mosquito abundance.

Predictive habitat suitability for all areas within the landscape was determined by the collective influence that habitat attributes (independent variables) had on mosquito abundance (dependent variable) at associated trap sites as determined by multiple regression analyses. More specifically, each habitat attribute constitutes a spatially continuous description of landscape pattern, such as digital satellite imagery enhancement (e.g., vegetation indices), land-use, hydrology, and soil properties represented in raster format. Independent variables were selected to represent maximum landscape heterogeneity in subsequent analyses while still maintaining a realistic degree of model generality. In support of regression results, importance values of various wetland types (e.g., estuarine, palustrine, riverine, lacustrine) to predicted mosquito abundance were calculated using a spatial overlay operation of National Wetland Inventory (USGS) maps and areas with high habitat suitability in HSIs using polar ordination analysis. Relational patterns associated with wetland-type importance were evaluated for dissimilarity using multivariate ordination analysis.

Forty-six of the 56 mosquito trapping sites sampled during 2004 had ≥ 5 nights of mosquito trapping (trap nights = TN). Capture data were normalized to account for variation in trapping effort among sites by dividing total captures of each species separately, and of all species combined, collected at each site by the number of TNs.

Capture data for individual species were grouped with other species based on similarities of habitat requirements, life-cycle types (after Crans, 2004), and vector potential (Turell et al., 2001 and 2005, among others). This was done to minimize complexity and increase usefulness of mosquito-habitat models. Because this HSI is spatially explicit, and much of the habitat attribute data is temporally static, model validation using capture data for alternate years when mosquitoes were collected (2003 and 2005) would be problematic and would also have spatial redundancies because many of the trapping sites sampled in 2004 were also used in 2003 and 2005. In addition, the number of trapping sites in 2003 with sufficient TNs is smaller than 2004, and when analyses were performed a complete set of 2005 capture data was not yet available. Cross-year comparisons (2003-2004) consisted of pair-wise correlation testing.

These models were derived from spatially explicit empirical data, thus making them useful for locating potential mosquito habitat within real landscapes. The use of data collected by remote-sensing techniques enables the integration and analysis, within the framework of a GIS, of large and diverse data sets with extents not feasible by field collection alone. Because these HSI models are applied (i.e., not merely theoretical), much attention was devoted to keeping them streamlined, user-friendly, and not cost-prohibitive, while retaining its ability to process empirical data in real landscapes.

Chapter III Overview

In this chapter, the semi-static HSI classification described for Chapter II was temporally augmented by a weekly predicted abundance model for the ornithophilic (bird-biting) mosquito, *Cs. melanura*. This was done in a GIS through the integration of a temporally

static topographic soil moisture index and spatially explicit "recent" weather data. *Cs. melanura* was selected for several reasons. It is not a biter of humans, and thus is not generally the issue in residential complaints, but it was, by far, the most frequently captured species in Chesapeake in 2004 (62.0% of all captures), and it is the primary enzootic vector for EEE (Nasci and Edman, 1984; Crans et al., 1994), making it the primary focus of the CMCC's adulticide efforts.

The environmental conditions that bring mosquitoes, the pathogens they transmit, and potential hosts together are often measurable (Shaman and Day, 2005). For example, spatial and temporal fluctuations in mosquito abundance are both directly and indirectly influenced by weather patterns (Rogers, 1967; Shaman et al, 2002; Reiter, 2001; Tong and Hu, 2001; USDA 2004, and others). Naturally occurring outbreaks of EEE are usually associated with periods of high temperatures and rainfall, creating conditions conducive to the rapid expansion of *Cs. melanura* and other mosquito species (USDA, 2004). Rainfall increases the diversity and abundance of habitats available to breeding mosquitoes and the resultant near-surface humidity increases both flight activity and host-seeking behavior (Shaman and Day, 2005). These associations make the geographic locations of breeding and host-seeking activities predictable, and therefore, potentially reveal the most judicious stages at which to interrupt viral epidemiologic cycles of mosquito-borne diseases.

Topography is a major influence on the flow direction, accumulation, and distribution of water within natural watersheds as well as on landscape-level soil moisture gradients (Yeh et al., 1998; Bernhardsen, 2002; Garbrecht and Martz, 2000). Researchers have long used topographic indices to predict relative soil moisture (e.g., Beven and

Kirkby, 1979, Urban et al., 2000). Others have suggested improved soil moisture indices that integrate topographic data and empirical soil data (Iverson et al., 1997, O'Loughlin, 1981 and 1986), especially in landscapes with little topography (Dirnböck et al., 2002). Chesapeake has low relief similar to the landscape studied by Dirnböck et al. (2002). Topographic indices permit the identification of saturated areas, with decent accuracy, especially where upslope accumulation exceeds local soil transmissivity (O'Loughlin, 1986), and thus reveals potential mosquito habitat.

I used Beven's (1997) topographic moisture index (TMI) to quantitatively identify areas where surface wetness was most likely to occur after precipitation events. The TMI was based on a 2-ft vertical (0.61 m) interval digital elevation model (DEM) of the city of Chesapeake (detailed in Chapter III Methods). This DEM was used to generate a hydrologic model (ArcGIS 9.1, Spatial Analyst extension) to quantify flow accumulation on a pixel-by-pixel basis. The National Hydrology Dataset (NHD: USGS) was used to determine the extent of the two watersheds Chesapeake lies within: Hampton Roads and the Albemarle Sound watersheds. Because the extent of these watersheds exceeds the boundary of Chesapeake, I clipped the area from the USGS's one-arc second DEM to quantify regional flow accumulation at the city's boundary. This regional accumulation raster was incorporated into the 2-ft vertical resolution hydrologic model of the city, thus accounting for all potential hydrologic contributions.

I used spatially explicit meteorological data (NEXRAD: ***NEX***t-generation [Doppler] ***RAD***ar) (National Oceanic and Atmospheric Administration [NOAA], National Weather Service [NWS]) to create weekly "accumulated precipitation" (PA) grids. NEXRAD (NOAA, NWS) is georeferenced radar data (Weather Service Doppler

Radar [WSR:88D]) that includes the 3-hr PA data used herein (Beringer and Ball, 2004). These data were preprocessed and overlaid into total weekly PA grids in ArcGrid format (detailed in Chapter III methods). Weekly PA grids were overlaid onto weekly temperature grids and the TMI grid (additively) to map areas with high probabilities of surface and subsurface wetness. *A priori* regression models were used to determine the weighted (multiplier) values for temperature, PA, and TMI grids before the overlay operation. Thus, knowing the spatial distribution of surface wetness, I was able to map which areas of suitable habitat, from Chapter II, are most likely to experience outbreaks of *Cs. melanura.*

From a prevention and control standpoint, it is critical that mosquito control agencies such as the CMCC have the ability to rapidly track the spatial and temporal distributions of potential arboviral vectors such as *Cs. melanura.* My weekly abundance models (maps) provide this ability. Weekly maps can be prepared quickly using a series of sub-models I created in ArcGIS ModelBuilder. These sub-models perform arduous data preprocessing in a streamlined and user-friendly manner. Most of the data needed are either free (e.g., NEXRAD, NHD, DEM, weather summaries) or generated by the agency itself (e.g., capture data). In addition, weekly maps are not hindered by biases associated with human population densities and residential complaints. They do, however, give mosquito control agencies the ability to respond quickly to distributional changes of *Cs. melanura*, thus lowering the transmission potential in nearby suburban and urban areas. Such knowledge will enable the agencies to apply insecticides in a more effective, timely, and economical manner, thereby reducing the health risks of EEE and similar diseases while reducing costs of chemicals and spraying efforts.

Chapter IV Overview

The purpose of this chapter is to provide the reader and potential users of the models presented in Chapters II and III with the necessary protocols for modeling the spatial and temporal distributions and abundances of mosquitoes, with emphasis on Cs. melanura, in real-world landscapes. Because of similarities in climate and mosquito assemblages, this sequence of models should be effective throughout coastal-plain and lower-piedmont areas in the MAR. However, the portability potential of these models in upper piedmont and montane regions of the MAR would need to be tested because of the ecological effects of elevation. Higher elevations replicate higher latitudes and generally have different assemblages of organisms. This is, in part, due to differences in climate (e.g., cooler temperatures, shorter active seasons) as well as differences in the mechanics of surface water distribution (e.g., soil type, slope, runoff and drainage potential). For example, *Cs. melanura* is present in lowland swamps throughout the MAR, but its range does not extend into the Appalachian range (Crans, www-rci.rutgers.edu).

The intended audience for this final chapter is primarily GIS analysts employed by mosquito-control and public health agencies. Environmental managers and decision makers of these agencies with limited experience in spatial modeling could also use these protocols to make more educated decisions regarding temporal and spatial mosquito monitoring and control practices.

Chapters II and III are designed for publication as separate entities. This chapter cogently summarizes the technical procedures of both chapters, with enough detail and background for the recreation of a seamless series of models for predicting mosquito outbreaks. Because most mosquito-control and public health agencies lack the ability to

conduct exhaustive *in situ* monitoring and environmental data collection, they would benefit from the application of models capable of predicting the temporal and spatial distributions of mosquitoes at a landscape scale (Shaman et al., 2002). Chapters II and III produce such a series of models.

In addition to providing protocols for generating models that predict habitat suitability and forecast mosquito outbreaks, this chapter presents suggestions for improving the quality of collected mosquito monitoring data. The sampling design and data collection techniques for mosquito captures used in Chapters II and III were developed by the CMCC, and thus not specifically tailored for integration into spatial models. Consequently, this fourth chapter contains a discussion, including recommendations, of modifications in sampling design and data collection that could be used to improve the accuracy and precision of habitat suitability and predicted abundance models, including issues with the selection of representative habitats to be sampled, number and distribution of trapping sites, and use of multiple trapping techniques for increasing the diversity of mosquito species collected.

This chapter also discusses the prognostic value of several augmenting datasets that could be easily processed into spatial format, including: larval monitoring and control data, bird surveillance (e.g., dead birds, sentinel bird flocks), and human demographics. Except for larval monitoring and control, these datasets would be more directly associated with reducing the risks of disease transmission than with efforts to control nuisance mosquito species. Pre- and post-larvicide monitoring data from both treatment and control sites could be used not only to quantify the effects of control efforts, but also to increase the predictive power of my models.

Dead bird data could be integrated into disease surveillance programs to provide an early warning system of viral activity in both mosquitoes and birds. This would be especially critical when dead bird reports spatially coincide with outbreaks of known vector species such as *Cs. melanura.*

Sentinel birds have long been used to monitor arbovirus activity (Moore et al., 2003). Similar to dead bird reports, sentinel bird data can also be used as an early warning system of viral activity and to quantify transmission rates (Komar, 2001). Because the geographic location of sentinel flocks is usually known, data are especially suited for spatial modeling.

Children and the elderly are at a higher risk for debilitating complications resulting from viral encephalitis (Whitley and Kimberlin, 1999; Peterson and Marfin, 2002). Because of these elevated risks, it is critical that locations where these two demographic groups congregate (e.g., nursing homes, retirement communities, schools, playgrounds) should be considered when monitoring arboviral activity. These locations could easily be incorporated into a GIS and used in an overlay analysis with predicted abundance maps

In summary, the ability to assess habitat suitability and predict outbreaks of mosquitoes using accurate landscape-level data is vital in the development of effective, efficient, and environmentally sound integrated pest management programs. This chapter provides a baseline protocol for achieving these objectives. Where appropriate, I have attempted to supplement my methods with short discussions regarding potential enhancements to experimental design, data collection technique, and the incorporation of

ancillary datasets that could be used to increase the predictive power these or similar models.

Conclusions

This sequence of models should be useful to mosquito-control agencies because it consists of a series of robust components designed to use real-world data. Chapter II involves the construction of a scale-appropriate HSI that establishes baseline models for mapping mosquito habitat based on species groups. The models in Chapter III integrated recent rainfall and temperature data with the results of Chapter II for locating, in near real time, which areas are the most likely to experience mosquito outbreaks. Lastly, Chapter IV provides the reader and potential users the necessary protocols for reconstructing the models in Chapters II and III in a real-world coastal landscapes in the MAR, with emphasis on *Cs. melanura*, the primary reservoir vector of EEE. These models should subsequently lead to the development of environmentally sensitive strategies that will not only lower chemical and manpower costs by increasing the efficiency of control efforts, but also reduce transmission risks of mosquito-borne diseases such as EEE and West Nile virus (WNV).

CHAPTER II

SPATIAL PREDICTION OF MOSQUITO HABITAT ON THE SOUTHERN COASTAL PLAIN OF VIRGINIA USING REMOTE-SENSING TECHNIQUES AND A GIS

Introduction

In the last 30 years geographic information system (GIS) technology has grown from relative obscurity to a worldwide industry that is expanding at a rate of more than 20 percent per year (Bernhardsen, 2002). Before the relatively widespread availability of GIS, global positioning systems (GPS), and remotely sensed techniques and data, the modeling of spatial and temporal heterogeneity of landscapes was often difficult, if not impossible. This difficulty was primarily associated with a general inability to manage, store, and analyze the huge volumes of data needed to model complex real-world patterns and processes (Johnson, 1993). Now, applications for GIS are as diverse as the broad range of data that can be applied to this technology; this is reflected in recent literature. A burgeoning source of such information, GIS, GPS, and digital satellite remote sensing provide promising data and analytical tools for applied and multi-disciplined study.

The use of digital satellite data in GIS is becoming a valuable approach in the study of vector ecology and disease transmission (Clarke et al., 1996; Kitron, 1998). Surveillance, monitoring, and subsequent health policies associated with the study of vector-borne emerging infectious diseases (EID), such as hantavirus (Glass et al., 2000), Lyme disease (Dister et al., 1997), Sin Nombre virus (Boone et al., 2000), and malaria

(Srivastava et al., 2001), are becoming more streamlined and functional through the integration of spatial, ecological, and epidemiological data (Clarke et al., 1996). A common thread in many such studies is an attempt to lower disease transmission rates by interrupting the epidemiological cycle.

Two arthropod-borne viruses (a.k.a. arboviruses) that are currently of particular concern in the eastern United States are West Nile virus ([WNV] Wonham et al., 2004) and eastern equine encephalitis ([EEE] Hassan et al., 2003). Mosquitoes, the primary vectors for both viruses, are broadly cast into two non-mutually exclusive groups: enzootic (reservoir) and epizootic (bridge) vectors. Both viruses remain enzootic in birds via bird-feeding (ornithophilic) mosquitoes, and become sporadically epizootic in wildlife, livestock, and human hosts via mosquitoes that feed on a wide variety of taxa (McLean et al., 2001; Hassan et al., 2003; Tate et al., 2005). These epizootic hosts, especially mammals, are generally considered "dead-end" hosts, as they rarely develop viremias high enough for transmission back to mosquitoes (Hassan et al., 2003).

WNV, the most recent major North American EID (Beasley et al., 2003), is a form of Japanese encephalitis (swelling of the brain) belonging to the taxonomic family Flaviviridae: *Flavivirus*. WNV was first isolated in 1937, from a woman in the West Nile province of Uganda. Human and equine outbreaks were restricted to the eastern hemisphere until 1999, when the first North American human case was reported in New York City (Devine, 2003). This began the largest documented arboviral epidemic recorded for the western hemisphere, and the largest worldwide for WNV (Makar and Stowell, 2004). Since the 1999 outbreak, WNV has spanned North America and moved south to Central America, resulting in $\approx$ 17,000 human cases including $\approx$ 670 deaths

(Kilpatrick et al., 2005). Primary reservoir vectors of WNV are ornithophilic mosquitoes of the genus *Culex* (Turell et al., 2005), although the virus has been recovered from 43 mosquito species from 11 genera (Dauphin et al., 2004) and eight genera of ticks (Higgs et al., 2004). Since the New York case, WNV has been detected in dead birds of 138 North American bird species, especially those of the family Corvidae ([crows and jays] Dauphin et al., 2004). Potential bridge vectors of WNV include opportunistic feeders such as *Aedes albopictus* and *Culex salinarius* (Turell et al., 2005). Vector maintenance and transmission efficiency of WNV of North American mosquito species is far from resolved because of the relatively recent introduction of the virus to a new suite of potential vector and host species (Turell et al., 2001 and 2005).

EEE and two other closely equine encephalitides, western (WEE) and Venezuelan (VEE) equine encephalitis, belong to the genus *Alphavirus* (Togaviridae). EEE was first isolated in North America during concurrent human outbreaks in Delaware, New Jersey and Virginia in 1933, and currently persists in the eastern North America, the Caribbean, and South and Central America (Weaver et al., 1999). EEE has a long North American history, and thus its epidemiology has been well studied.

In North America, EEE tends to be more prevalent in summer and fall, and foci are generally associated with freshwater swamps, which are the preferred habitat of the primary reservoir vector, *Culiseta melanura* (Weaver et al., 1999). Predominant reservoir hosts are gregarious passerine birds species that roost abundantly in swamp habitats (Komar et al., 1999). As with WNV, bird species of the family Corvidae are particularly susceptible to EEE (Hassan et al., 2003), making them poor enzootic hosts but good indicators viral presence. Once enzootic transmission is established, the virus becomes

available to epizootic bridge vectors such as *Coquillettidia perturbans* and *Aedes vexans*, which readily feed on mammals as well as birds (Hassan et al., 2003). As the name suggests, epizootics are the most commonly documented in horses and infections are usually fatal. Since 1964, there have been 200 confirmed human cases of EEE (Calisher, 2004) with a 30% mortality rate (CDC, 1992).

Persistence and transmission dynamics of arboviruses are functions of many factors, including vector competence, susceptibility and proximity and mobility of enzootic vertebrate hosts (Hassan et al., 2003). Additionally, transmission generally coincides spatially with environmental conditions conducive to vector breeding conditions found within habitats frequented by host species (Kitron, 1998; Kaya et al., 2004). Like many mosquito-borne viruses, there is no human vaccine available for EEE (Calisher, 2004) or WNV (Li, 2004) and the most effective preventative measure is mosquito control, i.e., regulation of mosquito populations.

Many life-history aspects that influence the distributions of organismal populations (e.g., competition, physiological and behavioral niche tolerances) are controlled by landscape-level gradients ([e.g., moisture] Kaya, et al., 2004; Bellows et al., 2001). Although direct observation of many disease vectors is not possible at large spatial scales, vector presence or the environmental conditions in which they flourish can be inferred via more visible indicators such as habitat type and attributes (Shuchman et al., 2002). Digital surrogates of habitat attributes are useful because direct measurement of habitat attributes is not practicable at the landscape-level (Goetz et al., 2000). Thus, selection of attributes for inclusion in this model is based, in part, on the ability to accurately represent, in digital format, critical niche dimensions of mosquitoes.

Recent advances in earth-observing sensors have made possible the generation of a wide range of spatially explicit environmental and biophysical features relevant to the ecology of disease vectors (Goetz et al., 2000). Common approaches are to use these data to map disease transmission risk or suitable vector habitat using landscape classification based on land cover/use (Overgaard et al., 2003; Pope et al., 2005; Kaya et al., 2004) and environmental characteristics, such as dominant vegetation type (Pope et al., 1994; Guerra et al., 2002), wetland type (Hayes et al., 1985; Lathrop et al., 2000), and soil properties (Beck et al., 1994; Glass et al., 1995; Patz, 1998).

Many studies have linked the presence of disease vectors to spatial and temporal vegetation characteristics via spectrally derived vegetation indices (VI) that represent various aspects of vegetative cover (e.g., vegetative moisture, biomass, photosynthetic activity) (Goetz et al., 2000). VI algorithms use mathematical operations between digital reflectance values of two different spectral bands (Campbell, 2002). They are generally designed to exploit the high absorption of visible red and high reflectance of near-infrared bands by photosynthetically active pigments and leaf mesophyll tissues (Hay et al., 1998).

First described by Rouse et al. (1974), the normalized difference vegetation index (NDVI) is one of the most widely used VIs for mapping primary production and leaf area index and, to a lesser degree, soil moisture gradients (Todd and Hoffer, 1998). NDVI has been used to map suitable vector habitat (Baylis et al., 1998; Estrada-Peña, 1999), to forecast disease outbreaks (Linthicum et al., 1999; Nihel et al., 2002), and to detect soil moisture gradients (Todd and Hoffer, 1998).

Another technique, Tasseled-Cap transformation (TC), computes biophysical scene characteristics associated with soils and vegetative vigor from multispectral satellite imagery (e.g., Landsat Enhanced Thematic Mapper [ETM+]) by condensing reflectance information for several weighted spectral bands onto a single transformation plane containing soil brightness, vegetation greenness, and wetness (soil and vegetation moisture) information (Crist and Cicone, 1984). TC concentrates data variability in three orthogonal axes (components) that are known to correlate with suitable arbovirus vector habitat (Beck et al., 2000). Dister et al. (1997) used TC to classify tick abundance and then generate transmission risk maps for Lyme disease. Barrera et al. (2001) used NDVI and TC to characterize VEE endemic foci in lowland tropical forests in western Venezuela.

The impact of factors influencing landscape- or ecosystem-level patterns, processes, and functions is scale-dependent (Turner, 1989). Further, Levin (1992) suggests that difficulties associated with the unification of population biology and ecosystem science can be attributed to problems of pattern and scale. Variation in the spatial heterogeneity among the environmental attributes is inherent, as is the variation in scale dependence among factors at the organismal level (Wiens, 1976). Therefore, the conception of a parsimonious set of measurable habitat attributes designed to collectively assess habitat suitability must incorporate issues of scale, i.e., the spatial scale of each attribute to which a species, or group of species, most strongly responds.

The primary objective of my study was to construct a set of predictive, spatially explicit, and scale-dependent habitat suitability indices (HSI) for mosquito species based on the "Hutchinsonian-niche concept" (Hutchinson, 1957). Particular attention is given to

the habitat requirements associated with soil properties for known vector species of WNV and EEE. These models are based largely on remotely sensed data (e.g., satellite imagery, land use/cover, soil surveys) formatted for use in a GIS and analyzed using inferential statistical models (i.e., multiple linear regression). Model results are predictive, and used to identify areas, or "patches," within the landscape in which mosquito species are most likely to occur. This approach requires the development of a baseline habitat classification model capable of identifying and ranking suitable habitat-based environmental characteristics.

Methods

Study Area

This study was conducted with the cooperation of the Chesapeake Mosquito Control Commission (CMCC), Chesapeake, Virginia. The spatial extent is the entire city of Chesapeake, Virginia (Figure 1). The city, located on Virginia's Coastal Plain physiographic region, has a total area of 91,427 ha, with a growing population of 214,725 (2004), up 20.8% from 1990. Chesapeake was selected for study because: 1) the structure of the landscape represents a diverse mosaic of land use that is representative of the region, 2) the CMCC is a well-established and nationally respected mosquito-control agency that strives to use current mosquito-control technology, and 3) ~30 mosquito species occurring within the city, including the major reservoir and bridge vectors of EEE, are listed as potential vectors of WNV (Appendix A) by the Centers for Disease Control (CDC) of the United States Department of Health and Human Services.

Suitable habitat for a broad range of mosquito species, including tidal and freshwater creeks and the Great Dismal Swamp National Wildlife Refuge (GDSNWR), with its canals and forested wetlands, lies embedded in the landscape mosaic. In addition, an extensive ditch network to allow for agriculture, and more recently, suburban development, drains much of southern Chesapeake. Thus, the close proximity of good mosquito habitat threaded among high densities of humans creates a landscape conducive to the transmission of WNV, EEE and other mosquito-borne diseases. This combination of extensive wildland-urban interface is deemed highly representative of current urbanization and emerging infectious arboviral diseases.

Dependent Variables

Mosquitoes were captured using CO_2-baited CDC light traps stationed at 56 permanent trapping sites throughout Chesapeake (Figure 1) from early April through early November, 2004. Only captures of females were used in analyses.

Only 46 of the 56 mosquito trapping sites were used for my analysis because the remaining 10 sites sampled during 2004 had ≤ 5 sampling nights (trap nights = TN). Capture data were normalized to account for variation in trapping effort among the 46 sites by dividing total captures of each species collected at each site by the number of TNs for that site.

Because this HSI is spatially explicit, and much of the habitat attribute data are temporally static, model validation using capture data for alternate years when mosquitoes were collected (2003 and 2005) would be problematic and have spatial

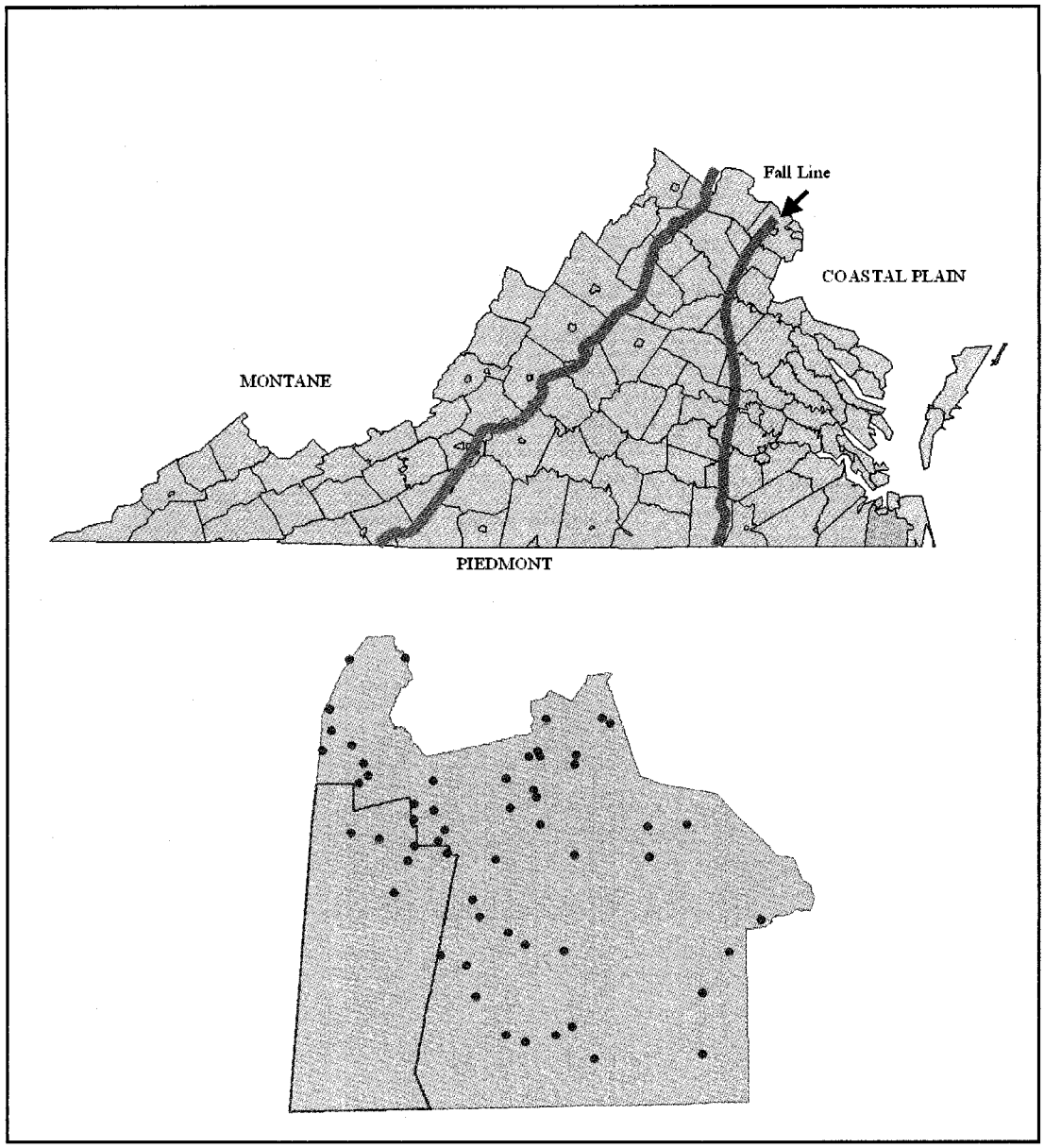

Figure 1. Location of the City of Chesapeake within the state of Virginia. Major physiographic provinces are indicated. Inset shows the location of 2004 trap sites (blue circles) and the Great Dismal Swamp National Wildlife Refuge (outlined in red).

redundancies because many of the trapping sites sampled in 2004 were also used in 2003 and 2005. In addition, the number of trapping sites in 2003 with sufficient TNs (N = 28)is smaller than 2004, and at the time analyses were run a complete set of 2005 capture data

was not yet available. Cross-year comparisons (2003-2004) to evaluate temporal patterns consisted of pair-wise *t*-test and correlation analysis of capture data for trapping sites common to both years (Zar, 1996).

CDC listing as a potential WNV vector species requires no determination of infection, dissemination, or transmission rates, but only that a species be collected in a "West Nile positive" pool (CDC: http://www.cdc.gov/ncidod/dvbid/westnile/). Because of the large number of potential vectors occurring in Chesapeake (Appendix A), generating a HSI for each listed species would be both cumbersome and impractical. The most abundant species, *Cs. melanura* (70.3% of modeled species [2004]), was modeled separately (CSMN; Table 1). *Culiseta melanura* is the primary enzootic vector for EEE and for this reason, it is the main target species of the CMCC control and surveillance program. This bias targeting *Cs. melanura*, is required because of its large numbers relative to the other species. Its inclusion in any multi-species model would have diluted the effects of the other species. In an effort to reduce the number of remaining models, only abundant species and species having high vector competence for WNV or EEE (N = 10) were considered. Vector competence is based on the susceptibility of mosquito species to disease dissemination from a host, and transmission back to a host (Sardelis et al, 2001). Capture data for these 10 species were combined into four separate groups: a single "competent-vector" group not including captures of *Cs. melanura* (ALSP), container-breeders [CONT], swamp species [SWMP], and ephemeral pool species [EPHM]; Table 1) based on similarities among habitat requirements, life-cycles (Crans, 2004), and vector competencies (after Vaidyanathan et al., 1997; Cupp et al., 2003; VDH,

2004; Turell et al., 2001, 2005). Although daily activity periods (i.e., diurnal, crepuscular, nocturnal), preferred host (e.g., avian, mammalian), and "maximum" known dispersal distance from site of emergence (Table 2) play critical roles in disease transmission, these factors were not considered in this classification. They will, however, be incorporated into the discussion of results.

Table 1. Total numbers of captured females in 2004. Total (Caps), percents of total females captured, life cycle types, and species group for each the 11 species are provided.

Species	Life cycle[†]	Total Caps (♀)	% Caps (♀)	Species Group[§]
Aedes albopictus [b, d, e]	2c	2,824	1.161	CONT
Culex pipiens [a]	3c	68	0.028	CONT
Culex restuans [a]	3c	1,497	0.616	CONT
Ochlerotatus triseriatus [b]	2c	339	0.139	CONT
Coquillettidia perturbans [d]	5a	6,025	2.477	SWMP
Culex erraticus [d]	3a	858	0.353	SWMP
Culex salinarius [a, b]	3b	21,991	9.042	SWMP
Ochlerotatus canadensis [b]	1c	32,288	13.276	SWMP
Aedes vexans [b]	2a	1,741	0.716	EPHM
Psorophora columbiae	2a	4,506	1.853	EPHM
Group total		72,137	29.661	ALSP
Culiseta melanura [c]	4a	171,071	70.339	CSMN
Total		243,208		

[a] Potential enzootic vector of WNV.
[b] Potential epizootic vector for WNV.
[c] Primary enzootic vector for EEE.
[d] Potential epizootic vector for EEE.
[e] Primarily diurnal
[†] From Crans, 2004. Summarized in Table 3.
[§] CONT = container, SWMP = swamp, EPHM = ephemeral, ALSP = all species except *Cs. melanura*, and CSMN = *Cs. melanura*

Table 2. Summary of daily activity periods, preferred host(s), and known flight ranges of modeled mosquito species. Activity periods: Diurnal = D, Crepuscular = C, and Nocturnal = N.

Species	1' Host Preference†	Flight Range[1]	D	C	N
Ae. albopictus	Humans[3]	~30-100 m	x[3, 8]	x[8]	
Ae. vexans	Generalist[3]	~16-40 km	x[4]	x[2]	x[2]
Cq. perturbans	Generalist[8]	~1.5-8 km	x[3]	x[3]	x[2]
Cx. erraticus	Birds[2]	~0-0.4 km			x[2]
Cx. pipiens	Birds[3, 8]	~0.4-0.8 km			x[3]
Cx. restuans	Birds[3, 8]	~1.5-3 km		x[8]	x[8]
Cx. salinarius	Generalist[5]	~1-8 km			x[5]
Cs. melanura	Birds[8]	~0.8-1.5 km		x[8]	x[8]
Oc. canadensis	Mammals[8]	~0.4-8 km	x[2, 3]	x[3]	x[3]
Oc. triseriatus	Mammals[6]	~0.8-1.5 km	x[8]	x[2]	
Ps. columbiae	Generalist[7]	~8-16 km	x[7]	x[7]	x[7]

†Not necessarily exclusive
[1]from Hopkins (2002)
[2]from Carpenter and LaCasse (1955)
[3]from Horsfall (1955)
[4]from O'Malley (1990)
[5]from Slaff (1990)
[6]from Walker (1992)
[7]from Meisch (1994)
[8]from Turell (2005)

Crans' (2004) classification of life-cycle types (LCT) is based largely on the timing, frequency, and habitats of reproductive events and larval development of mosquitoes. LCTs are named for representative species (e.g., LCT 1c = *Oc. canadensis* type [Table 3]). The 11 mosquito species modeled herein (Table 3) represent all but three of the 11 mosquito LCTs associated with CDC-listed species from Chesapeake.

Collectively, captures of mosquito species with these three unrepresented LCTs amount to only 0.0187% of females in 2004. By contrast, the least abundant vector species to be modeled, *Cx. pipiens*, is slightly more numerous (0.028%). Of the three unrepresented LCTs, *Ochlerotatus stimulans* type (1a) was not included, but differs from *Oc. canadensis* type only in the number of emergences from a single generation of eggs, *Ochlerotatus sollicitans* type (2b) was not included, but differs from similar type in that it is highly salt-tolerant, and *Orthopodomyia signifera* type (4b) is similar to the other treehole-breeding species included herein (e.g., *Oc. triseriatus*, *Ae. albopictus*), but it requires more winter protection.

Independent Variables

Predictive habitat suitability for all areas within the landscape was determined by the collective influence of habitat attributes (independent variables) on mosquito abundance (dependent variable) at associated trap sites. More specifically, each habitat attribute constituted a spatially continuous description of landscape pattern, such as digital satellite imagery enhancement (e.g., vegetation indices), land use, hydrology, and soil properties represented in raster format (Table 4). Independent variables were selected to represent maximum landscape heterogeneity while still maintaining a realistic degree of model generality.

Table 3. Life cycle types and primary larval habitat of mosquito species. Life cycle (LC) type, primary larval habitat (1' Habitat), duration of 1' habitat (temporary/permanent [T/P]), and microhabitat information was summarized from Crans (2004).

Species	LC[1a-5a]	1' Habitat	T/P	Microhabitat
Ae. albopictus	2c	container	T	Natural (e.g., treeholes, plant axils), artificial (e.g., discarded tires)
Ae. vexans	2a	ephemeral pool	T	Any fresh floodwater, especially river floodplains (open areas)
Cq. perturbans	5a	swamp/bog	P	Larvae attach to roots in aquatic vegetation in freshwater swamps
Cx. erraticus	3a	swamp/bog	P	Swamp and bog wetlands with abundant vegetation
Cx. pipiens	3c	manmade	-	Polluted (e.g., sewage treatment plants, landfills, containers)
Cx. restuans	3c	manmade	-	Polluted (e.g., sewage treatment plants, landfills, containers)
Cx. salinarius	3b	brackish marsh	-	Brackish habitat between salt marshes and upland drainage
Cs. melanura	4a	swamp/bog	P	Freshwater swamp habitats
Oc. canadensis	1c	swamp/bog	P	Many, especially in litter along water margins (floodplains)
Oc. triseriatus	2c	container	T	Natural (e.g., treeholes, plant axils), artificial (e.g., tires)
Ps. columbiae	2a	ephemeral pool	T	Any fresh floodwater, especially river floodplains (open areas)

1c Univoltine Aedine Life Cycle Types: *Oc. canadensis* type (spring hatch represents the bulk of a year's population, but often make successive appearances).

2a Multivoltine Aedine Life Cycle Types: *Ae. vexans* type (direct sunlight increases pool temperature for fast larval development before pools dry out).

2c Multivoltine Aedine Life Cycle Types: *Oc. triseriatus* type (floodwater species that develop in container habitats, *Oc. triseriatus* is common in suburban areas).

3a *Culex/Anopheles* Life Cycle Types: *An. quadrimaculatus* type (sparse in spring, most abundant in mid-summer to early fall).

3b *Culex/Anopheles* Life Cycle Types: *Cx. salinarius* type (larvae are only somewhat salt-tolerant).

3c *Culex/Anopheles* Life Cycle Types: *Cx. pipiens* type (tolerate pollution: high organic content, putrefied water).

4a Unique Life Cycle Types: *Cs. melanura* type.

5a Monotypic Life Cycle Types: *Cq. perturbans* Type: (larvae extract oxygen from the roots of aquatic plants).

Table 4. Summary characteristics of thematic layers representing independent variables. "Source" = the creator of the original data and the date it was created by the source, respectively.

Layer	Data Type	Source	Description	Code	Neighborhood Aggregation‡
Capture data§, §§	Vector (point; March-November, 2004)	CMCC*	Adult (♀) mosquito numbers at 46 permanent trap sites	n/a	n/a
Tasseled-Cap§,†	Raster: Landsat ETM+ (29 July 2002)	USGS	TC1 (Greenness) TC2 (Brightness) TC3 (Wetness)	TC1-3	Focal Mean
Land cover/use§,†	Raster: National Land Cover Data (NLCD; 2002)	USGS	Level I	-	Focal Majority
Soil data derivatives§, §§	Raster: Soil Surveys (SSURGO; 2004)	NRCS	Refer to Table 7	Table 7	Focal Mean
Hydrologic §, §§	Vector → Raster National Hydrology Dataset (ESRI Grid; July 2004) Vector → Raster Chesapeake Drainage Ditches (ESRI Grid: 2000)	USGS CMCC	Hydrologic sum, measure of spatial density of permanent water sources	HYDSM	Overlay and Neighborhood Sum

§ Using ArcGIS v9.0; Environmental Systems Research Institute (ESRI), Inc., Redlands, CA.

§§ Using ArcView v3.3; Environmental Systems Research Institute (ESRI), Inc., Redlands, CA.

† Using Erdas Imagine v8.7; Erdas, Inc. Atlanta, Georgia.

‡ Neighborhood attributes see Table 5.

*Chesapeake Mosquito Control Commission

Among the issues of scale associated with thematic representation is the inherent problem that increasing spatial scale results in a net loss of variation (Levin, 1992). I have accounted for a portion of this lost variation by creating a series of grids for each habitat attribute raster by operationally aggregating pixel data to increasingly larger scales (odd numbers, 1 x 1 through 21 x 21, 30-m/side pixels [Table 5, Figure 2]) using ArcGIS-9.1, Spatial Analyst and Model Builder extensions. Model Builder was used to generate a multi-stepped model capable of: 1) creating a set of new raster layers for each independent variable, one for each of the 11 scales, and 2) extracting values from these rasters that correspond to locations for each of the 46 trapping sites into a new shapefile.

Table 5. Spatial scales used as independent variables in habitat suitability indices. Length, side, and area are neighborhood (moving window) attributes.

Neighborhood (# of pixels)	Window	Length / side (m)	Perimeter (m)	Area (ha)
	1 x1	30	120	0.09
9	3 x 3	90	360	0.81
25	5 x 5	150	600	2.25
49	7 x 7	210	840	4.41
81	9 x 9	270	1,080	7.29
121	11 x 11	330	1,320	10.89
169	13 x 13	390	1,560	15.21
225	15 x 15	450	1,800	20.25
289	17 x 17	510	2,040	26.01
361	19 x 19	570	2,280	32.49
441	21 x 21	630	2,520	39.69

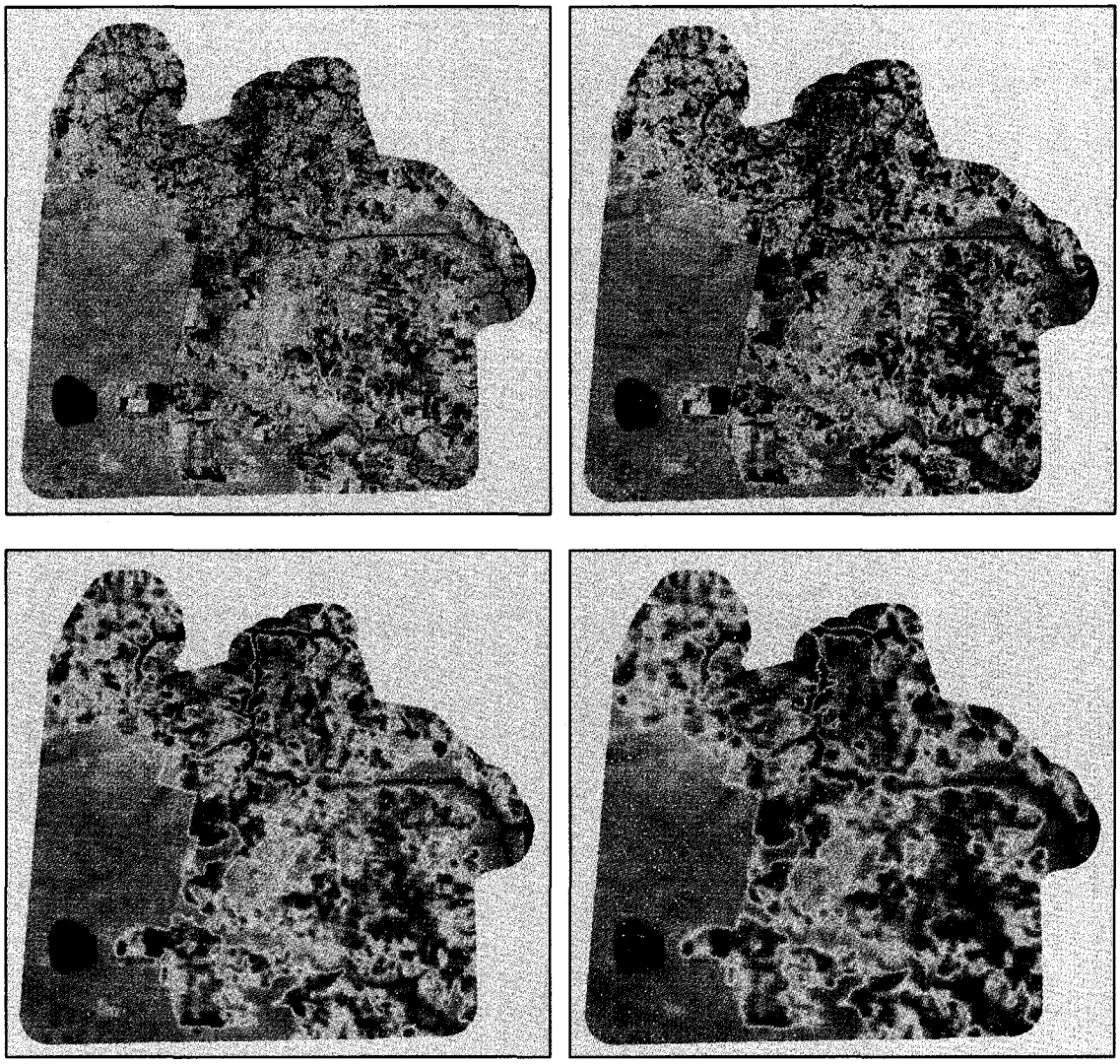

Figure 2. Tasseled-Cap (TC) greenness represented at four of the 11 spatially aggregated scales. Pixel values are derived from neighborhood statistics (i.e., means for TC) using a moving window. Pixel sizes at all scales remains 30 x 30m.

I used Pearson's correlation analysis to determine, for each habitat attribute, the spatial scale most strongly correlated with captures for each species group (Zar, 1996; Appendix B). Thus, the spatial scale of the habitat attributes in any given HSI will not

necessarily be consistent. A similar multiple-scale approach was used by Johnson et al. (2002) to predict the occurrence of several frog species within fragmented landscapes in the north-central United States. They achieved higher predictability with a multi-scale habitat occupancy model than those considering only a single spatial scale. In another study, Store and Jokimäki (2003), using multi-scale GIS models to predict habitat suitability for two bird species, were able to use habitat variables at different scales to create a multi-species HSI.

Data for most layers (e.g., spectral reflectance and soil property derivatives) were aggregated using a moving-window function that replaced raw attribute values with the focal neighborhood mean of all pixels within their respective spatial scales. A similar moving-window function to generate focal neighborhood sums was used to represent spatial density in binary data layers (e.g., water = 1, not water = 0). Neighborhood majorities were used to spatially aggregate categorical data (e.g., land-use). Because of variation in order of magnitude among the raw values of independent variables, all data layers were rescaled (standardized) to values between 0 and 1. It was expected that different aggregation scales among independent variables for each HSI would likely be inconsistent. However, in order to treat them as the same variable at differing spatial scales, I needed to determine that the 11 spatial scales were statistically autocorrelated (interdependent), and that the interdependencies exceeded the maximum aggregation resolution (Table 5). To justify potential multiple-scale models, I performed a preliminary analysis on continuous variables to determine the range, or on the ground distance, of spatial autocorrelation associated with each independent variable.

Tasseled-Cap Transformation (TC)

Landsat-7 ETM+ was used to compute TC for the City of Chesapeake because this imagery is readily available, recognized by most applicable software packages (e.g., ESRI products, Erdas IMAGINE), and relatively inexpensive. The ETM+ image, July 29, 2002 (acquired from the USGS's EROS Data Center), was cloud-free and in 30m x 30m-pixel size. This date represents the peak of the CMCC's mosquito trapping season.

Tasseled-Cap transformation was used, in lieu of NDVI, because its algorithms extract and condense spectral information pertaining to soil and vegetation characteristics (e.g., vegetative vigor = measure of photosynthetic [chlorophyll] activity) from all six Landsat bands, and not just red and near-infrared (NIR) bands as with NDVI, to which it is often compared. TC enhances spectral information for ETM+ by weighted transformation of brightness values (Crist and Cicone, 1984). Transformed values are reprojected onto three orthogonal axes (TC1-TC3). Output values for the TC1 (brightness [soil characteristics]) are the sum of weighted raw reflectances for bands 1-5 and 7. TC2 output values (greenness [vegetation characteristics]) are the weighted reflectance for band 4 (NIR) minus the weighted reflectances for bands 1-3, 5 and 7. Output values for the TC3 (wetness [soil and vegetation characteristics]) are the sum of weighted reflectances for bands 1-4 and minus bands 5 and 7. TC1-TC3 were used as independent (habitat) variables (Table 4). Axes were calculated using the following equation:

Equation 1. TC axis equations (ETM+) band weights (taken from Huang et al., 2002):

Axis	Blue (B1)	Green (B2)	Red (B3)	NIR (B4)	MIR* (B5)	FIR** (B7)
TC1 =	0.3561205	0.39722874	0.39040367	0.69658643	0.22862755	0.15959082
TC2 =	0.3343884	-0.35444216	-0.45557981	0.69660177	-0.02421353	-0.26298637
TC3 =	0.2626188	0.21406704	0.09260517	0.06560172	-0.76286850	-0.53884970

*Middle-infrared
*Far-infrared

Land-cover/land Use Data (LCLU)

Virginia LCLU data (National Land Cover Data [NLCD]: 2002) acquired from the USGS were subsetted to the extent of the City of Chesapeake with an additional 1.5-km buffer. The USGS Level II (e.g., deciduous[level I] forest[level II]) classification scheme (after Anderson et al., 1976 [Table 6]) was derived from Landsat TM digital satellite data (30 x 30m pixels) and validated by the USGS on a 5-state mid-Atlantic region using aerial photographs. Because of the large-scale validation by the USGS, I ran a preliminary accuracy assessment to determine the local usefulness of these data using a stratified random sampling design to select sample points (N = 1,016) throughout Chesapeake (Congalton and Green, 1999). Land cover/use of these sites was referenced using USGS digital orthophoto quarter-quads (DOQQ [1-m resolution]: USGS).

Soil Data

Soil survey data for the City of Chesapeake, Virginia (Soil Survey # va550, publication date: 10/05/2004) were exported in SSURGO format (***S***oil ***Sur***vey ***Geo***graphic Data) from the United States Department of Agriculture (USDA), Natural Resources Conservation Service's (NRCS, 2005) Soil Data Mart. SSURGO data describe the

characteristics and distribution of soil types within the landscape. These data are delivered in tabular (ASCII-delimited) and spatial (ArcView shapefile [polygons]: UTM Zone 18, Northern Hemisphere [NAD 83]) formats. SSURGO datasets for the City of Suffolk, Virginia (va800, 10/07/2004) and City of Virginia Beach, Virginia (va810, 10/07/2004) were also acquired, because several mosquito trap sites were located near boundaries of these cities (Figure 3). These additional datasets ensured that soil data were available for a minimum distance of 1.5 km for these border trap sites.

Table 6. Level-I reclassification scheme developed herein for the City of Chesapeake, Virginia. This scheme is based on the Level II land-cover/use classification scheme (after Anderson et al., 1976) used in USGS: NLCD (2002) datasets.

Level I	L I code	Level II	L II code
Water	1	Open Water	11
Developed	2	Low Intensity Residential	21
Developed	2	High Intensity Residential	22
Developed	2	Commercial / Industrial / Transportation	23
Developed	2	Transitional	33
Forested	4	Deciduous Forest	41
Forested	4	Evergreen Forest	42
Forested	4	Mixed (Evergreen and Deciduous) Forest	43
Herbaceous	8	Pasture / Hay	81
Herbaceous	8	Row Crops	82
Herbaceous	8	Urban / Recreational Grasses	85
Forested	4	Woody Wetland	91
Wetland	9	Emergent Herbaceous Wetland	92

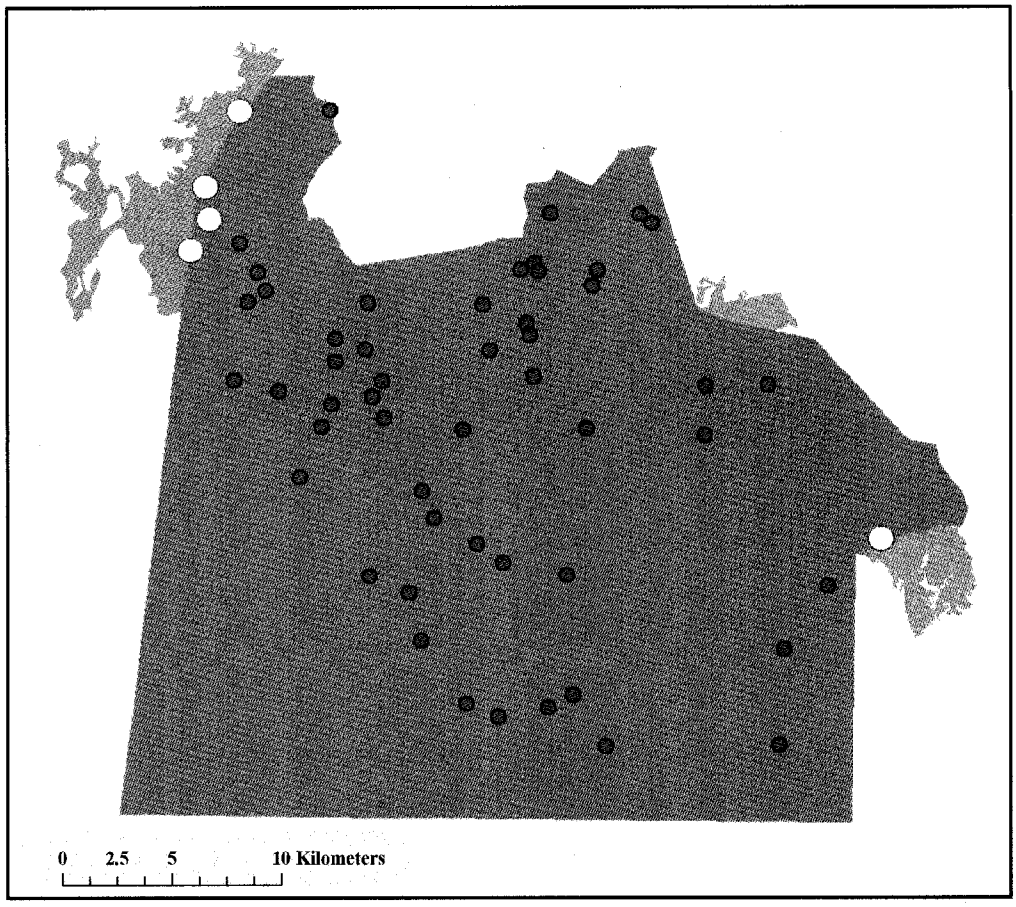

Figure 3. Spatial extents of SSURGO data for Chesapeake, Suffolk, and Virginia Beach. Circles represent trapping sites; those close to the city line are in yellow. Cheasapeake = blue, Suffolk (partial extent) = purple, Virginia Beach (partial extent) = green.

There are challenges associated with incorporating SSURGO spatial data into a GIS. Themes in thematic maps are based on map units; however, SSURGO map units are made up of one or more named soil types (components), each with a distinguishing suite of properties. As such, thematic representations of the soil properties of map units describing suitable mosquito habitat were created by pooling the properties (e.g., weighted averages) of each component as a function of the percent of map unit composition (Table 7). Pooling component properties resulted in a continuous single

value/pixel raster surface for soil properties associated with mosquito breeding habitats (Laird, 1988).

Table 7. SSURGO soil properties used as independent variables in habitat suitability regression models. Code and derivative equation for each property is provided. CV_{xi} refers to individual values for map unit components, CP_{xi} refers to the percent of composition for individual components in respective map units, and N_j is the number of possible values of CV_{xi}.

Soil Property Value (SPV)	Code	Equation	Applicable CV_{xi}[†]
Percent Hydric Composition (Soil meets requirements for hydric soil)	HYDPC	A	0 = not hydric 1 = hydric
Drain Potential (Degree of hydraulic conductivity and low water-holding capacity)	DRAIN	B	1 = well drained 2 = moderately well drained 3 = somewhat poorly drained 4 = poorly drained 5 = very poorly drained
Runoff Potential (Degree of potential water loss by overland flow)	RUNOF	A	1.00 = negligible 0.75 = very low 0.50 = low 0.25 = medium
Water Table Depth (Minimum value for the range in depth to the seasonally high water table April-June)	WTDAJ	N/A	Continuous (provided by NRCS) Values inverted on a 1-5 scale
Available water storage (25 cm) (Maximum value for the range of available water in plant root zones)	AWS25	N/A	Continuous (provided by NRCS)

Equations:

A) $SPV = (CV_{1i} \times CP_{1i}) + (CV_{2i} \times CP_{2i}) \ldots (CV_{ni} \times CP_{ni})$

B) $SPV = (CV_{1i} \times CP_{1i}) + (CV_{2i} \times CP_{2i}) \ldots (CV_{ni} \times CP_{ni}) / N_j$

[†] For more technical criteria of component attributes refer to NRCS (1995).

Hydrologic

Two vector datasets, the National Hydrology Dataset ([NHD, 2002] USGS) and a digitized map of Chesapeake canals and ditches (CMCC [2000]), were overlaid, combined as a single polygon shapefile, and then converted to raster to create a binary grid representation (water = 1, not water = 0) of Chesapeake water bodies, including the GDSNWR. This binary grid was spatially aggregated using a focal neighborhood sum, resulting in multi-scale (Table 5) representations of water prevalence (Table 4).

Regression Models

Multiple (linear) regression models were used to quantify habitat suitability based on the hypothesis that mosquito abundance is a function of the variation in measurable environmental (habitat) attributes. These habitat attributes were represented by digital thematic layers in a GIS. Linear regression models are commonly used in studies seeking to describe relationships between organismal abundance and environmental factors; however, they are easily misused (Johnson, 2002). Ecological phenomena are often complex, and data sets often have inherent anomalies and background variation that can produce results that are analytically unreliable (Matthews et al., 1994; McCune, 1997; Maurer, 1999).

I used all possible regressions (APR) to quantitatively select the most parsimonious set (model) of independent variables (habitat attributes) to be used in multiple regression models for each species group. All regression analyses were made using Number Cruncher Statistical Software (NCSS) v2000. Correlation analysis between mosquito captures and each of the 11 aggregation scales (described above) for each

independent variable enabled the selection of the best spatial scale for variables to be represented in subsequent regression models (Appendix B). These results were used to reduce the number of scales/variable used in all possible regressions to one, thereby determining the suite of independent variables, including the scale of representation, that was most important to each species group. Final independent variables and the scale of representation of each variable in the five group-specific multiple regression models were based on a combination of high R^2-values and low root mean^2 errors in APR models. Multiple regression models were validated by rerunning each of the five group analyses in 15 trials after randomly removing the data associated with one trapping site/trial. Chi-square analysis was used to determine if R^2-values and root mean squared errors were statistically similar to initial models (Wrigley, 1985).

Habitat Suitability Maps

A habitat suitability map for each species group was produced in a GIS (using ArcGIS v9.1) using linear regression equations to perform an arithmetic overlay operation. Standardized raster-formatted data layers (X) for each independent variable (described above) were weighted using the associated partial regression coefficients (b), and overlaid using the generalized equation below (a = Y-intercept).

Equation 2: $$Y = a + b_1(X_1) + b_2(X_2) + ... + b_n(X_n)$$

Following the overlay operation, final maps were ranked for suitability (5 equal intervals [20% each]), i.e., for predicted mosquito abundance (Y).

In order to get a sense of the local conditions associated with mapped areas of predicted high mosquito abundance, spatial data were extracted from National Wetland Inventory (NWI) maps (USFWS, 2006) and overlaid on ranked habitat suitability maps. Areas ranked most suitable (80-100%) on habitat maps were clipped and converted to shapefile format. These new shapefiles were used as a mask to extract, or cookie-cut, Level-I classification data (i.e., System-Level classes: estuarine, lacustrine, palustrine, riverine, and upland; after Cowardin et al., 1979) from NWI maps. A wetland class importance value (WTI_{ij}) for each wetland class (WT_i) in each species group regression model (SM_j) was calculated using the following equation:

Equation 3:

$$WTI_{ij} = \left(\frac{\text{Number of } WT_i \text{ pixels for } SM_j \text{ in clipped scene}}{\text{Number of } WT_i \text{ pixels for } SM_j \text{ in entire scene}} \right) \text{x } 10$$

Bray-Curtis polar ordination (PCORD for Windows) was used to describe habitat affinity patterns of mosquito species groups for each NWI wetland type based on WTIs. Bray-Curtis ordination was selected because it has low sensitivity to noisy data present in most ecological data sets (Gauch and Whittaker, 1972) and because it calculates end point selection on the two most dissimilar species groups (Ludwig and Reynolds, 1988). I used Euclidean distance measure because it emphasizes major differences in species distributions among habitats, or in this case, wetland types (Ludwig and Reynolds, 1988). Pearson's correlations (R) based on ordination results quantified relationships between each species group and the five wetland types (Zar, 1996).

Results

Dependent Variables

Of the 46 permanent trapping stations where mosquito capture data were collected, 28 were located in or near (<200m) palustrine wetlands, six near (<200m) estuarine wetlands and the remaining 22 within (<200m) upland habitats. Thirty-eight trapping stations were <400m from palustrine wetlands, well within the potential dispersal distances of *Cs. melanura* and the three SWMP species. This habitat is the primary breeding habitat of *Cs. melanur*a, the CMCC's target species. No traps were located in or near lacustrine or riverine wetlands. These locational assessments were made using System-Level NWI maps (USFWS, 2006).

In all, 275,726 female mosquitoes, representing the 29 CDC-listed WNV vector species (Appendix A), were captured in 2004. Of these, 243,208 (≈ 88% [242.24 captures/TN]) are accounted for by captures of the 11 modeled species (Tables 1 and 3). Numbers of modeled species ranged from 171,071 individuals for *Cs. melanura*, ≈ 70.3% of 2004 captures for these 11 species, to 68 for *Cx. pipiens*. Unless otherwise stated, future references of captured mosquitoes will include only the 11 representative species modeled in Tables 1 and 3.

There was no significant difference in captures by species between 2003 and 2004 ($P = 0.094$, $t = 1.850$, $df = 10$ [Table 8; Figure 4]). Additionally, capture numbers of each species were highly correlated between 2003 and 2004 ($R = 0.931$). These results indicate temporal similarity of capture patterns at trap sites between the two years, and indirectly justify the analysis of 2004 capture data only.

Table 8. Results of a preliminary two-tailed *t*-Test comparing the number of captured females for 2003 and 2004. Values were normalized by trapping nights. Descriptive statistics and Pearson's correlation coefficient (*R*) are provided.

Species	2003/TN	2004/TN
Cx. pipiens	0.16	0.07
Oc. triseriatus	0.59	0.34
Cx. erraticus	0.50	0.85
Cx. restuans	5.87	1.49
Ae. vexans	21.29	1.73
Ae. albopictus	1.53	2.81
Ps. columbiae	4.18	4.49
Cq. perturbans	1.42	6.00
Cx. salinarius	47.64	21.90
Oc. canadensis	117.93	32.16
Cs. melanura	206.36	170.39
Total	407.49	242.24
Mean	37.04	22.02
Standard Deviation	66.47	50.28

Results		
Pearson Correlation (*R*)	0.931	
H_o: Mean Difference =	0	
Observations	11	11
df	10	
t Stat	1.850	
P($T \leq t$) two-tailed	0.094	
t Critical two-tailed	2.228	

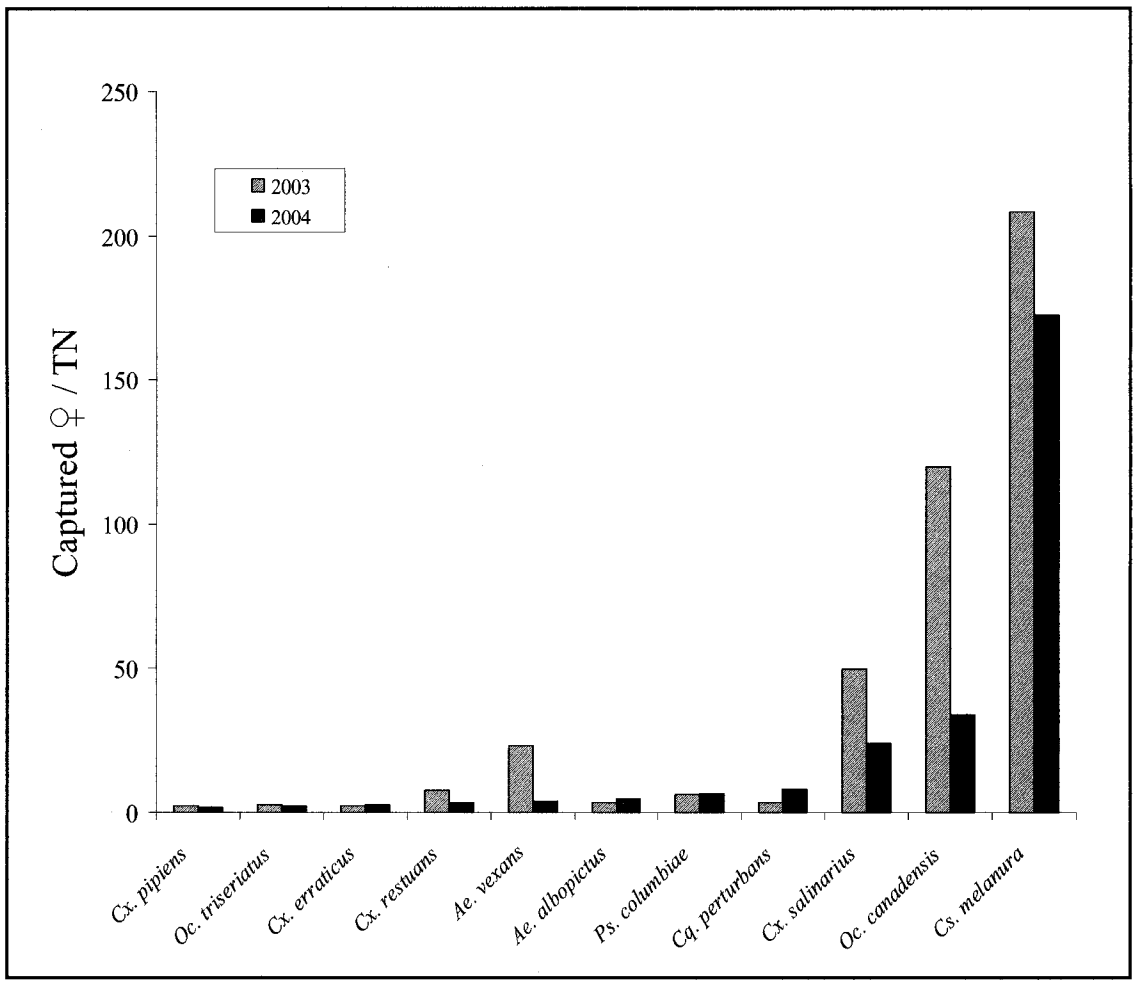

Figure 4. Numbers of captured females for modeled species for 2003 and 2004. Values represent captures/trap night (2003 = gray bars; 2004 = black). Results for a two-tailed *t*-test are provided in Table 8.

Land-cover/land Use Data

Results of the preliminary accuracy assessment of the USGS Land cover/use (NLCD) data ($K^{\Lambda} = 0.232$, overall accuracy = 28.84%) were well below the accepted standard ($K^{\Lambda} = 0.8$), and were largely due to the lack of mutual exclusion between land-cover and land-use classes (e.g., failure to distinguish between various forest types and light residential or natural and recreational grasses). For example, many sites classified as upland forest

were actually forested residential, and other sites classified as forested uplands were actually forested wetlands. In addition, a portion of the remaining error can be attributed to the added variation within land cover/use classes on a 5-state region compared to the spatial variation within the City of Chesapeake. The data were reclassified to a Level I classification scheme (Table 6) to reduce confusion among classes and then reassessed. The reclassification still produced results below the accepted standard ($K^{\Lambda} = 0.664$, overall accuracy = 76.28% [Table 9]), resulting in my decision to drop land cover/land use as an independent variable in the development of useful HSI models.

Table 9. Error matrix and accuracy summaries for the reclassified Level I scheme of the USGS: NLCD Level II land-cover/use dataset for the City of Chesapeake, Virginia (2002). Kappa statistic [K^{Λ}] is provided.

Classified	Class 1	Class 2	Class 4	Class 8	Class 9	Row total
Class 1	47	3	0	0	0	50
Class 2	0	272	22	9	0	303
Class 4	0	88	282	17	0	387
Class 8	0	51	42	133	0	226
Class 9	0	7	2	0	41	50
Col Total	47	421	348	158	41	1016

Producer's Accuracy	User's Accuracy
Class 1 = 100.00%	Class 1 = 94.00%
Class 2 = 64.61%	Class 2 = 89.77%
Class 4 = 81.03%	Class 4 = 72.87%
Class 8 = 83.65%	Class 8 = 58.85%
Class 9 = 100.00%	Class 9 = 82.00%

Overall Accuracy = 76.28%
K^ = 0.664

Multiple Regression Models

Maximum ranges for statistically significant spatial autocorrelation of independent variables (except NLCD data) ranged from 6,815m to 42,227m (Table 10). All ranges were well in excess of the maximum aggregation resolution (630m). As a result, I assumed that the 11 spatial scales for each independent variable (Table 5) are interdependent, and in turn justify the use of different spatial scales of representation among variables within the same HSI.

Table 10. Summary of semivariance analysis for the base spatial scale of each continuous independent variable. Scales (01x = 30x30m pixel resolution) are described in Tables 4 and 7. Range represents the distance (on the ground) beyond which data are not spatially autocorrelated. Error values are provided.

Variable	Maximum Range (m)	Mean^2 Error
HYDPC_01x	12,655	0.079
DRAIN_01x	7,537	0.036
RUNOF	9,331	0.058
WTDAJ_01x	12,510	0.015
AWS25_01x	6,815	0.027
TC1_01x	42,227	0.005
TC2_01x	26,679	0.004
TC3_01x	28,739	0.004

Multiple regression results for each species group are provided in Tables 11 through 15, and collectively summarized in Table 16. The number of independent variables used in the regression models, for all possible regression results, for each of the five species groups ranged from four (SWMP: swamp species) to seven (CONT: container species). The maximum variance inflation factor (VIF) any variable in any of the five regression models was 3.488 for DRAIN_17x in CSMN model. Consequently, I can assume that there was no multicollinearity among independent variables.

Results of regression model validation trials were consistent with the initial models. R^2-values (Appendix C) and root mean square errors (Appendix D) for validation trials were not dissimilar ($P>0.05$, $df = 14$) to those computed in all five initial group regression models. *P*-values for the validation trials are provided in Appendix E.

All five regression models suggested significant relationships ($P<0.05$) between captures of female mosquitoes and independent variables. However, the large number (50%) of negative relationships between captures and independent variables was unexpected (Tables 11-16). The species group with the lowest percentage of negative relationships was CSMN (40%), which is the target species of the CMCC. The group with the highest percentage was CONT (57%); the remaining three groups all had 50% negative. There were, however, several noteworthy patterns. Available water storage (AWS25) was negatively associated with abundance for all species groups except EPHM, where it was not a model factor. Similarly, Tasseled-Cap wetness (TC3) was negatively associated with predicted abundances of ALSP ($R = -0.357$), CONT ($R = -0.206$), and SWMP ($R = -0.261$), but positively associated with the abundance of the target species group CSMN ($R = 0.314$). TC3 was not a model factor for EPHM. Percent hydric soil

Table 11. Multiple regression results for the all species group. Reports for independent variables (described in Tables 4 and 7) include variance inflation factors (VIF > 5.0 suggests multicollinearity problems) and regression and correlation coefficients.

ANOVA

Source	*df*	SS	MS	*F*	*P*
Intercept	1	1.441	1.441	2.8832	0.0201
Model	6	0.655	0.109		
Error	39	1.476	0.038		
Total	45	2.130	0.047		

Root Mean^2 Error = 0.195

R^2 = 0.3073

Y-intercept = 0.485

Independent Variable	VIF	Coefficient	Partial *R*
TC3_07x	1.127	-0.383	-0.357
HYDSM_05x	1.283	0.209	0.308
DRAIN_01x	1.379	-0.224	-0.255
RUNOF_17x	1.248	0.155	0.159
AWS25_09x	1.501	-0.257	-0.191
WTDAJ_21x	1.526	0.059	0.034

Table 12. Multiple regression results for the container species group. Reports for independent variables (described in Tables 4 and 7) include variance inflation factors (VIF > 5.0 suggests multicollinearity problems) and regression and correlation coefficients.

ANOVA

Source	*df*	SS	MS	*F*	*P*
Intercept	1	9.469	9.469	7.8593	0.000007
Model	7	54.701	7.814		
Error	38	37.783	0.994		
Total	45	92.484	2.055		

Root Mean^2 Error = 0.997

R^2 = 0.5915

Y-intercept = 2.461

Independent Variable	VIF	Coefficient	Partial *R*
TC2_21x	1.569	0.068	0.004
TC3_01x	1.401	-1.368	-0.206
HYDSM_11x	1.273	0.008	0.181
HYDPC_11x	2.049	-0.616	-0.151
RUNOF_11x	1.273	-1.468	-0.306
AWS25_11x	1.969	-3.151	-0.379
WTDAJ_01x	1.304	4.978	0.664

Table 13. Multiple regression results for the swamp species group. Reports for independent variables (described in Tables 4 and 7) include variance inflation factors (VIF > 5.0 suggests multicollinearity problems) and regression and correlation coefficients.

ANOVA

Source	*df*	SS	MS	*F*	*P*
Intercept	1	0.898	0.898	2.6726	0.0453
Model	4	0.402	0.101		
Error	41	1.542	0.038		
Total	45	1.944	0.043		

Root Mean^2 Error = 0.194

R^2 = 0.2068

Y-intercept = 0.328

Independent Variable	VIF	Coefficient	Partial *R*
TC3_09x	1.041	-0.277	-0.261
HYDSM_03x	1.061	0.159	0.300
RUNOF_17x	1.055	0.087	0.095
AWS25_01x	1.049	-0.329	-0.301

Table 14. Multiple regression results for the ephemeral species group. Reports for independent variables (described in Tables 4 and 7) include variance inflation factors (VIF > 5.0 suggests multicollinearity problems) and regression and correlation coefficients.

ANOVA

Source	*df*	SS	MS	*F*	*P*
Intercept	1	0.466	0.466	7.7116	0.000017
Model	6	1.160	0.193		
Error	39	0.978	0.025		
Total	45	2.138	0.048		

Root Mean^2 Error = 0.158

R^2 = 0.5426

Y-intercept = -1.884

Independent Variable	VIF	Coefficient	Partial *R*
TC1_17x	1.227	2.160	0.674
TC2_21x	2.167	0.583	0.564
HYDSM_03x	1.087	-0.051	-0.124
DRAIN_05x	1.941	-0.268	-0.268
RUNOF_19x	1.348	0.171	0.203
WTDAJ_01x	1.114	-0.168	-0.198

Table 15. Multiple regression results for *Cs. melanura*. Reports for independent variables (described in Tables 4 and 7) include variance inflation factors (VIF > 5.0 suggests multicollinearity problems) and regression and correlation coefficients.

ANOVA

Source	*df*	SS	MS	*F*	*P*
Intercept	1	1.159	1.159	5.2537	0.000842
Model	5	0.817	0.163		
Error	40	1.244	0.031		
Total	45	2.061	0.046		

Root Mean^2 Error = 0.176

R^2 = 0.3964

Y-intercept = -0.460

Independent Variable	VIF	Coefficient	Partial *R*
TC2_21x	2.851	-0.254	-0.224
TC3_21x	1.228	0.271	0.314
DRAIN_17x	3.488	0.970	0.513
RUNOF_17x	1.379	0.010	0.107
AWS25_07x	2.061	-0.446	-0.295

Table 16. Summary of results for multiple regression models for each of the five species groups (Tables 11-15) defined in Table 1. Positive (+) and negative (-) relationships and variable scale (e.g., 9x [Table 5]) are indicated. Partial R values > 0.250 but < 0.499 are underlined, and partial R values > 0.500 are double-underlined.

Variable(*)	ALSP	CONT	SWMP	EPHM	CSMN
AWS25	9x (-)	11x (-)	21x (-)		7x (-)
DRAIN	1x (-)			5x (-)	17x (+)
HYDPC		11x (-)			
HYDSM	5x (+)	11x (+)	3x (+)	3x (-)	
RUNOF	17x (+)	11x (-)	17x (+)	19x (+)	17x (+)
TC1				17x (+)	
TC2		21x (+)		21x (+)	21x (-)
TC3	7x (-)	1x (-)	9x (-)		21x (+)
WTDAJ	21x (+)	1x (+)		1x (-)	

*Defined in Tables 4 and 7.

(HYDPC) was unexpectedly a poor predictor of mosquito abundance and was only a factor in the CONT (R = -0.151) species group, where it was negatively associated. Soil runoff potential (RUNOF) was positively related to predicted mosquito abundance in all species groups except CONT (R = -0.306). Tasseled-Cap brightness (TC1) was a poor predictor of mosquito abundance for all species groups except EPHM, where it was the best predictor (R = 0.674). Most unexpected were the negative relationships between predicted abundance of EPHM and [inversely ranked] soil drainage (DRAIN; R = -0.268)

and water table depth (WTDAJ; R = -0.198), and the negative relationship between CSMN and Tasseled-Cap greenness (TC2; R = -0.224). TC2 was positively related with CONT (R = 0.004) and EPHM (R = 0.564) abundance.

Only CSMN responded relatively consistently with regard to spatial scale; all predictor variables for this group but AWS (210m aggregate resolution [7x, Table 5]) were most reliable at the largest scale used (21x). Spatial scales of predictors for EPHM were large for positive relationships (RUNOF = 19x, TC1 = 17x, TC2 = 21x) and smaller for negative relationships (DRAIN = 5x, HYDSUM = 3x, WTDAJ = 1x). A similar, but not as consistent pattern, was seen for ALSP. Patterns in spatial scale of predictors were not evident for CONT and SWMP species groups (Table 16). Additional spatial-scale relationships will be reviewed in the discussion of these results.

Habitat Suitability Maps

Habitat suitability maps for each of the five species group regression models are presented (Figures 5-9), showing the most suitable areas (80-100%) in red. These maps are the results of an overlay operation of weighted raster values using the regression equation. Wetland type importance (WTI) values resulting from the extraction and overlay of wetland class data from NWI maps onto habitat suitability maps suggest that upland habitat had the highest WTIs for CONT, EPHM, and SWMP groups. WTIs for ALSP were highest for estuarine wetlands, and WTIs for CSMN were highest for palustrine wetlands (Table 17). However, the corresponding maps (Figures 10–19) suggest that upland/wetland ecotones are hot spots of mosquito abundance. This pattern was most evident when an additional overlay of drainage ditches (ArcView shapefile

format) is added. Nearly all upland habitat predicted to be most suitable for CSMN (Figures 18 and 19), EPHM (Figures 16 and 17), and SWMP (Figures 14 and 15) was within a ditched network. The CONT group was predicted to be most abundant in uplands bordering permanent water bodies (Figures 12 and 13); and ALSP group abundance was primarily associated with permanent water bodies, and, to a lesser extent, ditches (Figures 10 and 11).

Table 17. Summary of areal extent of the five System-Level National Wetland Inventory wetland classes for the City of Chesapeake. Also provided are the areal extents (in 30m x 30m pixels) and wetland type importance values (WTIs) for these classes for the most suitable habitat (80-100%) for each of the five species group (described in Tables 4 and 7) regression models. The wetland class with the highest WTI for each species group is underlined.

	Upland	Palustrine	Riverine	Estuarine	Lacustrine
Pixels					
NWI Chesapeake	531,483	211,135	5,438	21,543	1,753
ALSP	5,428	2,232	1,603	8,801	1,112
CONT	12,840	225	7	346	0
SWMP	8,445	1,127	263	598	164
EPHM	9,484	130	59	0	0
CSMN	57,034	66,788	250	705	8
WTI					
ALSP	0.102	0.042	0.030	<u>0.166</u>	0.021
CONT	<u>0.242</u>	0.004	< 0.001	0.007	0
SWMP	<u>0.159</u>	0.021	0.005	0.011	0.003
EPHM	<u>0.178</u>	0.002	0.001	0	0
CSMN	1.073	<u>1.257</u>	0.005	0.013	< 0.001

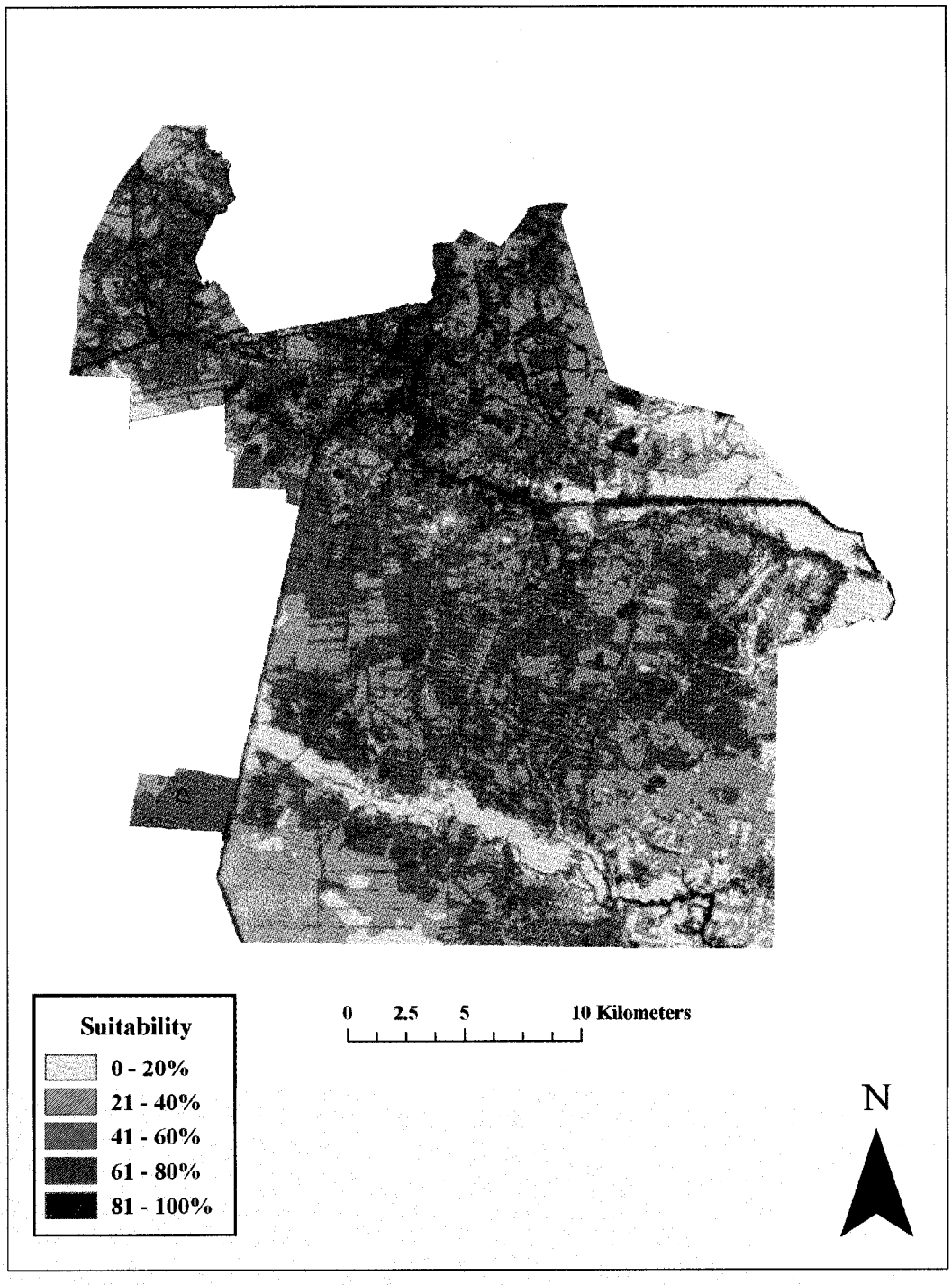

Figure 5. Habitat suitability map for the all species (ALSP) group based on multiple regression results. Areas with the highest degree of suitability (81 – 100%, using equal-interval breaks) are indicated in red.

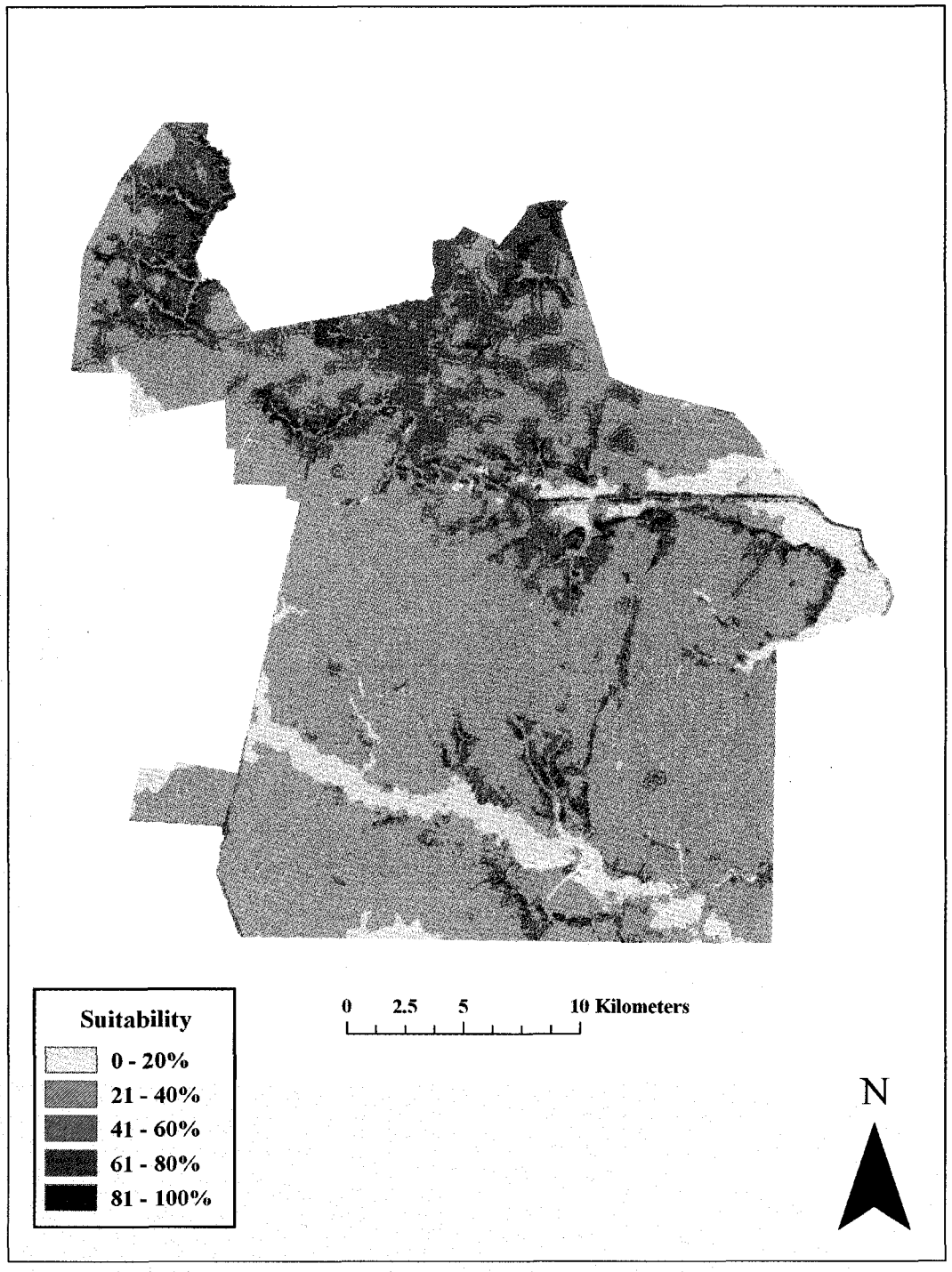

Figure 6. Habitat suitability map for container (CONT) species group based on multiple regression (equation) results. Areas with the highest degree of suitability (81 – 100%, using equal-interval breaks) are indicated in red.

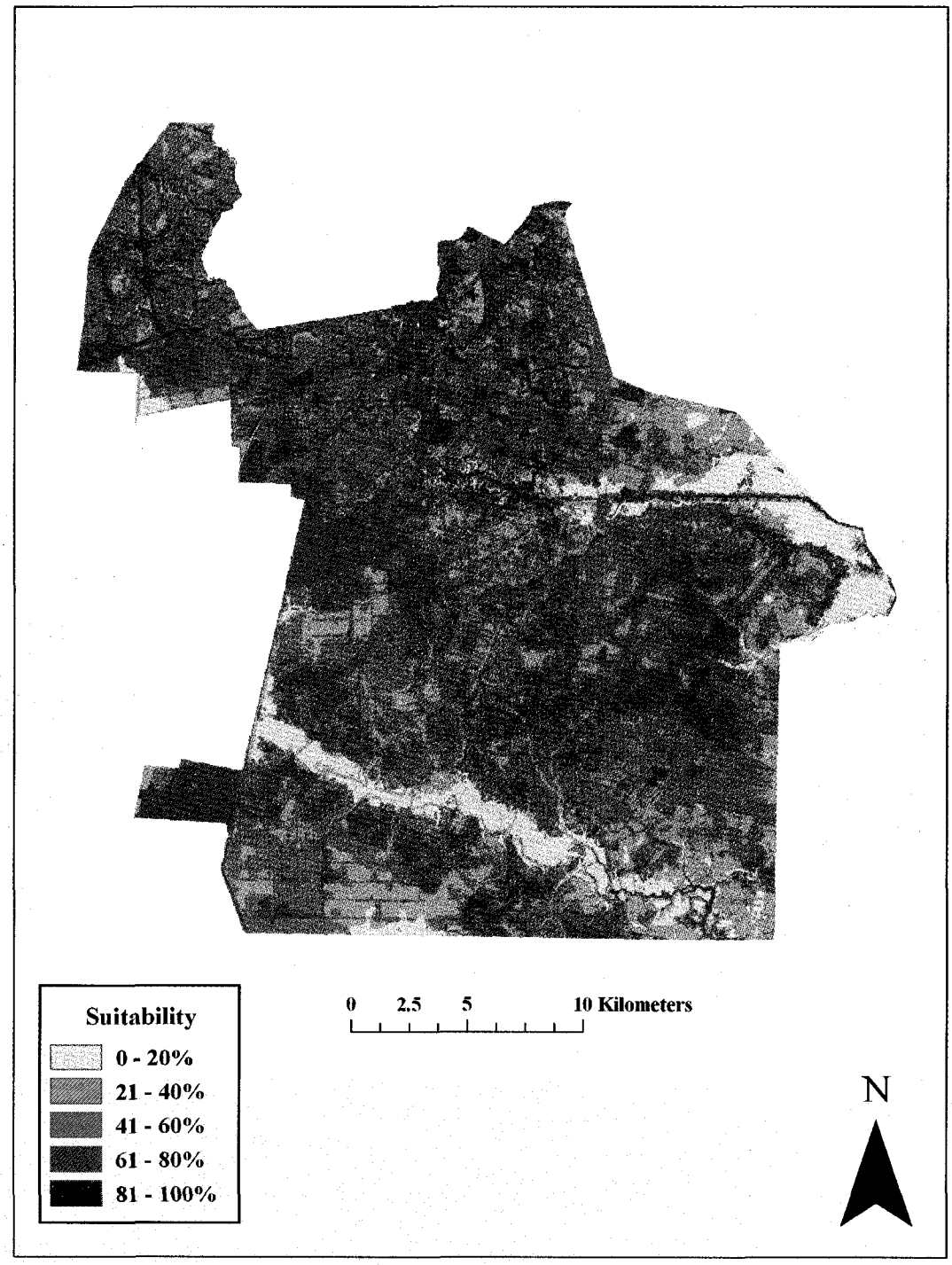

Figure 7. Habitat suitability map for swamp (SWMP) species group based on multiple regression (equation) results. Areas with the highest degree of suitability (81 – 100%, using equal-interval breaks) are indicated in red.

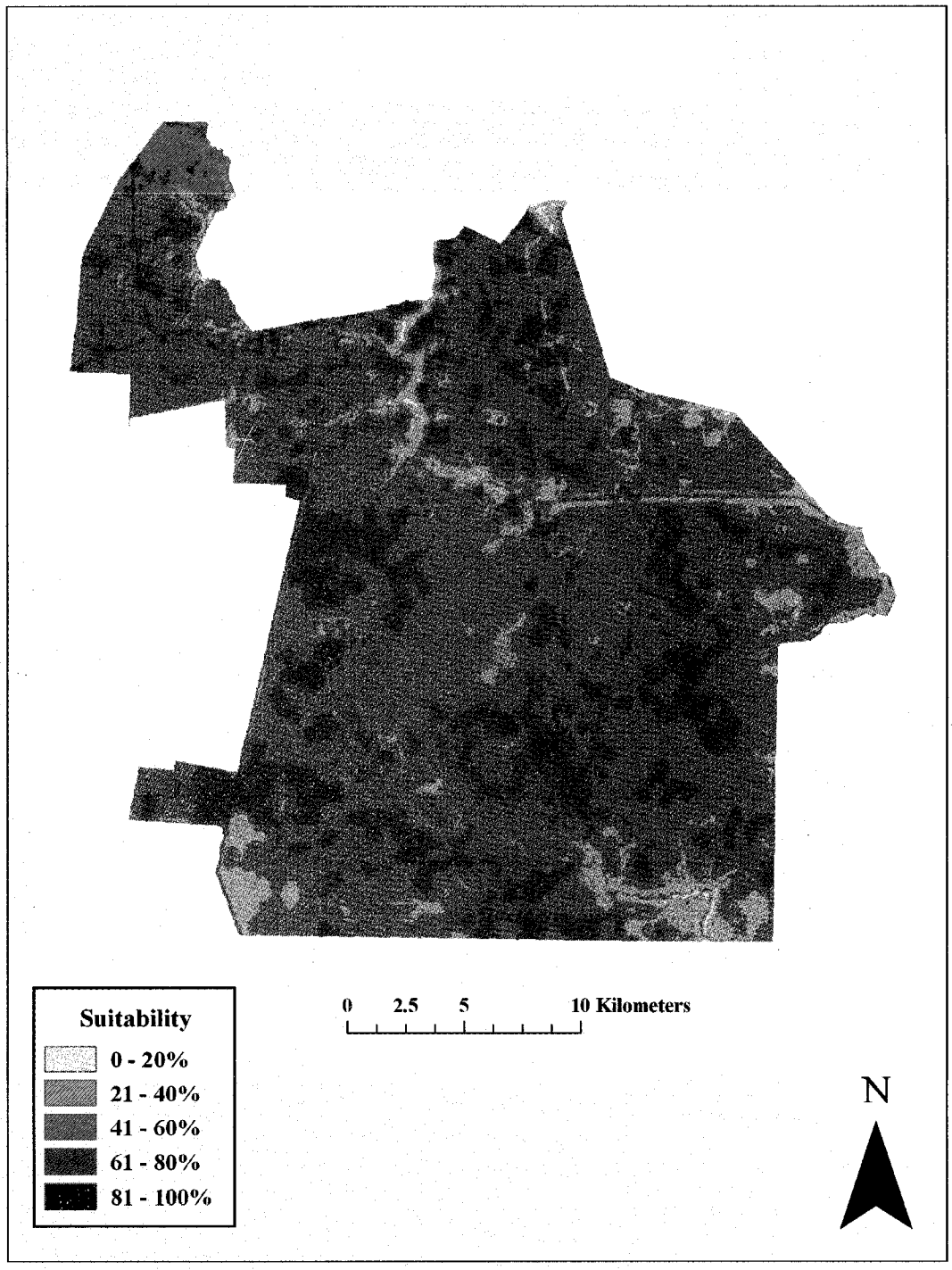

Figure 8. Habitat suitability map for ephemeral (EPHM) species group based on multiple regression (equation) results. Areas with the highest degree of suitability (81 – 100%, using equal-interval breaks) are indicated in red.

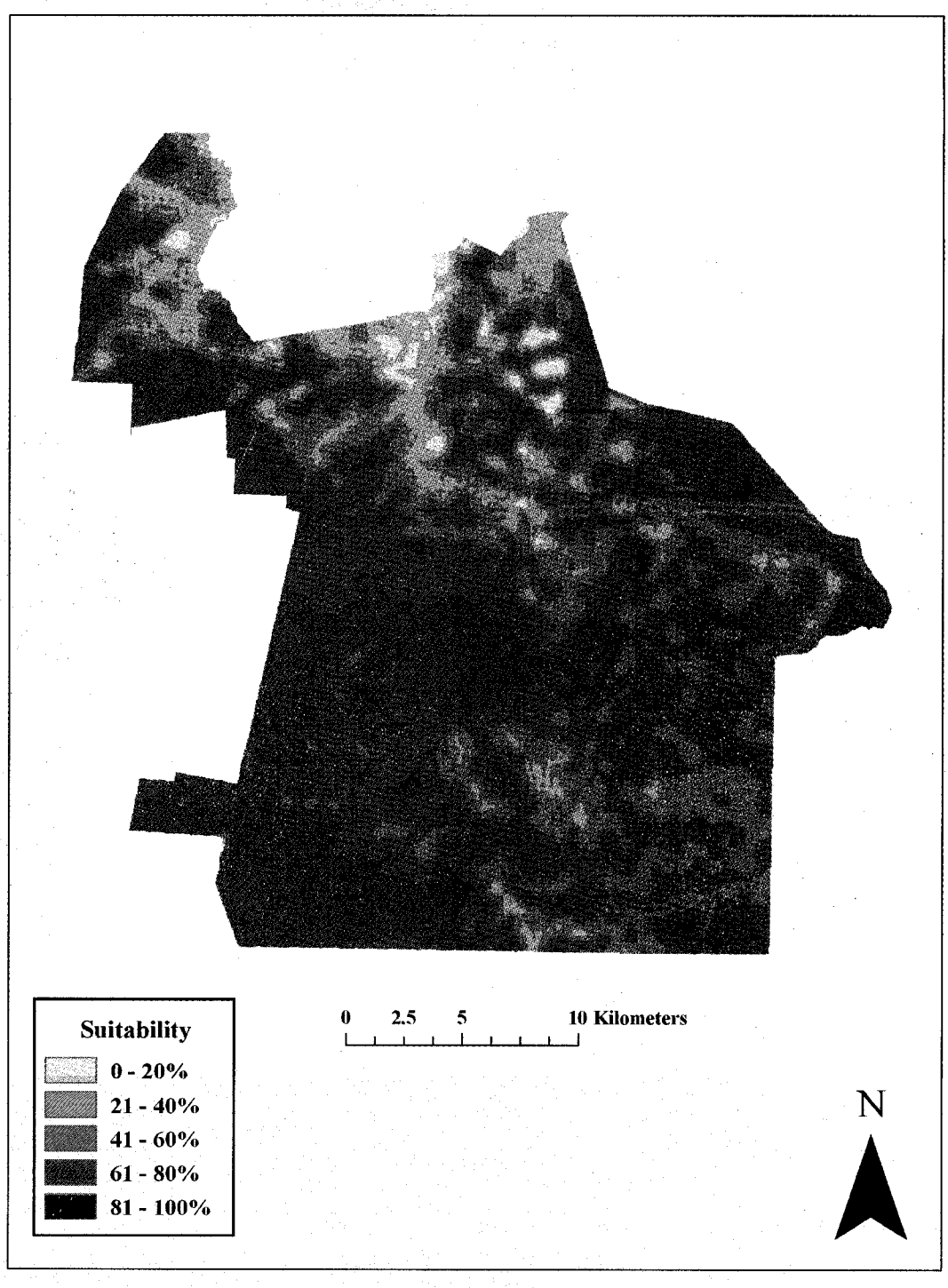

Figure 9. Habitat suitability map for *Cs. melanura* based on multiple regression (equation) results. Areas with the highest degree of suitability (81 – 100%, using equal-interval breaks) are indicated in red.

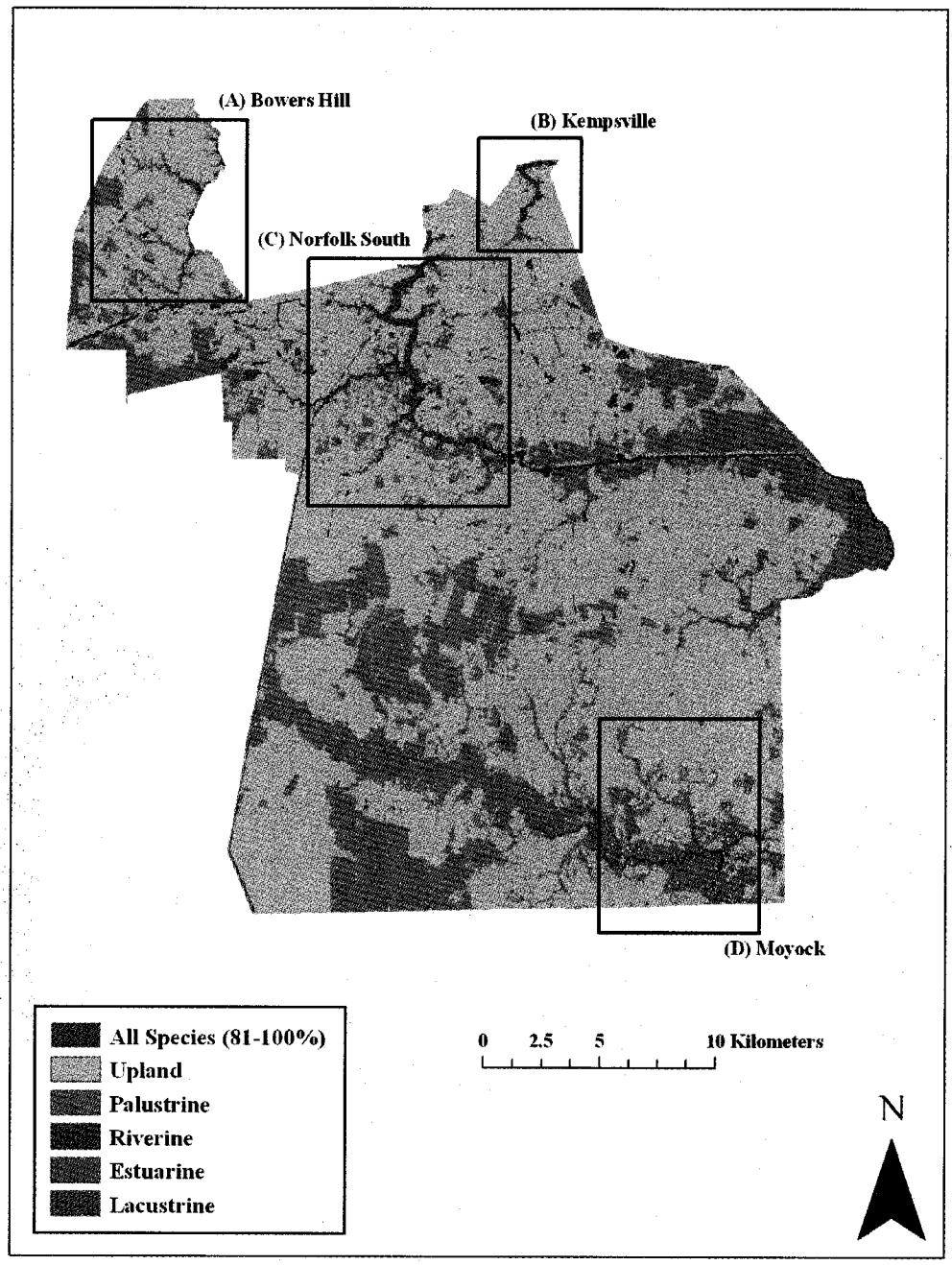

Figure 10. Visual overlay of the most suitable habitat (80-100%, red polygons) for the all species group and the System-Level NWI map for the City of Chesapeake, Virginia. Names of boxes A-D correspond to the nomenclature of the National Wetland Inventory Map subsection in which each is primarily located in; these boxes are represented at smaller scales (increased detail) in Figure 11.

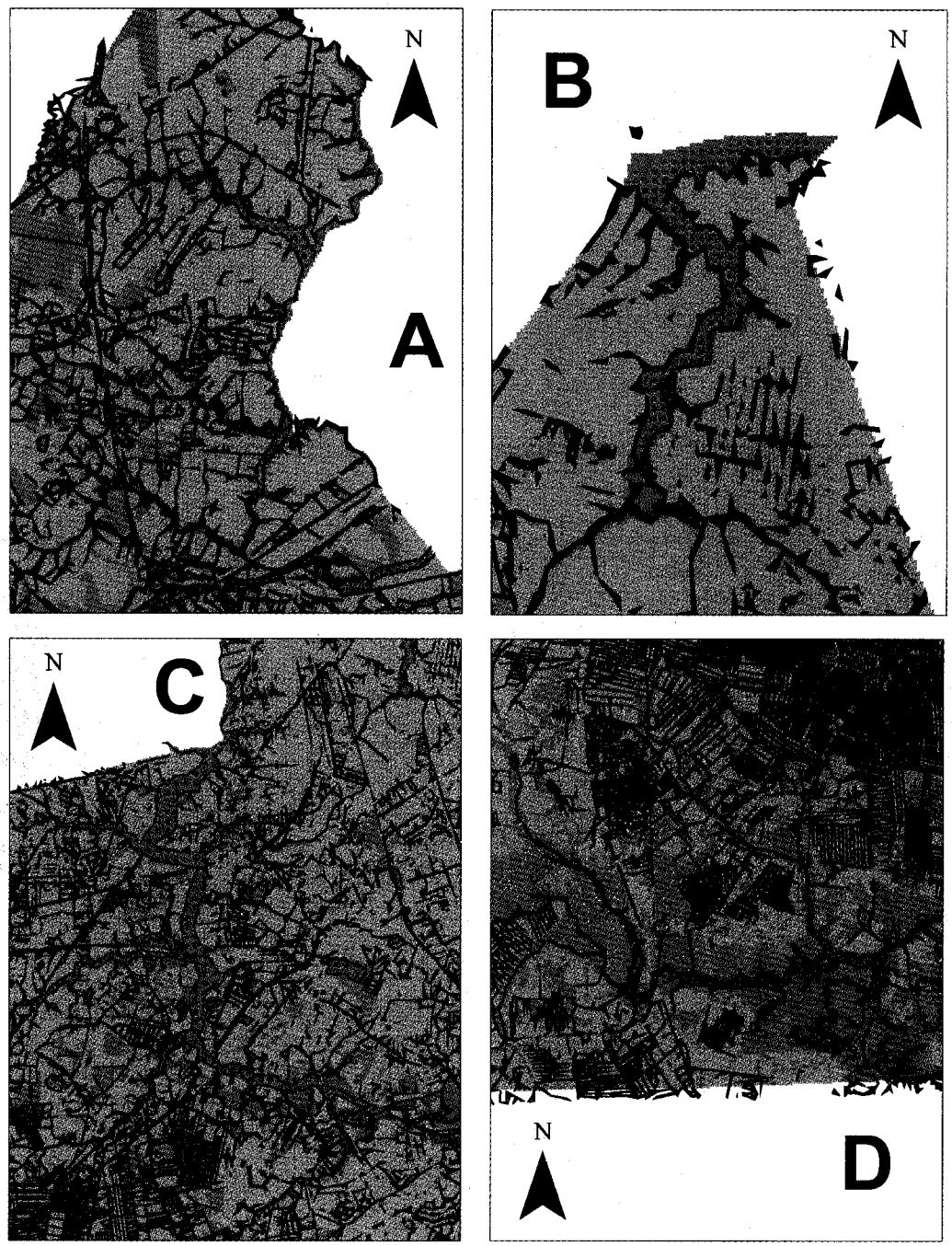

Figure 11. Representative sections of the overlay of National Wetland Inventory maps and the habitat suitability index for the all species group. Sections (boxes A-D, Figure 10) showing high levels of suitability (80-100%; red stippling) in relation to System-Level wetland classes described in Figure 10 and drainage ditches (in black). Scales are relative to the box sizes in Figure 10.

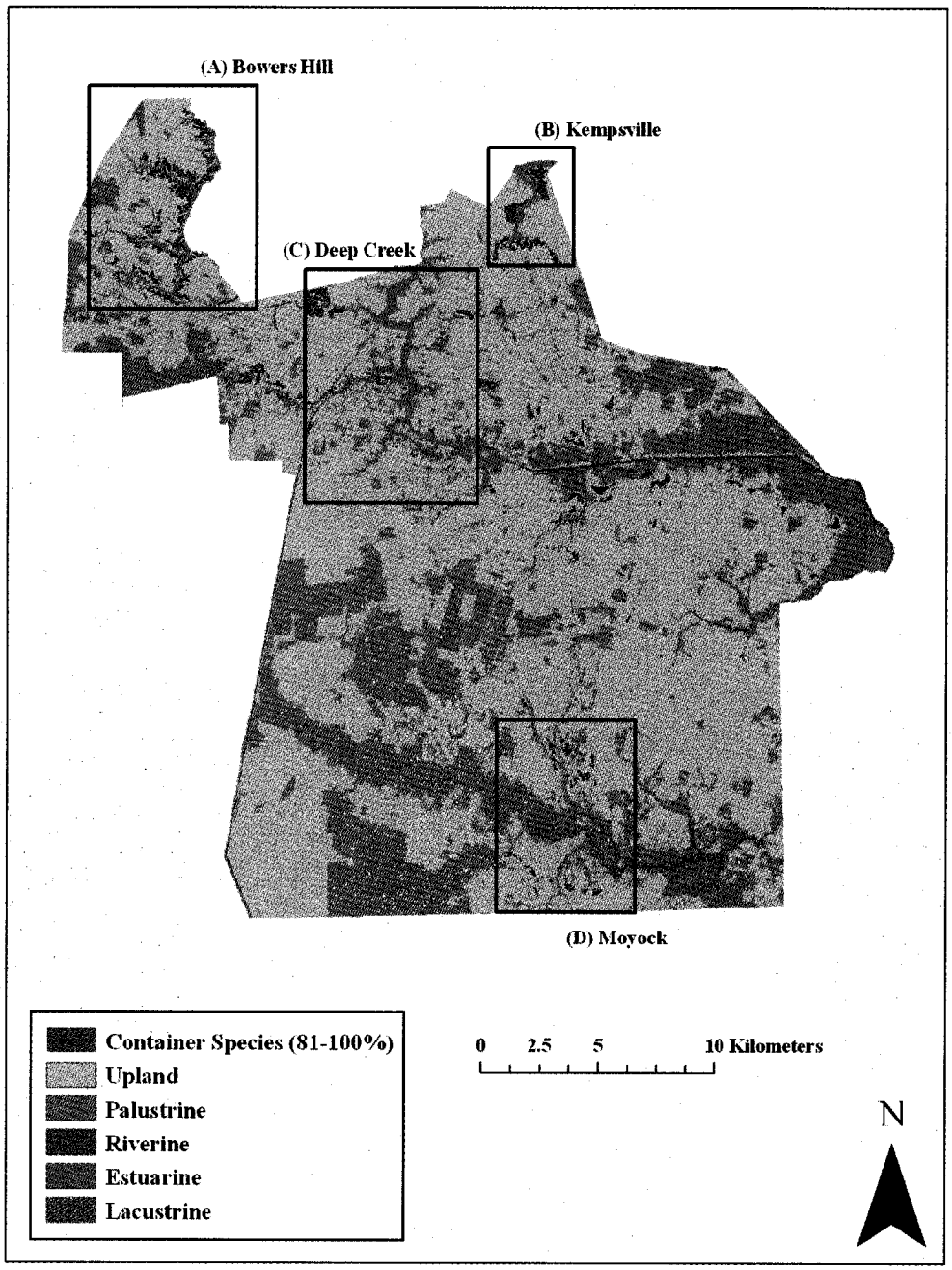

Figure 12. Visual overlay of the most suitable habitat (80-100%, red polygons) for the CONT group and the System-Level NWI map for the City of Chesapeake, Virginia. Names of boxes A-D correspond to the nomenclature of the National Wetland Inventory Map subsection in which each is primarily located in; these boxes are represented at smaller scales (increased detail) in Figure 13.

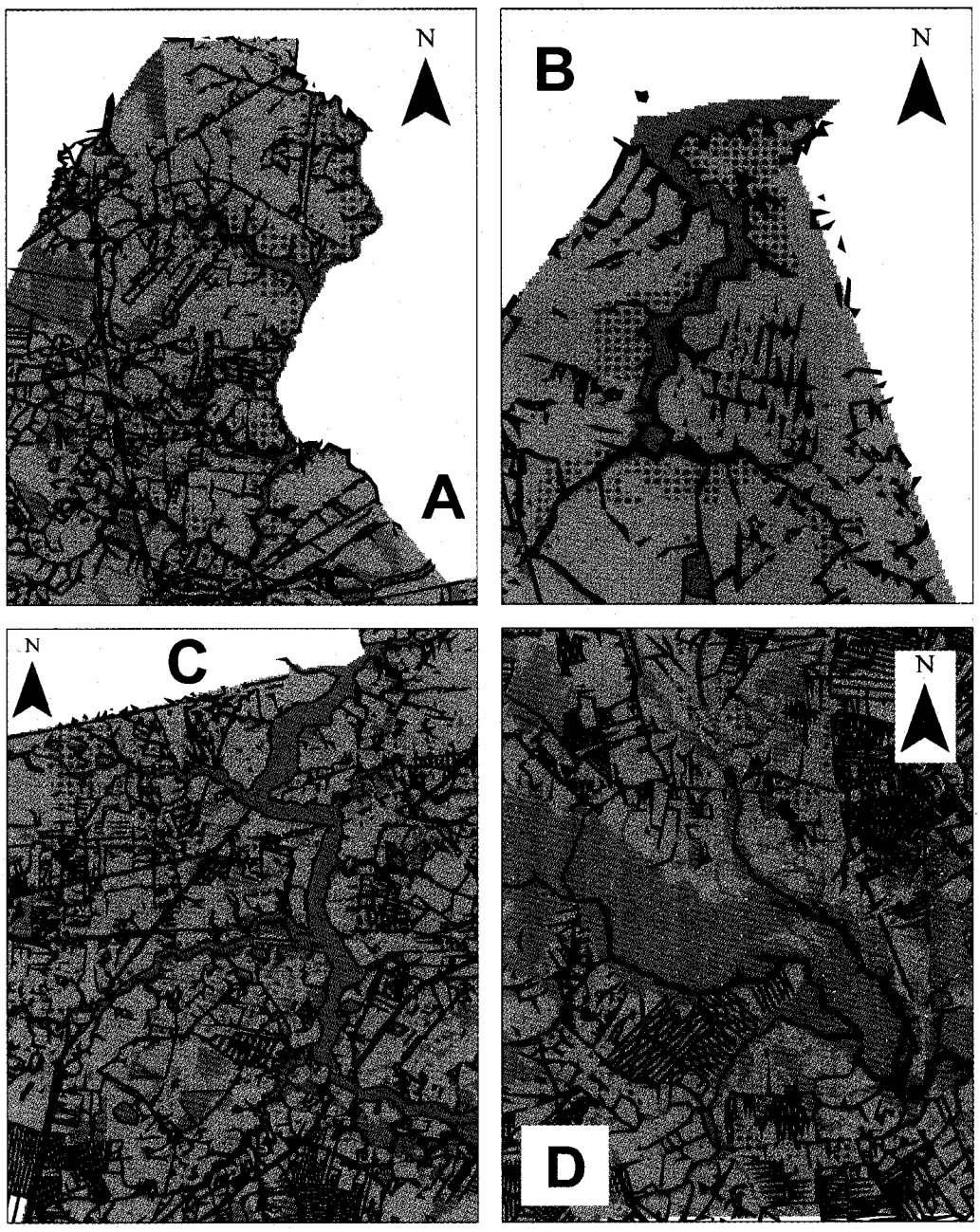

Figure 13. Representative sections of the overlay of National Wetland Inventory maps and the habitat suitability index for the container species group. Sections (boxes A-D, Figure 12) showing high levels of suitability (80-100%; red stippling) in relation to System-Level wetland classes described in Figure 12 and drainage ditches (in black). Scales are relative to the box sizes in Figure 12.

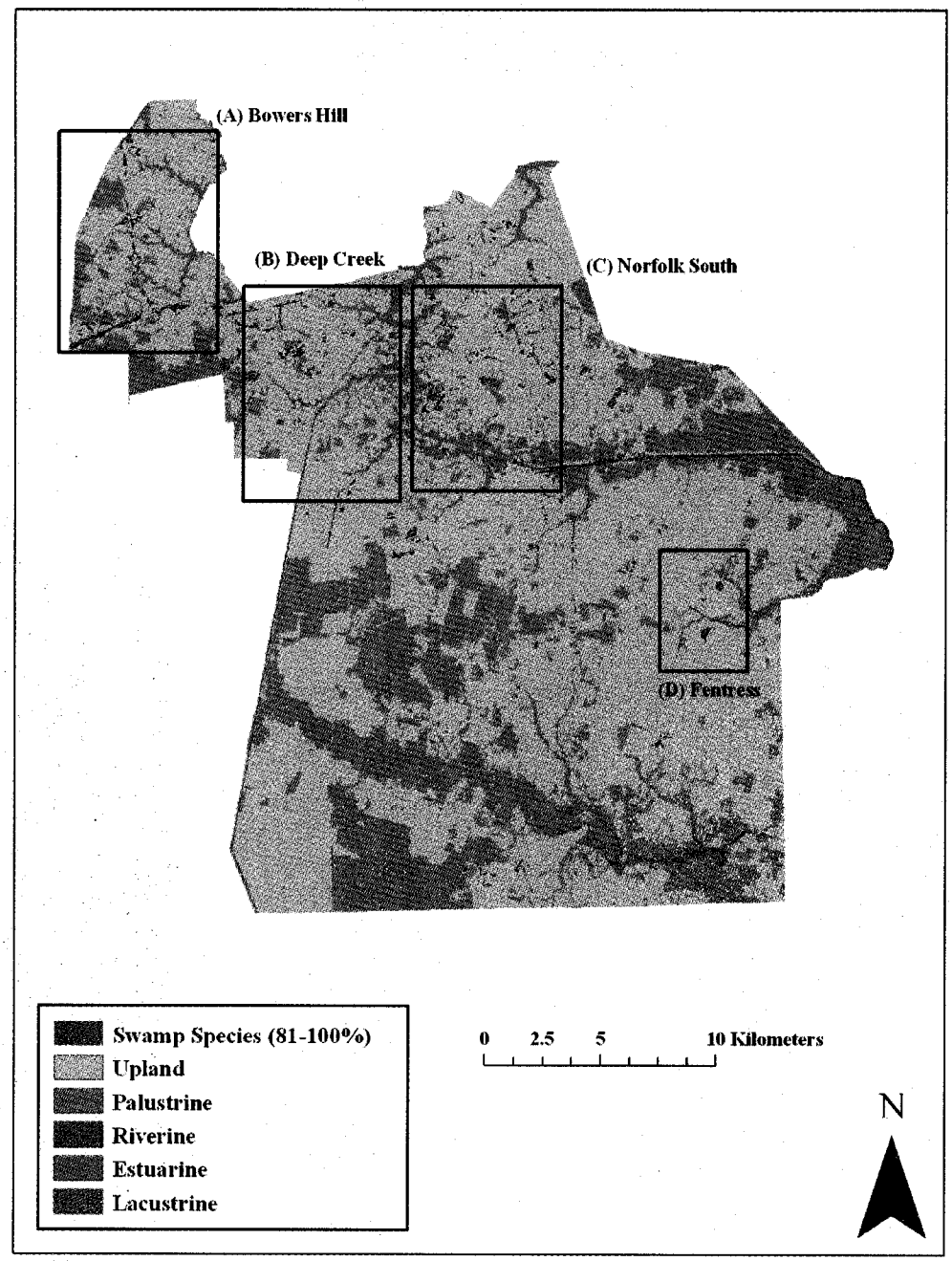

Figure 14. Visual overlay of the most suitable habitat (80-100%, red polygons) for the SWMP group and the System-Level NWI map for the City of Chesapeake, Virginia. Names of boxes A-D correspond to the nomenclature of the National Wetland Inventory Map subsection in which each is primarily located in; these boxes are represented at smaller scales (increased detail) in Figure 15.

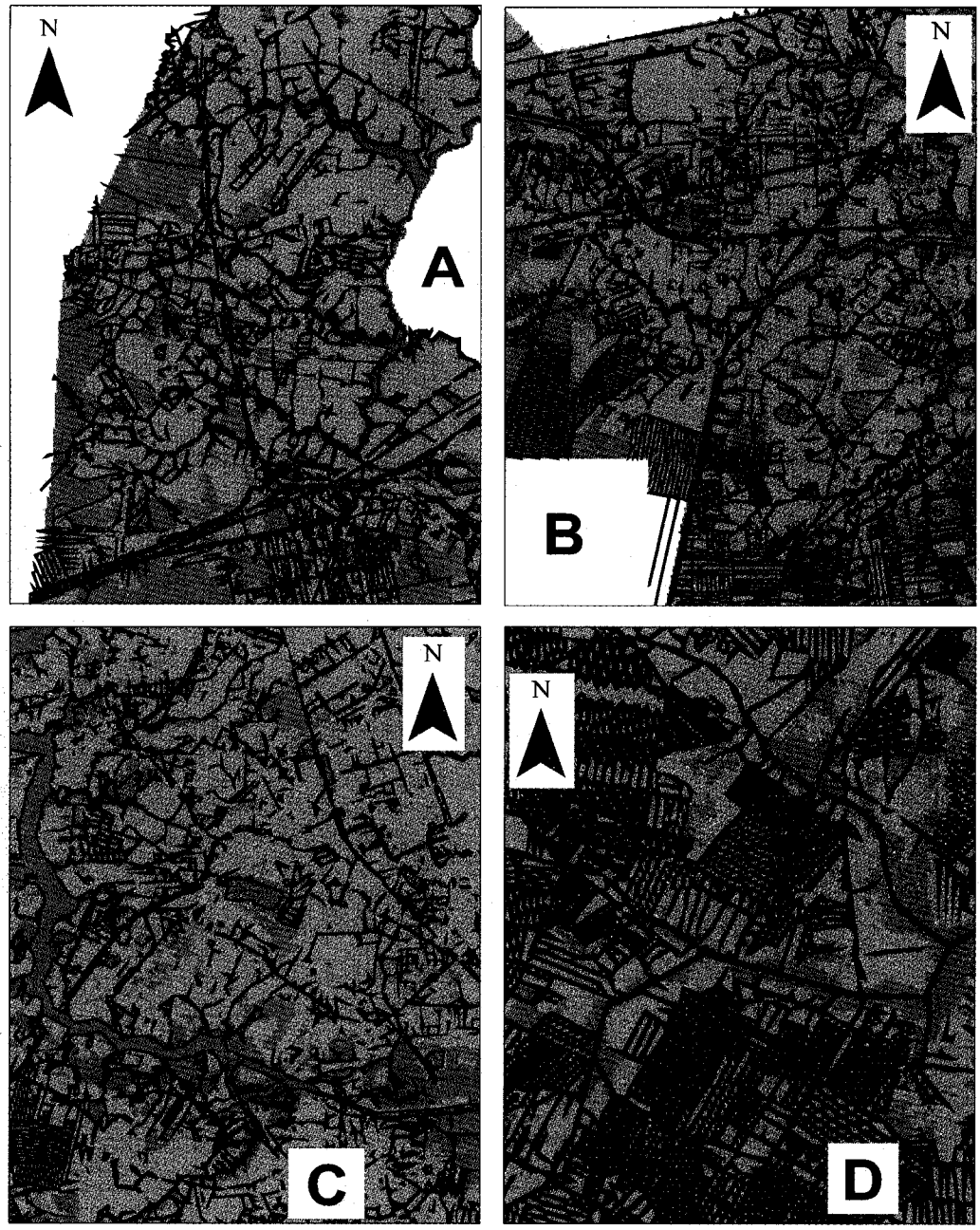

Figure 15. Representative sections of the overlay of National Wetland Inventory maps and the habitat suitability index for the swampl species group. Sections (boxes A-D, Figure 14) showing high levels of suitability (80-100%; red stippling) in relation to System-Level wetland classes described in Figure 14 and drainage ditches (in black). Scales are relative to the box sizes in Figure 14.

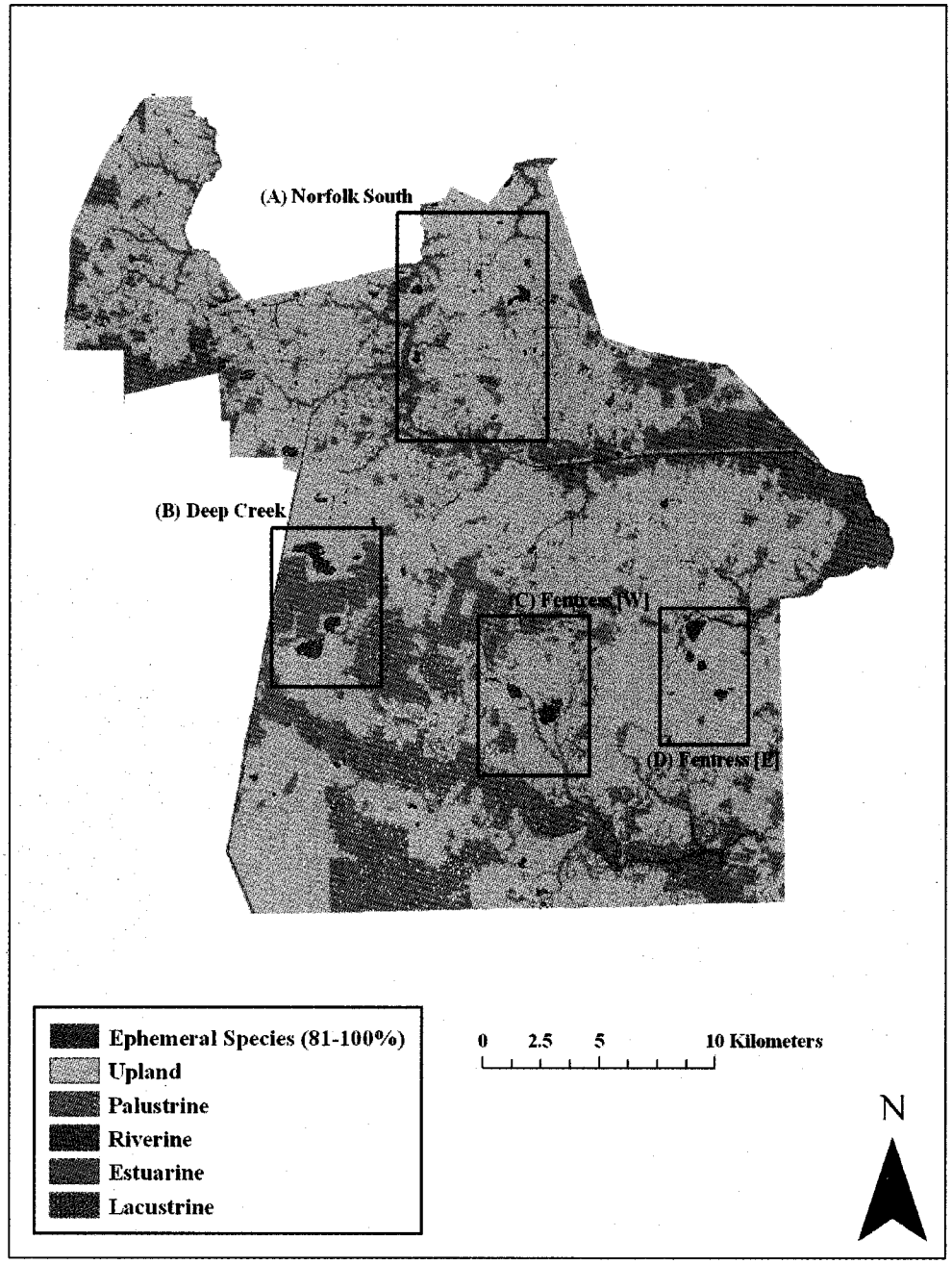

Figure 16. Visual overlay of the most suitable habitat (80-100%, red polygons) for the EPHM group and the System-Level NWI map for the City of Chesapeake, Virginia. Names of boxes A-D correspond to the nomenclature of the National Wetland Inventory Map subsection in which each is primarily located in; these boxes are represented at smaller scales (increased detail) in Figure 17.

Figure 17. Representative sections of the overlay of National Wetland Inventory maps and the habitat suitability index for the ephemeral species group. Sections (boxes A-D, Figure 16) showing high levels of suitability (80-100%; red stippling) in relation to System-Level wetland classes described in Figure 16 and drainage ditches (in black). Scales are relative to the box sizes in Figure 16.

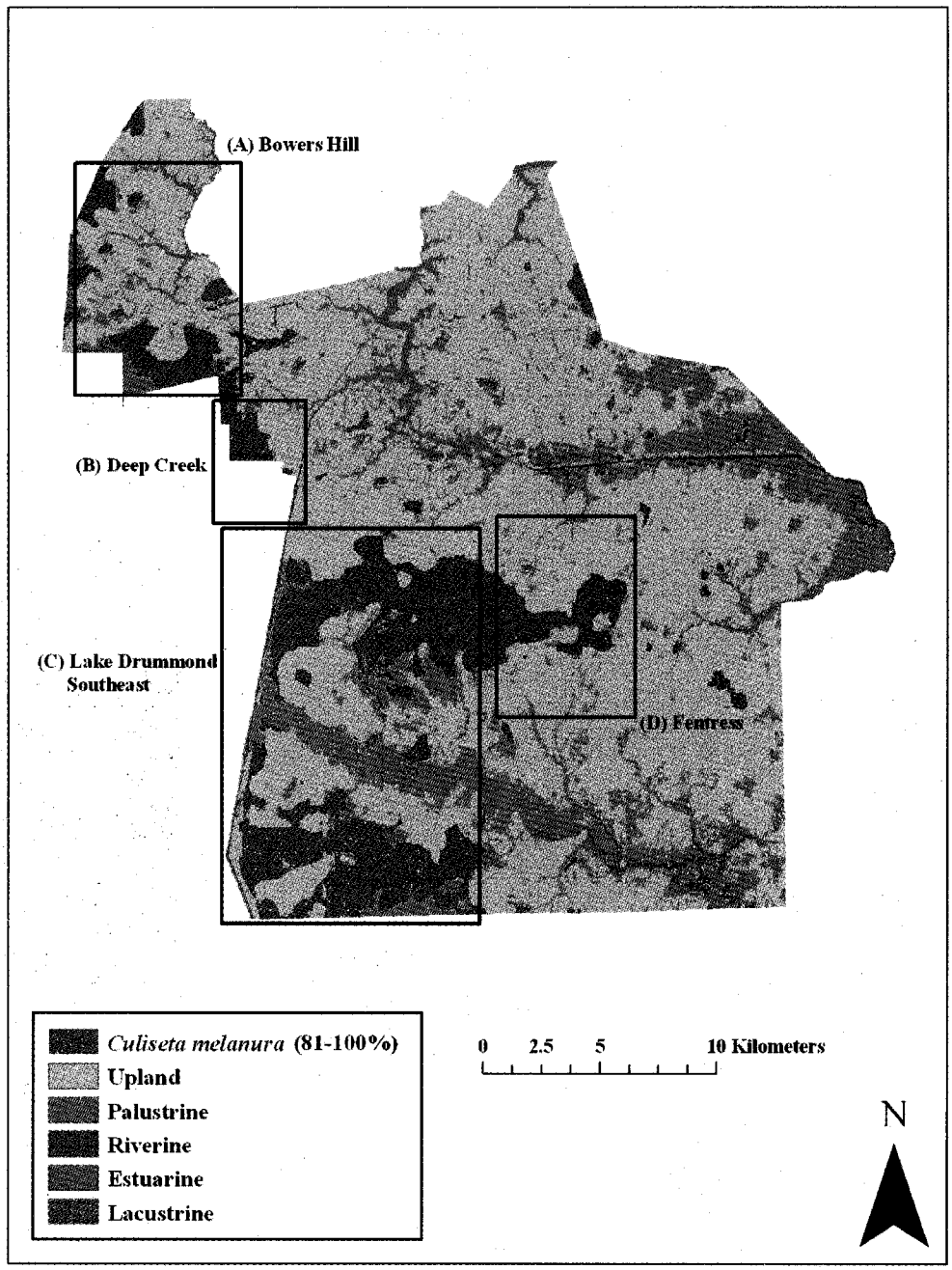

Figure 18. Visual overlay of the most suitable habitat (80-100%, red polygons) for the CSMN group and the System-Level NWI map for the City of Chesapeake, Virginia. Names of boxes A-D correspond to the nomenclature of the National Wetland Inventory Map subsection in which each is primarily located in; these boxes are represented at smaller scales (increased detail) in Figure 19.

Figure 19. Representative sections of the overlay of National Wetland Inventory maps and the habitat suitability index for *Cs. melanura*p. Sections (boxes A-D, Figure 18) showing high levels of suitability (80-100%; red stippling) in relation to System-Level wetland classes described in Figure 18 and drainage ditches (in black). Scales are relative to the box sizes in Figure 18.

Variation in WTIs based on species group predicted abundance among the five NWI wetland types was explained nearly completely (99.8%) by the first two Bray-Curtis polar ordination axes (Axis 1 = 97.7%, Axis 2 = 2.1%). Endpoints for Axis 1 were CSMN and a cluster of the other four species groups (Figure 20 A-E). Endpoints for Axis 2 were CSMN and ALSP. It is important to remember that negative correlation coefficients in Bray-Curtis ordination indicate only the direction of a dissimilarity gradient along the ordination axis, and not negative relationships. Variation among species groups dissimilarities for Axis 1 largely explained the predicted abundance of CSMN for palustrine (r = -0.998) and upland habitats (r = -0.996), and to a lesser degree, ALSP in estuarine habitat (r = 0.239; Figure 20). A much smaller proportion of the variation in WTIs based on species group predicted abundance among the five NWI wetland types was explained by Axis 2 (2.1%). Endpoints for Axis 2 were CSMN and CONT (Figure 20 A-E). Ordination scores for both axes were driven primarily by the results for CSMN.

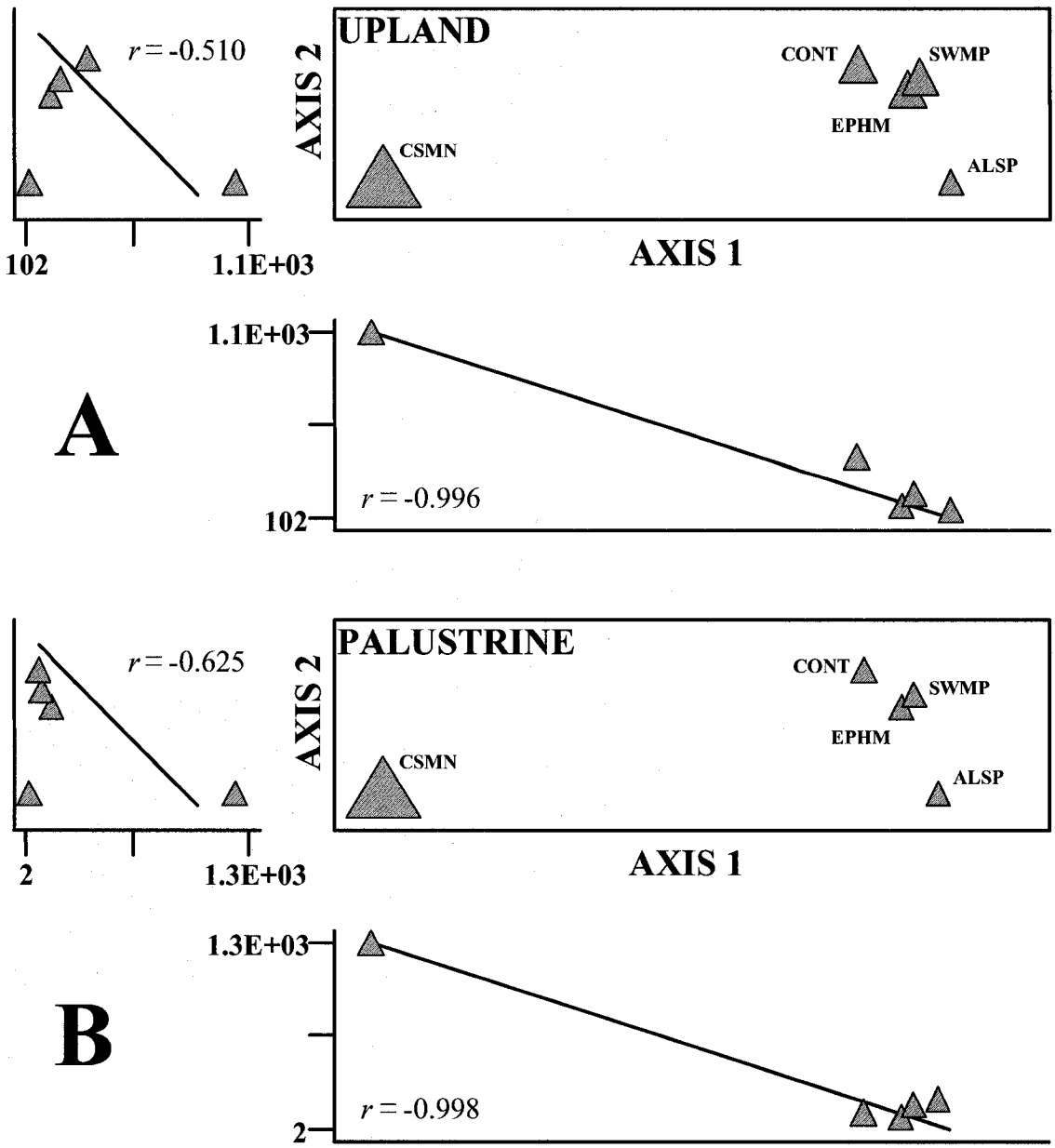

Figure 20. Bray-Curtis Polar ordination plots of the five wetland types based on wetland-type importance values for species groups. Distances between species groups along an axis reflect potential differences among species group abundances for that National Wetland Inventory wetland type (A-E). Included are graphic overlays of WTI values on ordination diagram points. The size of the triangles (representing species groups) indicates potential wetland affinities for each species group as described by that axis. Scatterplots quantify the relationships (Pearson's correlation coefficients [r]) between species groups and the explained variance of each axis with regard to each wetland type.

Figure 20. Continued

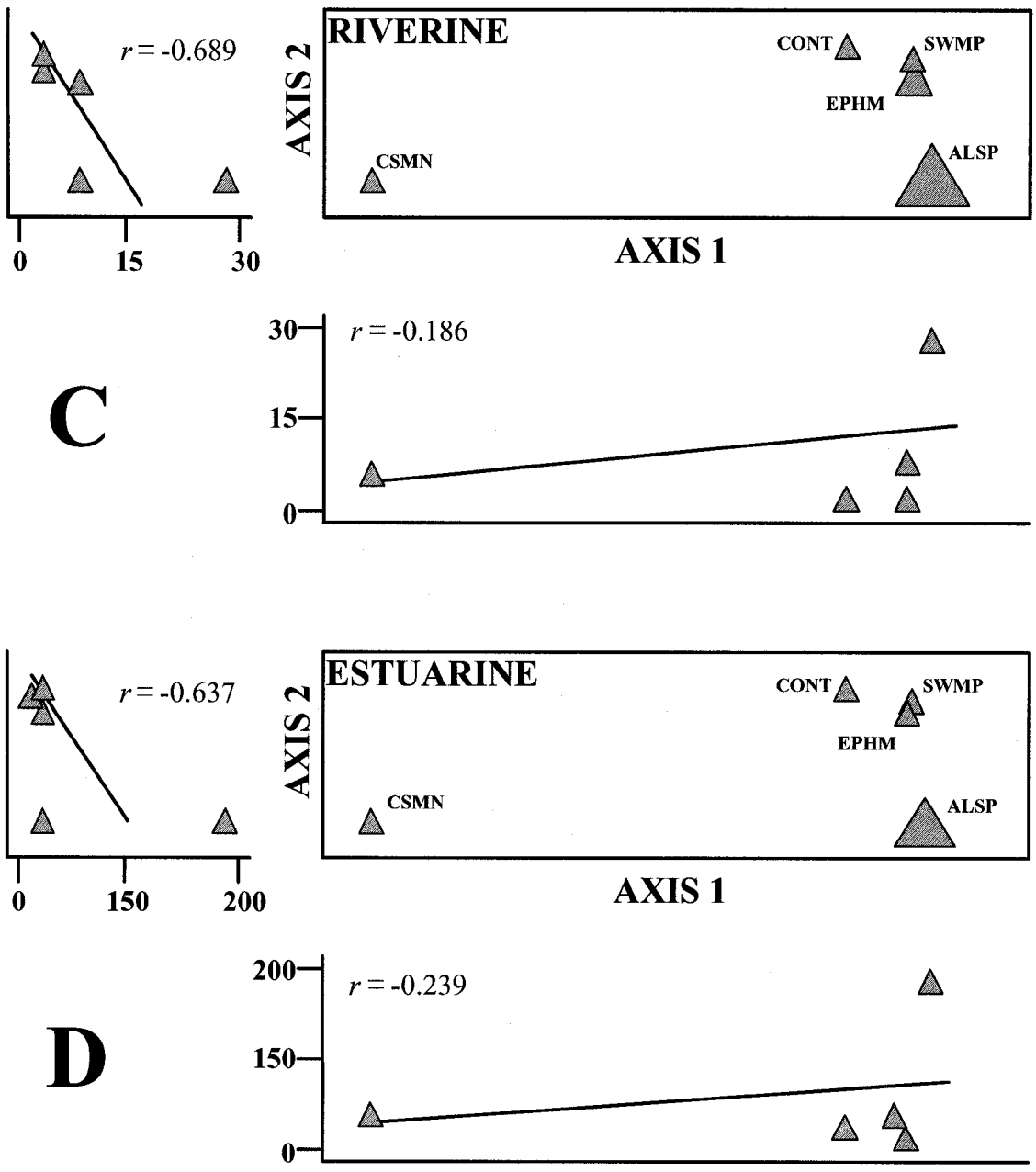

Figure 20. Continued

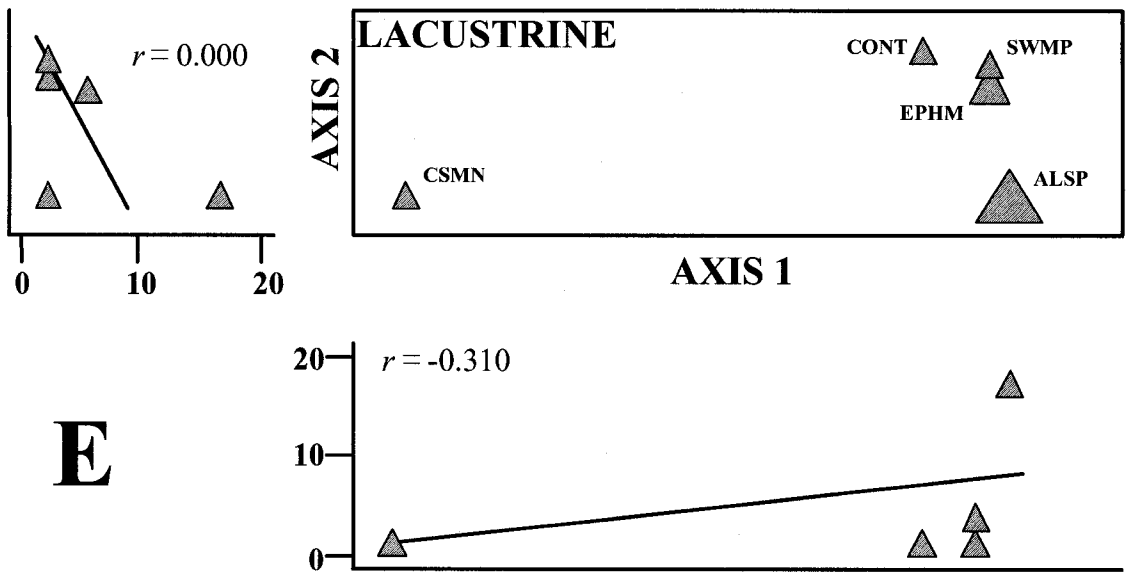

Discussion

The models in this study were designed to predict adult mosquito abundance based on environmental factors associated with larval habitat (i.e., soil condition, vegetative vigor, permanent bodies of water). Predicting mosquito emergence using adult capture data is not unprecedented. Shaman et al. (2002) used captures of adults from New Jersey light traps in conjunction with soil moisture indices to successfully predict mass emergence of adults from modeled larval habitats. As with my study, Shaman et al. experienced both positive and negative relationships between mosquito captures and environmental factors that were expected to have only positive effects on predicted abundance. They concluded that these counterintuitive results were a function of variations in the biology of each species. They also suggested that larval monitoring data, which they did not have, might have enhanced the predictive power of their models. However, due to the recent isolation

of WNV in North America (1999), many mosquito control and surveillance programs have only recently begun to collect larval data. For example, the CMCC, the source of capture data for my study, is currently developing a larval monitoring program (personal communication with Melissa Cushing, CMCC [January 2006]). Thus, a dataset for larval captures was not available.

One factor not addressed by Shaman et al. (2002) was the flight, or dispersal, distance of adult mosquitoes from their natal habitat. This would likely have an effect on adult abundance models that use larval habitat attributes. For the species modeled in my study, distances traveled from larval habitats to capture sites were unknown; however, the literature suggests these distances vary from a few hundred meters to several kilometers depending on the species (Table 2).

Many studies have examined the spatial distributions of dispersing cohorts of flying insect populations (Rogers, 1977; Botterweg, 1982; Zumr, 1992; Zolubas and Byers, 1995; Duelli et al., 1997; Liew and Curtis, 2004). Most of these studies suggest that without external effects, such as wind speed and direction, numbers of individuals captured are inversely proportional to the distance from the initial source. Therefore, I assumed that any single adult female captured at any given trapping site was likely to be much closer to where it emerged than its maximum dispersal potential. Dispersal potential of adult mosquitoes was, in part, my justification for using a broad range of spatial scales to predict mosquito abundance.

Some mosquito species (e.g., *Culex* spp., *Oc. triseriatus*) are not always most accurately represented by CDC light traps, and are often better represented by using gravid traps (CDC, 2003; USACE, 2005). Gravid traps attract females to an oviposition

medium in lieu of a blood meal attractant (CO_2). The CMCC had made limited use of gravid traps, and these data were not made available for my study. In Louisiana, Godsey et al. (2005) reported ~3.4 times the number of captures of *Culex* spp. in gravid traps than in light traps baited with dry ice. This included *Cx. salinarius*, which they captured ~11.7 times more frequently in light traps than in gravid traps. In north-central Ohio, White et al. (2003) captured 17 mosquito species from four genera using gravid traps; *Cx. pipiens* and *Cx. restuans* were the two most abundant species. In my study, *Cx. erraticus*, *Cx. pipiens*, and *Cx. restuans* collectively represented only 0.89% (Table 1) of all captures, whereas *Cx. salinarius* represented 8.03% (Table 1). My results were similar to those of Godsey et al. (2005, without gravid trap data). Moreover, the CMCC deployed light traps from late afternoon to early morning (personal communication with Melissa Cushing, CMCC [January 2006]); thus, diurnal species such as *Ae. albopictus* (1.03%, Tables 1 and 2) were potentially underrepresented in the CMCC's capture data. These issues of trapping technique efficiency may have affected the numbers of captures for all four species in the CONT and one (*Cx. erraticus*) of the four species of the SWMP group.

Finally, an inherent source of error that had unquantifiable effects on the numbers of mosquitoes captured at trapping stations was the variation in spatial coverage of the CMCC's adulticide efforts. Shaman et al. (2002) suggested that increased mosquito abundance at one of their study areas might have been due to an absence of mosquito control in that area. At the time of my research, the CMCC was instituting a computer-based program to quantify the spatial and temporal distributions mosquito adulticide use. As a result, records for how much, where, and when adulticides were sprayed were not

available. However, the lack of a significant difference in capture trends between 2003 and 2004 suggests that residual adulticide effects were minimal.

I expected that properties associated with increased vegetative vigor and soil moisture content would increase habitat suitability for mosquitoes, but this was not found in my study. In fact, predicted abundances for all five species groups were negatively related to at least one of the five independent variables derived from SSURGO data and at least one of the three Tasseled-Cap variables (Table 16). Although these negative relationships were not expected, many are explainable and supported by the literature (e.g., Shaman et al., 2002; Keating et al., 2004; Rey et al., 2006). In addition, many are supported by positive relationships. It is, however, noteworthy that all R values > 0.500 had positive relationships on predicted mosquito abundance (Table 16).

For instance, small-scaled, negative relationships between Tasseled-Cap wetness (TC3) and the predicted abundances of ALSP (R = -0.357; 7x [Table 11]), CONT (R = -0.206; 1x [Table 12]), and SWMP (R = -0.261; 9x [Table 13]) may be an indirect function of canopy cover (TC2), which is considered to carry more explanatory power than TC3 (Campbell, 2002). An alternative explanation is that spectral reflectance values are largely influenced by the uppermost layer in the scene and thus increased summer foliage would have decreased the detectability of underlying soil wetness (TC3).

With only two species, *Ps. columbiae* and *Ae. vexans*, EPHM is the smallest non-target species group (Table 1). Both species have similar life histories (*Ae. vexans* type 2a, from Crans, 2004 [Table 3]), and tend to lay eggs directly on soils in areas with dense vegetative cover and prone to frequent inundation (O'Malley, 1990; Meisch, 1994). Thus, the large-scale (21x) positive relationship between Tasseled-Cap greenness (TC2) and

predicted abundance of EPHM ($R = 0.674$) was expected because higher values for TC2 would indicate high vegetative vigor. However, I did not expect the conflicting and nearly equal positive response of EPHM abundance ($R = 0.564$ [Table 14]) to increases in Tasseled-Cap bareness (TC1). I am unable to explain this relationship with my data because these species rarely lay eggs on bare soils (Gjullin et al., 1950, O'Malley, 1990). Also unexpected was the negative relationship between predicted abundance of CSMN ($R = -0.224$ [Table 15]) and TC2. Similar to the findings of Keating et al. (2004), this relationship is likely a function of a propensity to use more developed upland habitat that has been heavily ditched. This generalized preference of *Cs. melanura* and other species groups for ditched areas and upland/wetland ecotones is clearly evident from visual examination of wetland maps (Figures 10-19), but is not apparent in WTIs or ordination scores alone (Table 17 and Figure 20 A-E).

The predictable pattern of soil moisture negatively affecting mosquito abundance is seen by negative relationships between available water storage (AWS) and four of the mosquito species groups (Table 16). AWS may not be a good indicator of potential surface wetness. Soils with higher AWS values are typically those not prone to surface wetness (flooding), but instead represent soils in which soil moisture is most available in plant root zones. These soil layers tend to be deep and well drained, with a large number of small pores that can hold great volumes of water (personal communication with David Kriz, National Soil Conservation Service, Richmond, VA [February 2007]). I was unable to find any recent studies that addressed effects of AWS on the quality of mosquito breeding habitat. Because most mosquito species require standing water to breed, soils that retain water deep within horizons, in part, explain the negative relationships between

AWS and the predicted mosquito abundances for modeled species groups, regardless of spatial scale.

Nevertheless, several studies have reported that soil characteristics generally assumed to increase the suitability of mosquito breeding habitat have sometimes had the opposite effect. For example, Shaman et al. (2002) analyzed 15 yr of data and found the prevalence of *Cx. pipiens*, a container species associated with polluted waters, to be negatively associated with local wetness models in nine years, and positively related to a swamp species, *Anopheles walkeri* (negative only one year) and an ephemeral habitat species *Ae. vexans* (negative only two years). Their local wetness models, like mine, were derived from soil moisture variables (e.g., water table depth, runoff, surface saturation). The generally positive influence of runoff (RUNOF) on predicted mosquito abundance in my study is supported by Shaman et al. (2002). This validation can be extended to include the container-breeding species (*Cx. pipiens* et al.), in which RUNOF negatively affected predicted abundance (R = -0.306). It is somewhat intuitive that runoff might not increase local abundance for mosquito species that rely primarily on containers (e.g., scrapped tires, nursery pots) and tree holes for breeding sites; Shaman et al. (2002) suggested that unmeasured factors (e.g., dry conditions leading to eutrophication) can promote reproduction in some species and not others.

It is difficult to say with confidence that my results either agree or disagree with those of Shaman et al.'s for two opposing reasons: 1) I used species groups instead of individual species, no doubt contributing more ecological noise than their single-species models, and 2) my models addressed soil characteristics separately whereas their model combined them. However, it is still interesting and puzzling that any mosquito species,

which in eastern Virginia all need standing surface water for larval development, would be negatively associated with factors that increase the probability of surface wetness.

Another apparent soil moisture/mosquito abundance anomaly was reported by Keating et al. (2004), who collected more anopheline mosquito larvae in regions with well draining soils than those with poorly drained soils. Well-drained areas tended to be more developed and contained more suitable manmade breeding habitats (e.g., drained swimming pools, water tanks, ditches) than areas with poorly drained soils. They attributed this finding of increased suitable breeding microhabitats to local human activity (e.g., community-level development and infrastructure) and socioeconomics, and thus higher mosquito densities were only indirectly associated with mosquito ecology. Rey et al. (2006) also found certain species to be more associated with human activity than with natural habitats.

The results of Keating et al. (2004) are relevant in other, but similar, ways to my study. Much of the area within the City of Chesapeake (ca. 20%, Figure 1) is coincident with the Great Dismal Swamp. Since colonial times this forested wetland has been under assault by potential developers. In William Byrd's account of the Great Dismal Swamp (*circa*1728-1737; edited by Swem, 1922) he states:

> "The Dismal then being so utterly useless to the crown, and such a nusance [sic] to the neighboring country, and the advantages of draining it being so many, there remains no difficulty but to find out a method of doing it without leading his majesty into an expence [sic]."

Because efforts to drain the Great Dismal Swamp predate the earliest geographic data for the region, the original extent of the swamp may never been accurately established (Oaks and Whitehead, 1979). However, Shaler (1890), a century and a half after Byrd proposed

his plan to drain the swamp, estimated that the Great Dismal Swamp occupied ~3900km^2; presently, the swamp occupies ~500km^2. Most of this reduction in area was accomplished via a drainage network of canals and ditches that continues to be expanded today; ditching is especially prevalent in the western and southern areas of the city. This "Tulloch ditching" is the purposeful draining of wetlands by digging ditches and carefully removing the dredge spoil to an offsite location. The practice is designed to convert (drain) wetlands into land that is no longer subject to wetland regulations, and thus, is made available for alternate uses (Hershner, 1999).

Although this extensive system of canals and ditches may have effectively transformed land into habitat more readily useful for agriculture and urban development, these activities may have inadvertently resulted in the creation of residual microhabitats for breeding mosquitoes such as reported by Keating et al. (2004). Many areas correctly classified as "upland" in NWI maps have been Tulloch ditched (Figures 11, 13, 15, 17, 19). As of 1999, the City of Chesapeake has Tulloch ditched seven times more wetland acreage than all other municipalities in the Hampton Roads region combined; further, the city has plans to double this acreage (Hershner, 1999).

Although ditching creates upland habitat from wetland, the ditches remain excellent mosquito breeding sites (Laird, 1988) embedded in otherwise unsuitable habitat. This pattern was most clearly seen in the predicted spatial abundances of *Cs. melanura*, the target species of the CMCC, but also was evident for the EPHM and SWMP groups. The influence of the system of ditches and canals is further reflected in the positive responses of most of the regression models of species groups. The independent variable HYDSUM accounted for the spatial distribution of ditches and

canals (Table 4). As expected, predicted abundance increased for most species groups in heavily ditched areas because of the potential for good breeding habitat in these disturbed areas (Laird, 1988). The negative relationship between HYDSUM and predicted abundance of EPHM (R = -0.124) was likely a result of a general affinity for temporary habitats not represented by a factor describing permanent bodies of water. All but two trapping stations were located within <200m of a ditch or canal. This close proximity of trapping stations to canals and ditches may have had a two-pronged effect. HYDSUM was not a good predictor variable for CSMN because this group responded most strongly to independent variables at consistently broad spatial scales. Therefore, the variation in HYDSUM values among trapping stations would have been diluted as scale was increased, possibly to a point where any statistical relationship wais lost. On the other hand, ALSP (R = 0.308), CONT (R = 0.181), and SWMP (R = 0.300) groups responded positively to increases in HYDSUM at much smaller spatial scales, thus preserving the variation of HYDSUM among trapping stations.

Moreover, the increased responses of the predicted abundance of *Cs. melanura* to independent variables at broad spatial scales was supported by visual examination of the wetland maps for this species (Figure 18 and 19), where large and contiguous areas of high predicted abundance dominate. This spatial-scale consistency in both suitability maps and independent variables is likely to be a function of habitat selection by *Cs. melanura*. It cannot be overemphasized that *Cs. melanura* was the target species, contributing to a bias in the placement of traps when the present trapping regime began in 2002. Again, the vast majority of trapping effort has been in close proximity to palustrine wetlands, the preferred habitat of *Cs. melanura*.

The remaining four species groups all had smaller and more localized areas of high predicted abundance; this was also seen in the scale of independent variables they most positively responded to. I suggest that the within-group variation of spatial scales for these groups was due to environmental variables I did not consider. Although species group-specific explanations for the variations in spatial scale are difficult to parse with the data I analyzed, or for lack of data I did not analyze, the fact remains that the predictability of mosquito abundance in my regression models was increased by the incorporation of differing spatial scales. Rey et al. (2006), who studied habitat segregation by mosquito species in south Florida, also found that species respond to habitat variables at different spatial scales from $30m^2$ to $630m^2$.

Summary

The methods used herein provide a simplified series of species-group models based on similarities in mosquito life histories. The data used in these models were provided (i.e., mosquito captures, City of Chesapeake hydrology [canals and ditches], both from CMCC), downloaded at no cost (i.e., national hydrology dataset [USGS seamless data], soil data [SSURGO, NRCS]) or relatively inexpensive (i.e., Landsat ETM+). My decision not to incorporate land cover/use data (USGS: NLCD) in my models was based on three real problems: 1) the inability to achieve an acceptable level of accuracy in the Level II classification that equated to less than desirable data reliability, 2) not all NLCD Level II classes were represented by trap-site locations, which would have made ranking of city-wide habitat suitability more difficult with many land use/cover classes

disproportionately represented or omitted, and 3) these data were categorical and would have required independent analysis. The latter is the least problematic of the three.

Although it has long been known that mosquitoes require standing water for breeding, there is much variation in habitat affinities among species (Howard et al., 1912; Shannon, 1931; Carpenter and LaCasse, 1955; Horsfall, 1955). In order to develop effective and efficient mosquito control programs, it is necessary to understand these species-specific differences and to be able to model habitat suitability using accurate landscape-level data. My HSIs were derived from spatially explicit empirical data, thus making them useful for locating potential mosquito habitats within real landscapes. The use of data collected by remote-sensing techniques enables the integration and analysis, within the framework of a GIS, of large and diverse data sets to an extent not feasible by field collection alone. Because my HSI models are applied in nature, much attention was devoted to keeping them streamlined, user-friendly, and not cost-prohibitive, while retaining the ability to process empirical data in real landscapes.

CHAPTER III

PREDICTION OF *CULISETA MELANURA* (COQUILLETT) ABUNDANCE ON THE SOUTHERN COASTAL PLAIN OF VIRGINIA IN RESPONSE TO RECENT WEATHER EVENTS USING REMOTE SENSING TECHNIQUES AND A GIS

Introduction

Besides being a general nuisance, mosquitoes are vectors of many diseases (a.k.a., arboviruses [arthropod-borne viruses]) that have threatened public health in North America since Colonial times (Fischer and Schweigmann, 2004; Andersen, 2006). One such example was the yellow fever outbreak that killed over 2,000 people in the port cities of Norfolk and Portsmouth, Virginia, between July and October 1855 (Goldfield, 1873). Years later, Walter Reed discovered that this viral disease was transmitted by a mosquito, *Aedes aegypti* (Vainio and Cutts, 1998).

One modern mosquito-borne arbovirus in the eastern United States is eastern equine encephalitis ([EEE] Hassan et al., 2003). First isolated in North America during simultaneous human outbreaks in Delaware, New Jersey and Virginia in 1933, EEE persists in the eastern North America, the Caribbean, and South and Central America (Weaver et al., 1999). Because of the relatively long history of association with North America, the epidemiology for EEE is well understood.

The persistence and transmission dynamics of EEE are functions of distribution, competence of vectors, and the proximity and mobility of their enzootic vertebrate hosts (Hassan et al., 2003). Thus, arboviral foci generally coincide spatially within habitats frequented by host species where environmental conditions are favorable for breeding mosquitoes (Kitron, 1998; Kaya et al., 2004). My study addresses the spatial and temporal distribution, within the City of Chesapeake, Virginia, of the primary enzootic vector of EEE, the bird-feeding mosquito *Culiseta melanura* (Nasci and Edman, 1984; Crans et al., 1994). Foci of EEE are generally associated with palustrine habitat, the preferred habitat of *Cs. melanura* (Weaver et al., 1999) and gregarious passerine birds species that serve as reservoir hosts (Komar et al., 1999). Once enzootic transmission is established, the virus becomes available to epizootic bridge vectors that readily feed on mammals as well as birds (Hassan et al., 2003). As its name suggests, epizoonoses are most commonly documented with horses, and infections are usually fatal. However, since 1964, 200 human cases of EEE have been confirmed (Calisher, 2004) with a 30% mortality rate (CDC, 1992).

Many environmental conditions that bring together mosquitoes, the pathogens they transmit, and potential hosts are measurable (Shaman and Day, 2005). For example, spatial and temporal fluctuations in mosquito abundance are directly and indirectly influenced by weather patterns (Rogers, 1967; Reiter, 2001; Tong and Hu, 2001; Shaman et al., 2002; USDA, 2004; and others). Naturally occurring outbreaks of EEE usually are associated with periods of high temperatures and rainfall, creating conditions conducive to the expansion of *Cs. melanura* and other mosquito species (USDA, 2004). Rainfall often increases the diversity and abundance of habitats available to breeding mosquitoes

and the resultant near-surface humidity increases both flight activity and host-seeking behavior (Shaman and Day, 2005). These associations make the geographic positions of breeding and host-seeking activities predictable, and therefore potentially reveal the most judicious stages at which to interrupt viral epidemiologic cycles of mosquito-borne diseases.

The distribution and accumulation of rainwater within natural watersheds at both macro- and micro-scales are intimately tied to topography (Yeh et al., 1998; Bernhardsen, 2002; Garbrecht and Martz, 2000; Shaman et al., 2002). Although researchers have long used topographic indices to predict relative soil moisture and potential surface wetness (Beven and Kirkby, 1979; Urban et al., 2000), others advocate the use of improved soil moisture indices that integrate topographic data with empirical soil data (Iverson et al., 1997; O'Loughlin, 1981 and 1986), especially in landscapes with little topographic relief (Dirnböck et al., 2002). The integration of soil characteristics and topography enables the detection of areas where upslope water accumulation can potentially exceed soil transmissivity (O'Loughlin, 1986), and thus reveals locations susceptible to flooding or ponding. Chesapeake is nearly flat, similar to the landscape studied by Dirnböck et al. (2002), so a model that integrates a topography-based soil moisture index and empirical soil data should be more useful than models in which only topography is considered (e.g., Beven and Kirby, 1979).

The integration of digital satellite data in GIS-based modeling of disease vector abundance and disease transmission is becoming a more broadly used approach in arboviral research (Beck et al., 1994; Washino and Wood, 1994; Kaya et al., 2004; and others). Recent advances in Earth-observing sensors have spurred the development of a

wide variety of spatially explicit environmental data applicable to the ecological study of disease vectors (Goetz et al., 2000). Because of these advances, surveillance, monitoring, and subsequent health policies associated with the study of arboviruses have taken on a more applied nature through the integration of spatial and epidemiological data (Clarke et al., 1996). However, because most mosquito control and public health agencies are unable to conduct exhaustive *in situ* monitoring, they would benefit from the application of models capable of predicting the temporal and spatial distributions of mosquitoes at a landscape-scale (Shaman et al., 2002). My study produces such a potentially useful model.

In Chapter II of this dissertation, I created semi-static habitat suitability indices (HSI) for five groups of mosquito species based on life-history characteristics from Crans (2004). These HSIs quantified the affinities of each group to measured soil and vegetation attributes. One group contained a single species, *Cs. melanura*, the target species for the Chesapeake (Virginia) Mosquito Control Commission. The HSI for *Cs. melanura* predicted highest abundances in relatively large, poorly drained areas with high degree of surface wetness.

The primary objective of this chapter was to augment the semi-static HSI model for *Culiseta melanura* (generated in Chapter II) with a dynamic GIS-based model incorporating weather patterns and a soil moisture index based on topographic derivatives to predict mosquito abundance. This "dynamic" model is capable of predicting not only *where*, but also *when* adult *Cs. melanura* are likely to emerge in large numbers. To achieve this predictability, I used spatially explicit meteorological data (NEXRAD: ***NEX***t-generation [Doppler] ***RAD***ar, National Oceanic and Atmospheric Administration

[NOAA], National Weather Service [NWS]) to create weekly "accumulated precipitation" grids that would be overlaid onto topographic soil moisture indices in order to map areas with high probabilities of surface and subsurface wetness. NEXRAD (NOAA, NWS) is georeferenced radar data (Weather Service Doppler Radar [WSR:88D]) that includes precipitation accumulation (Beringer and Ball, 2004). Thus, knowing current rainfall amounts and distributions, and the developmental period of mosquitoes, I can map which areas of suitable breeding habitat, from Chapter II, are most likely to experience outbreaks of adult mosquitoes. Such knowledge will enable the mosquito control agencies to apply insecticides in a more effective, timely, and economical manner, thereby reducing the health risks of EEE and similar diseases while reducing costs of chemicals and spraying efforts, and perhaps achieving a more effective level of control.

Methods

Study Area

This study, conducted with the cooperation of the Chesapeake Mosquito Control Commission (CMCC), encompasses the entire City of Chesapeake, Virginia (Figure 1). Located in the Coastal Plain physiographic province, Chesapeake has an area of 91,427 ha and a 2004 population of 214,725.

The climate of Chesapeake is humid subtropical and similar to the rest of Virginia east of the Blue Ridge Mountains (Woodward and Hoffman, 1991). Monthly temperatures range from –1.8°C (January) to 31.6°C (July) based on 30-yr averages (1971 – 2000; NCDC, 2002) collected at NWS Station KAKQ, Wakefield, Virginia

located at Wakefield Municipal Airport (Lat/Long: 36.9839°N, 77.0072°W), about 50 km west of Chesapeake. Temperature extremes are moderated by proximity to the Chesapeake Bay and the Atlantic Ocean. Annual average precipitation is 114.4 cm (45.05 inches) based on 30-yr averages (1971 – 2000; NCDC, 2002). The growing season (frost-free days) for the region is 185 – 200 days (Palone and Todd, 1998).

Chesapeake was selected for study not only because its landscape mosaic represents the regional diversity of land use, but also because of the known occurrence and relative distributions, within the city, of ~30 mosquito vector species of EEE and West Nile virus (WNV). Tidal and freshwater creeks, palustrine habitats, and an extensive network of ditches are embedded in the landscape mosaic, providing good mosquito habitat is threaded within and among high densities of humans, creating a landscape conducive to the transmission of EEE and other mosquito-borne diseases. Moreover, the primary reservoir vector for EEE, *Cs. melanura*, is, by far, the most numerous species captured by the CMCC during monitoring efforts. Equally important is the technologically advanced program of mosquito control and surveillance of the CMCC, dating from 2003, and the system of ditches, built since the 1880s, which drained low-lying, waterlogged soils, and plays a significant role in mosquito population dynamics.

Culiseta melanura *Captures*

Culiseta melanura were captured using CO_2-baited CDC light traps at 56 permanent trapping sites throughout Chesapeake (Figure 1). Populations were monitored from early April through late October and only females were used in analyses.

Only 46 of the 56 sites for 2004 were used in analyses because the others had ≤ 5 trap nights (TN). Capture data were normalized to account for variation in trapping effort among the 46 sites by dividing total captures of each species collected at each site by the number of TNs for that site.

Model validation (years and sites) using capture data for other years when mosquitoes were collected (2003 and 2005) would have been problematic because the number of trapping sites in 2003 (N = 30) was smaller than in 2004, and at the time analyses were run a complete dataset of 2005 *Cs. melanura* captures was not yet available. Cross-year comparisons for 2003 and 2004 to evaluate temporal patterns consisted of ANOVA (years) and correlation analysis (sites) of *Cs. melanura* capture data for the trapping sites common to both years (Appendix F). Single-factor ANOVA (α = 0.05) was used to evaluate differences in mean captures/TN of *Cs. melanura*, by trapping site, between 2003 and 2004 (Zar, 1996). Pearson's correlation was used to compare captures/TN at individual trapping sites between 2003 and 2004 (Zar, 1996).

*Weather Lag-Time Analysis (*a priori*)*

A series of multiple linear regression models was used to test the *a priori* hypothesis that fluctuations in weekly captures of *Cs. melanura* in 2004 were, in part, functions of current average daily temperature and recent precipitation accumulation (PA). Six time-sequential regression analyses were run (α = 0.05); in each successive regression, weekly captures of *Cs. melanura* were regressed against average weekly air temperature (AWAT) for the same 1-week PA period for successively earlier weekly intervals (see Table 18). Weekly intervals of the three datasets (i.e., captures, AWAT, PA) used in

these regressions were calculated for 32 weeks (April 4 – October 10, 2004; Appendix G). Temperature and precipitation data for the City of Chesapeake were provided by the CMCC. Regression models were made using Number Cruncher Statistical Software (NCSS) v2000.

Digital Elevation Model

Because the vertical resolution used in USGS's digital elevation model (DEM) that includes Chesapeake (5 ft [1.52 m]) is insufficient to accurately describe the ecological influence of elevation in this relatively flat coastal landscape, I created a 2-ft interval DEM (ESRI Grid format [30m x 30m pixels]) of the study area (ArcGIS v.9.1, ArcToolbox, Spatial Analyst Extension) from a 2ft-interval contour map of the City of Chesapeake provided by the CMCC. The contour map used to create this DEM did not include data for the Great Dismal Swamp, a forested wetland that abuts the western margin of Chesapeake (Figure 1).

To construct this higher vertical resolution DEM, I first extracted elevation values (*Z*-values) for all nodes on the CMCC's 2-ft contour map (Figure 21 [partial extent]) to a new point shapefile (Figure 21 [partial extent]). I then interpolated the *Z*-values from the point shapefile to produce a 2-ft (0.61 m) interval continuous and hydrologically correct surface of elevation (Figures 21 and 22 [30m x 30m pixels]). The interpolation method was *Topo to Raster* (ArcGIS 9.1, Spatial Analyst Extension). However, Chesapeake's extensive ditch network was not represented in the contour map. To correct for this, I used a stream-burning technique (Saunders, 2000) to incorporate the deviations in elevation values associated with ditches. An ArcView shapefile of the ditches for

Chesapeake was provided by the CMCC (Figure 23 [partial extent]). In order to acquire empirical data, I measured the depths of 63 ditches throughout the city. The CMCC's

Table 18. Summary of the six *a priori* time-lag regression models. Dependent and independent variable datasets used in these regression models used to test the hypothesis that fluctuations in weekly (wk) captures of *Cs. melanura* in 2004 (4 April through 30 October) are a function of current average weekly air temperature (AWAT) and past precipitation accumulation (PA).

Variable Dataset	1-wk lag	2-wk lag	3-wk lag	4-wk lag	5-wk lag	6-wk lag
†Current week: *Cs. melanura* captures	●	●	●	●	●	●
§Current week: AWAT	●	●	●	●	●	●
§One week prior: total weekly PA	●					
§Two weeks prior: total weekly PA		●				
§Three weeks prior: total weekly PA			●			
§Four weeks prior: total weekly PA				●		
§Five weeks prior: total weekly PA					●	
§Six weeks prior: total weekly PA						●

†Dependent variable (2004)
§Independent variable, prior to *Cs. melanura* weekly capture dataset (2004)

ditch network shapefile was converted to grid format and assigned a constant value representative of the calculated average of depth (~1.5 m) and burned into the 2-ft DEM to create a more locally appropriate final DEM for the city (Figures 23 and 24; ArcGIS-9.1, ArcToolbox, Spatial Analyst).

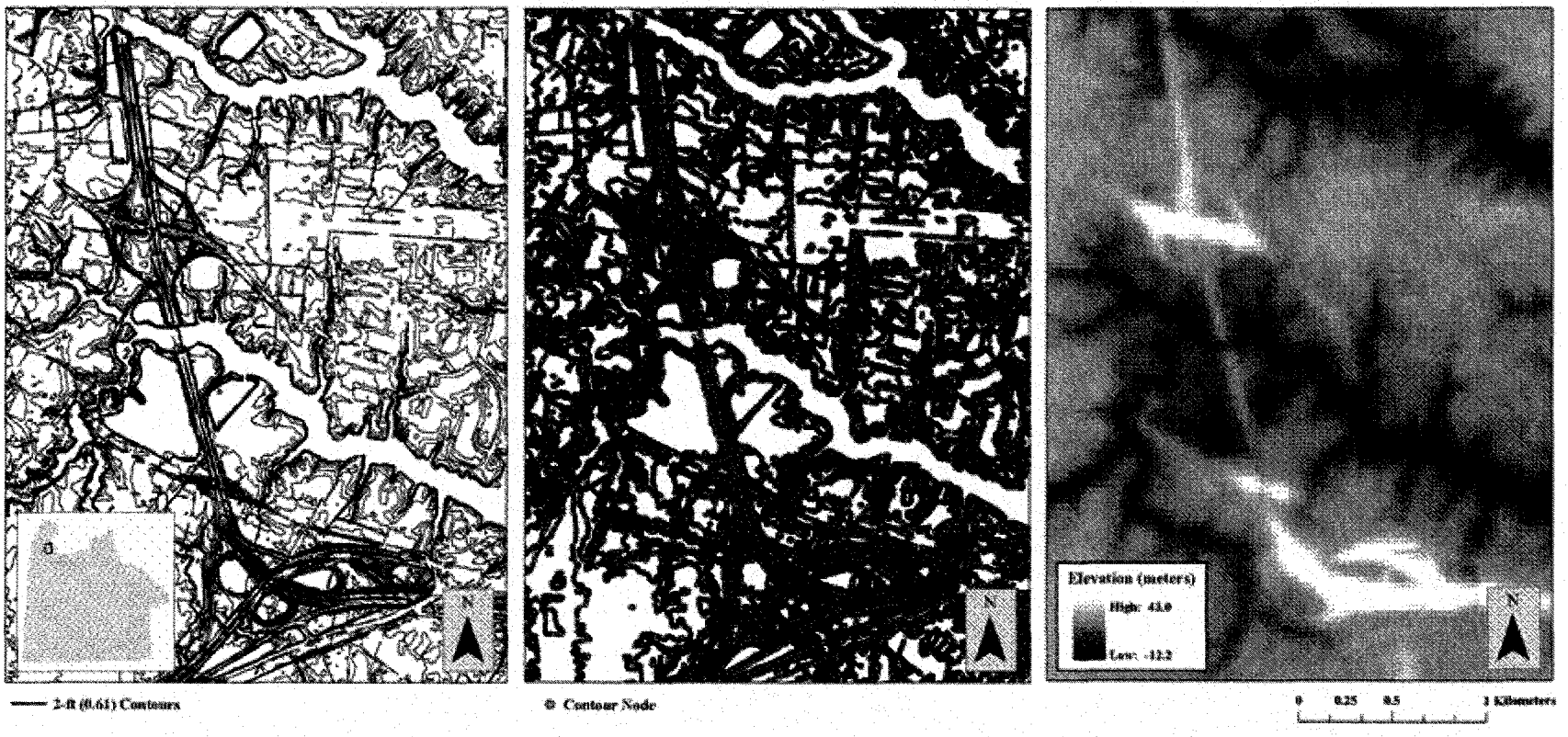

Figure 21. Creation of 2-ft (0.61-m) DEM from a contour map. Representative section of the contour map provided by the CMCC showing 2-ft (0.61 m) interval contour (left), the point shapefile created from the nodes of the 0.61-m interval contour (center), and the elevation surface interpolated from the point shapefile of the nodes of the 0.61-m interval contour (right). The inset shows the location of the section (red box) within the City of Chesapeake (light green). The rivers are tributaries of the western branch of the Elizabeth River.

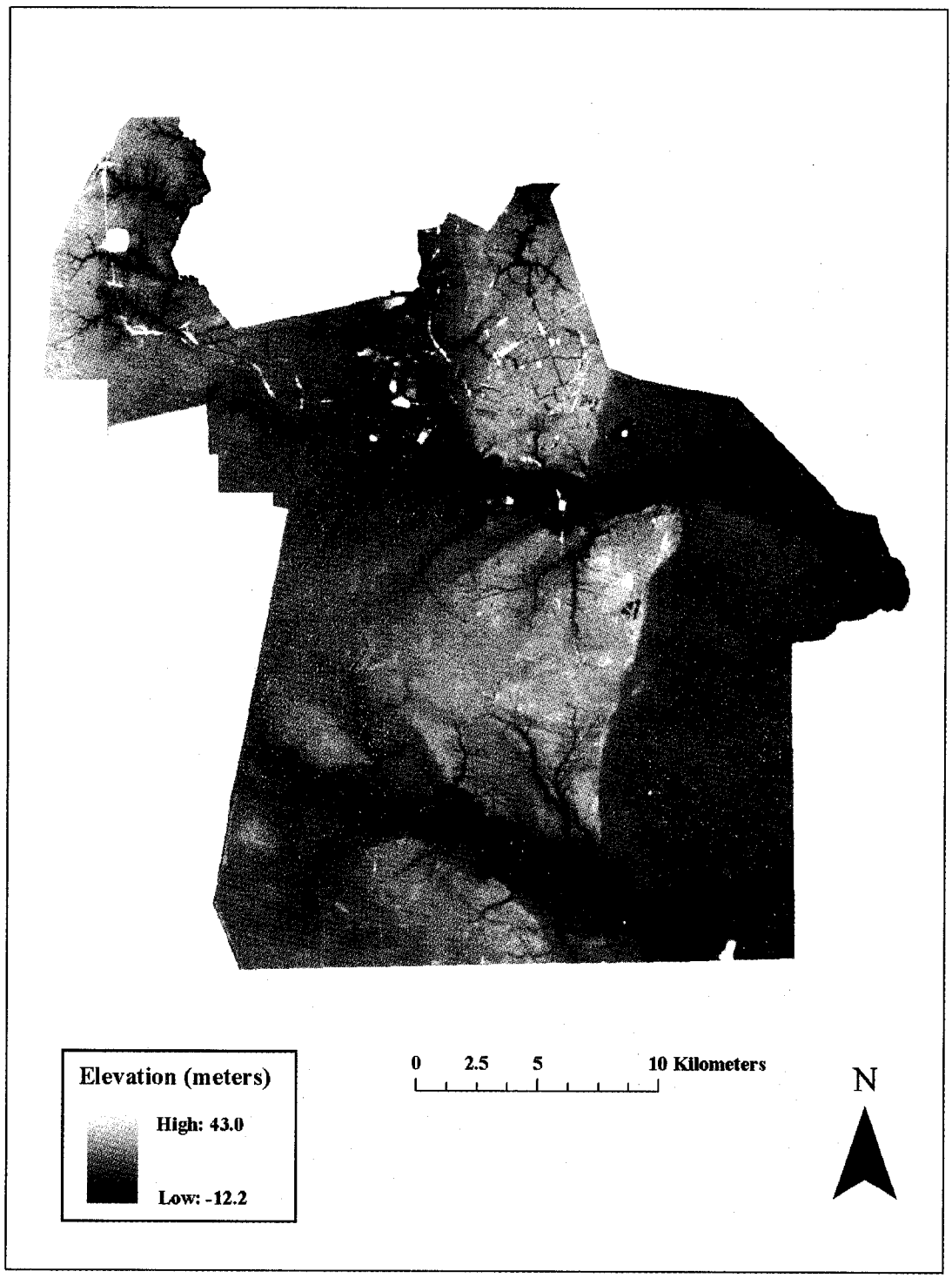

Figure 22. The digital elevation model interpolated from the 2-ft (0.61 m) contour map. The Great Dismal Swamp is not included in the extent.

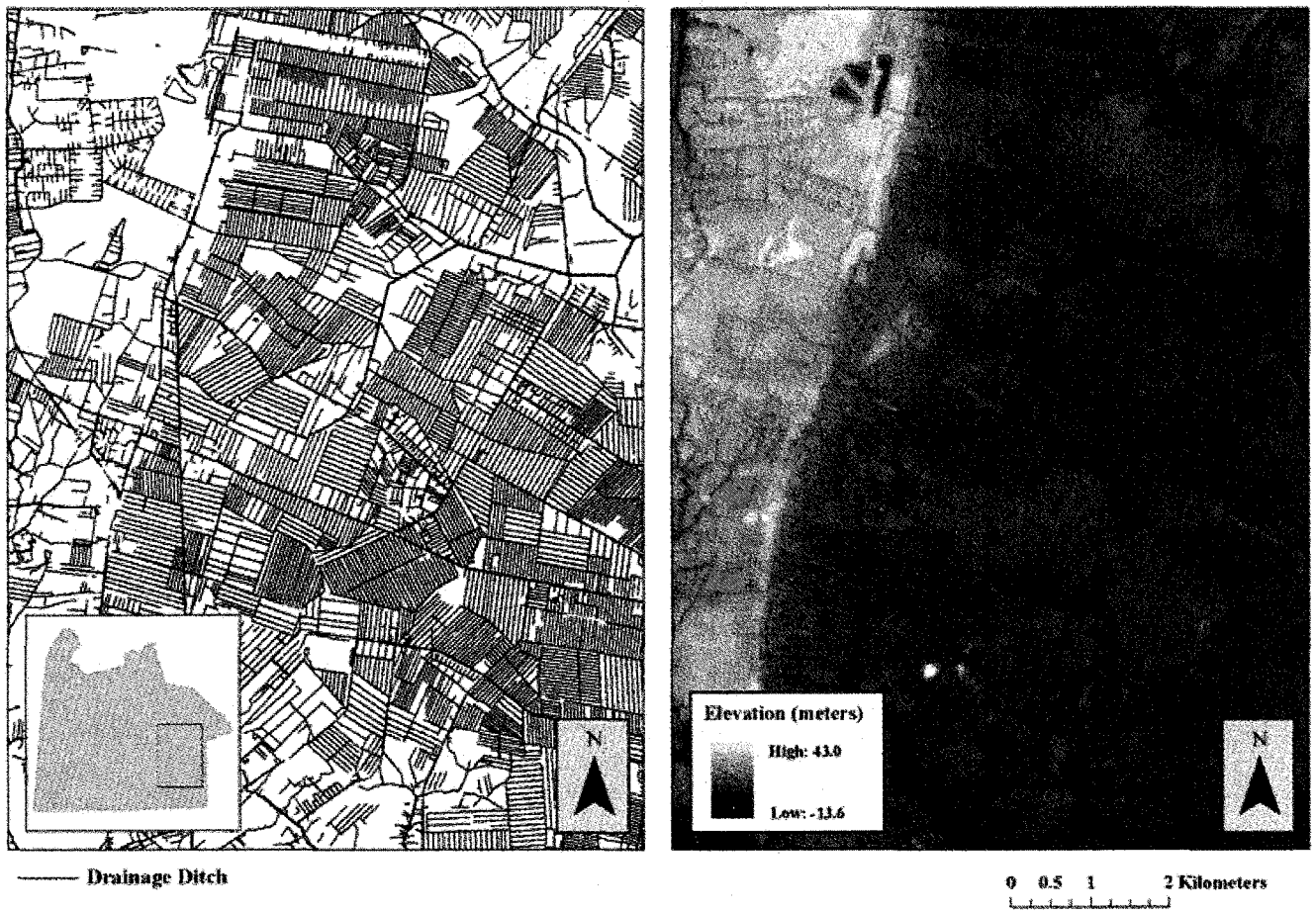

Figure 23. Stream-burning the ditch-network into the DEM. Representative section of the ditches shapefile (left; provided by the CMCC) used in the stream-burning process on the interpolated 2-ft (0.61 m) interval DEM (Figure 3). The same section after stream-burning the ditch network (right). The inset shows the location of the section (red box) within the City of Chesapeake (light green). The Pocaty River is shown in the northwest corner of the image and a tributary of the Northwest River is shown in the Southwest corner of the image.

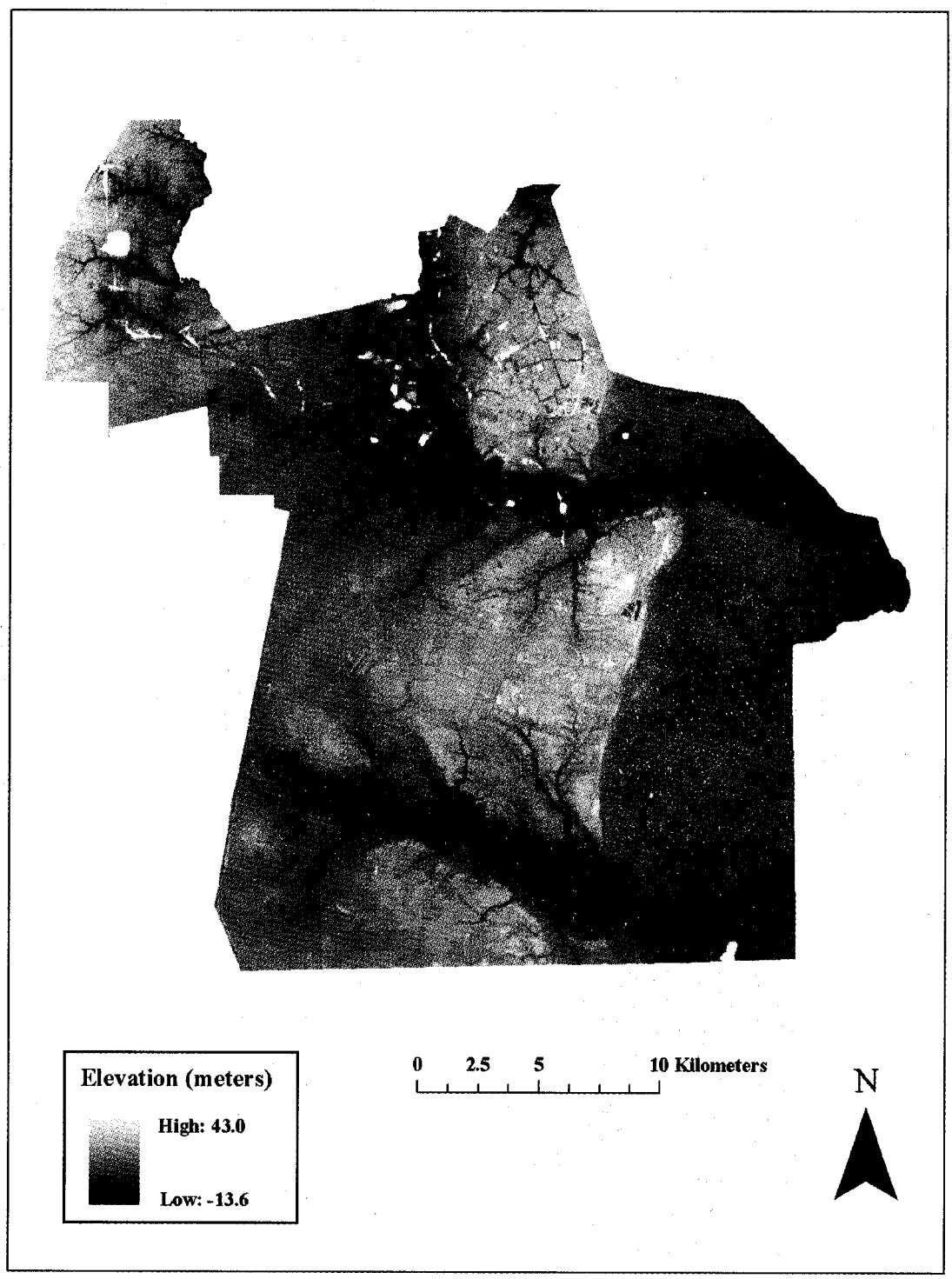

Figure 24. The 2-ft interval DEM after stream-burning in the ditch network. The Great Dismal Swamp is not included in the extent.

Hydrologic Model

The National Hydrology Dataset (NHD: USGS) was used to determine the extent of the two watersheds in which the City of Chesapeake lies: Hampton Roads and the Albemarle Sound. These watersheds extend beyond the boundary of Chesapeake, and thus upslope values influence drainage values within the city. Consequently, I created a total watershed flow accumulation grid from the USGS 5-ft vertical resolution (30m x 30m pixel) DEM using ArcGIS-9.1, ArcToolbox, Spatial Analyst extension. Next, I extracted a 1-pixel (30m x 30m) wide grid along the city boundary to quantify regional flow accumulation from outside Chesapeake. This regional flow-accumulation raster was integrated with the 2-ft (0.61 m) vertical resolution flow-direction raster of the city to produce a more accurate local flow-accumulation raster (Figure 25 [partial extent]) that accounted for regional flow accumulation (ArcGIS-9.1, ArcToolbox, Spatial Analyst). This local-accumulation raster was used to create a topographic soil moisture index (TMI), described below.

Topographic Soil Moisture Index (TMI) Grid

Soil moisture characteristics (SSURGO Soil Surveys # va550, va800, va810: USDA, Natural Resources Conservation Service [NRCS] Soil Data Mart) were inherent in the *Cs. melanura* HSI (from Chapter II) used in this study. As such, the use of soil characteristics in the soil moisture index would likely result in statistical redundancies. Therefore, I used a more complementary TMI (after Beven, 1997) to circumvent these issues in lieu of Iverson et al.'s integrated soil moisture index (1997) because the TMI uses only topographic derivatives. As a result, my model will have the theoretical

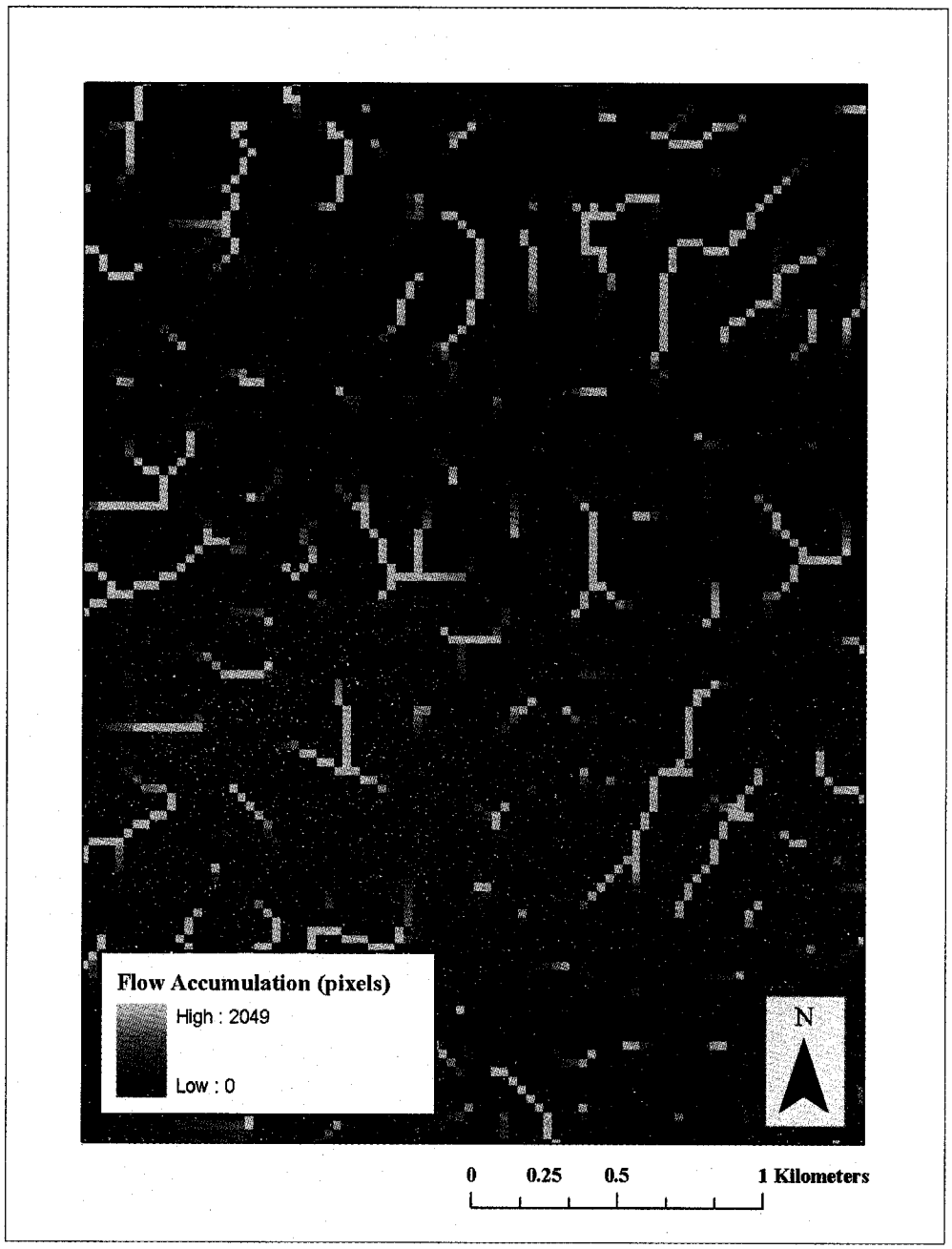

Figure 25. Flow-accumulation grid after stream-burning. The same section as Figure 21 showing of the local flow-accumulation grid from the interpolated 2-ft (0.61 m) interval, stream-burned, DEM and the regional flow-accumulation grid. Pixel values represent the number of 30m x 30m upslope pixels. The location of the inset within the city of Chesapeake is defined in Figure 21.

equivalent of a soil moisture index with both soil and topographic properties.

The construction of a TMI surface model for the City of Chesapeake was based on the following equation (after Beven, 1997):

Equation 4: $$TMI = \ln(A / \tan \beta)$$

Where pixel values for A = flow accumulation surface (Figure 25 [partial extent]) and β = DEM slope surface (Figure 26). The final TMI surface was created in grid format (Figure 27 [30m x 30m pixel]) using ArcGIS-9.1, ArcToolbox, Spatial Analyst extension.

Soil moisture values that coincided spatially with the locations for each of the 46 trapping sites were extracted from the TMI grid to create a soil moisture point shapefile. Extracted TMI values (from Equation 4) were used as the independent variable in a linear regression model ($\alpha = 0.05$) to test the hypothesis that variation in captures of *Cs. melanura* among trapping sites (dependent variable) is related to spatial variation in the calculated TMI values (Zar, 1996). Because the interpolated DEM used to create this TMI did not include the Great Dismal Swamp, TMI values for trapping sites located in the Swamp were not included in this analysis. This regression model was made using NCSS, v2000.

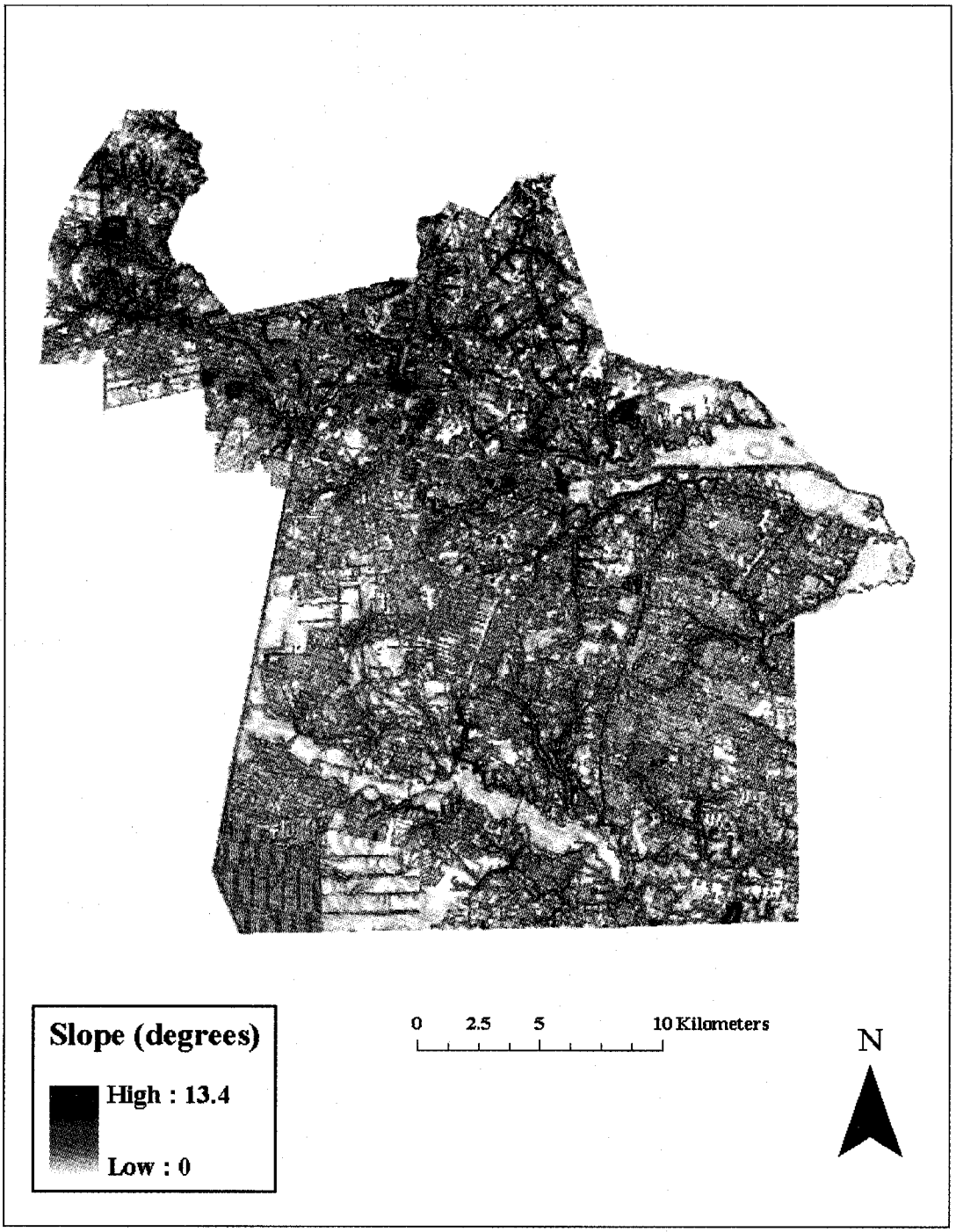

Figure 26. Slope surface of the interpolated 2-ft (0.61 m) interval, stream-burned, digital elevation model.

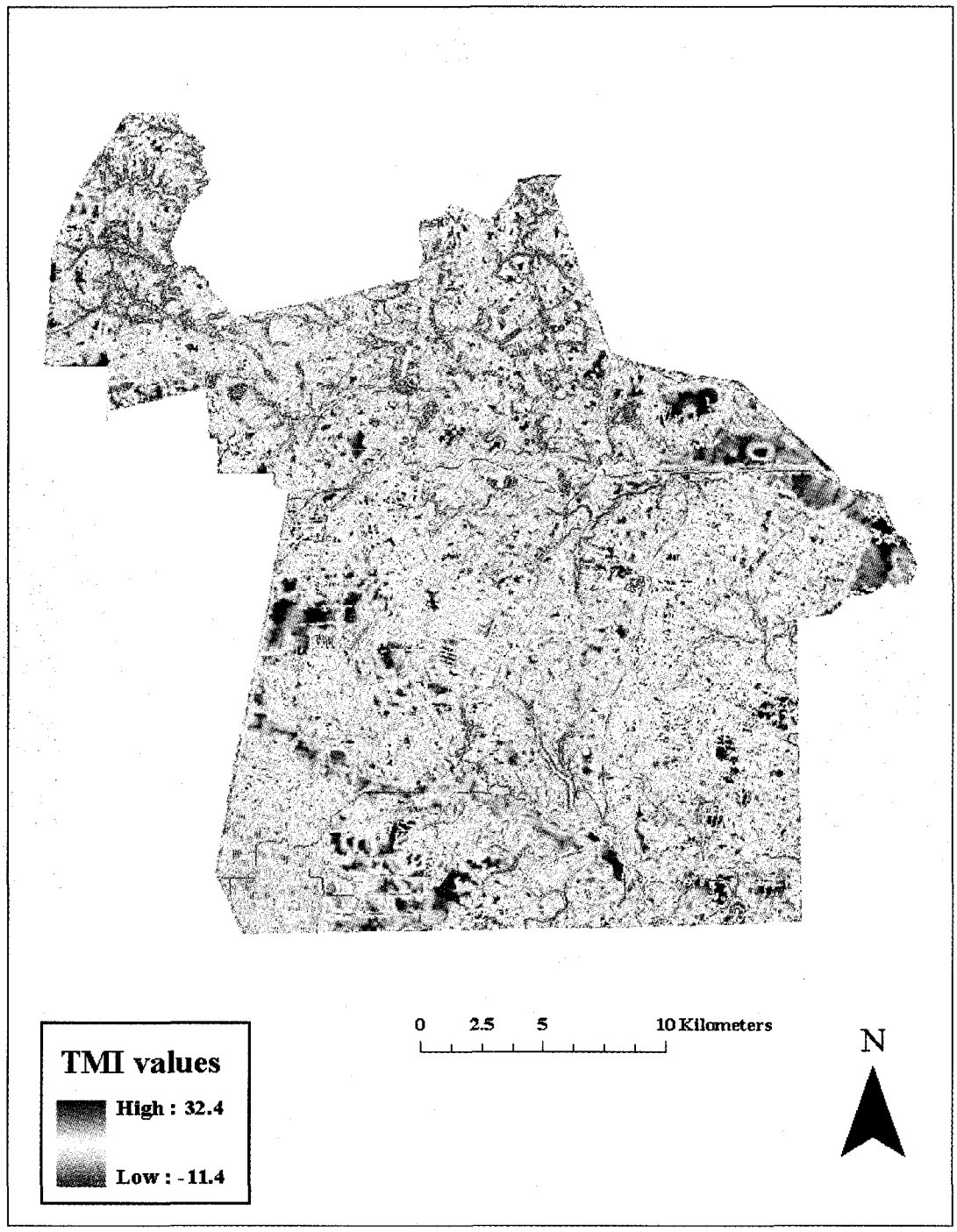

Figure 27. Topographic [soil] moisture index (TMI) surface. Pixels values were calculated using Equation 4.

The final TMI grid was normalized and rescaled before integration into the final dynamic predicted abundance models (below) with the following equation:

Equation 5:
$$TMI_r = \frac{(TMI_O - TMI_{min})}{(TMI_{max} - TMI_{min})} \text{ x } 100$$
$$TMI_{min})$$

Where TMI_r = normalized and rescaled TMI pixel values, TMI_O = calculated TMI vales (Equation 4), TMI_{min} = the lowest pixel value in the calculated TMI, and TMI_{max} = the highest pixel value in the calculated TMI.

Weekly Weather Grids

Neither the *Cs. melanura* HSI (from Chapter II) nor the TMI described above are prone to temporal changes because the factors involved in their creation are relatively static (e.g., topography, soil characteristics, vegetation patterns). The primary role of weekly weather data grids described below was to provide a dynamic and environmentally based aspect to the abundance models created in this study.

Integration of temperature and precipitation data into a single output is problematic because they are represented by different data types (intervals for temperature and ratio for precipitation) and relative scales. Consequently, both datasets were normalized and rescaled using the following equations:

Equation 6 (temperature): $$X_r = \frac{(X_O - X_{min})}{(X_{max} - X_{min})} \text{ x } 100$$

Equation 7 (precipitation): $$X_r = (X_O \div X_{max}) \text{ x } 100$$

Where X_r = the normalized and rescaled value (0-100), X_O = the observed value, X_{min} is the historical minimum, and X_{max} is the historical maximum. Minimum and maximum extremes were derived from different data sources and referenced below, where appropriate.

Some of the data needed for the construction of weekly weather grids were not available for 2004 (i.e., 3-hr PA data), the period when the capture data were collected. Instead, I used weather data collected in 2006. This use of 2006 data in my model construction is not an issue because the relationships between mosquito activity and variations in weather (i.e., temperature and precipitation) are so well documented.

Weekly Average Air Temperature (AWAT; constant-value) Grids

Spatially explicit temperature data for the study area are not available; as a result AWAT grids incorporated into these models had a constant, citywide value. AWAT in 2006 (X_{rt}) for Chesapeake were calculated using Equation 6 and transferred to constant-value AWAT grids using Quality Controlled Local Climatological Data from the National Climatic Data Center (QCLCD: NCDC) collected at the NWS Station at Chesapeake Regional Airport ([KCPK] 36.6639°N, 76.3306°W; Appendix H). Historical minimum

(X_{min} = 2.8 C) and maximum (X_{max} = 32.2 C) AWAT values (March – October) were based on 30-yr monthly records from 1971-2000 (NCDC, 2002) collected at station KAKQ.

Weekly Precipitation Accumulation (PA) Grids (NEXRAD Level-III Precipitation Data Acquisition and Preparation)

NEXRAD Level-III (WSR:88D), 3-hr PA data (NOAA, NCDC) were used to create spatially explicit, georeferenced weekly "accumulated precipitation" grids. These data may be downloaded at no cost (http://www.ncdc.noaa.gov/nexradinv) in ArcView shapefile format using the NEXRAD Data Exporter (Figure 28; [Java] BETA v.1.3.3). The NEXRAD data source closest to Chesapeake is KAKQ, Wakefield, Virginia (a.k.a., National Doppler Radar Site, Norfolk/Richmond).

NEXRAD 3-hr PA shapefiles were preprocessed into weekly PA (WPA) grids using a series of models created in ArcGIS v.9.1, Modelbuilder. These models make the creation of WPA grids streamlined and highly repeatable.

WPA grids were created in ArcGrid format by batch-conversion of 3-hr PA shapefiles for a given day (Figure 29; 1km x 1km pixels, NAD-1983, State Plane, Virginia [South], FIPS-4502 Ft. Projection: Lambert Conformal, Conic). Only shapefiles with coverage (polygons) within Chesapeake were used in this model; thus, the number

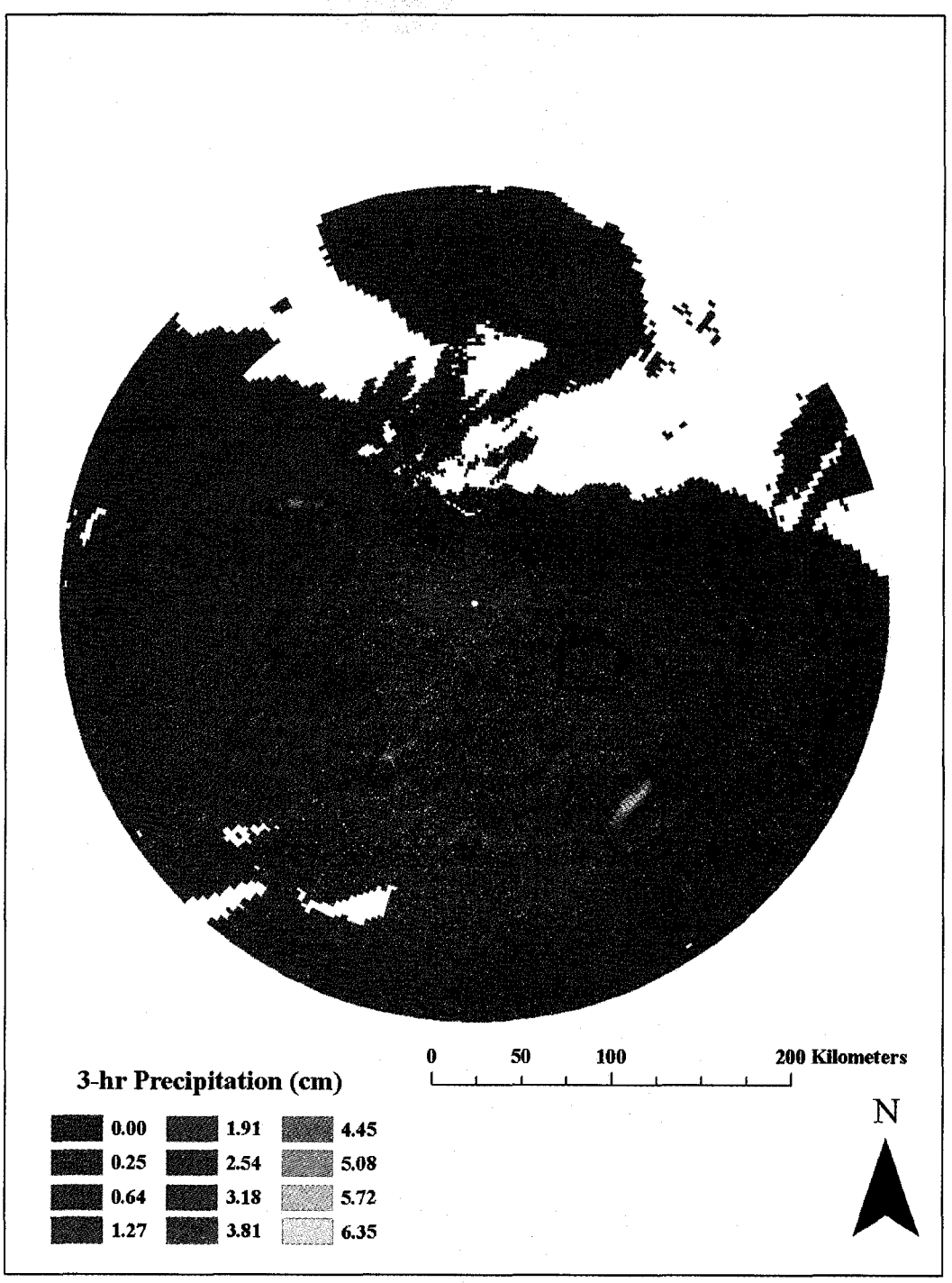

Figure 28. Sample of NEXRAD 3-hr precipitation accumulation data in ArcView shapefile format. Data (14 May 2005 [0214-0514 EST]) were collected at KAKQ, Wakefield, Virginia (Lat/Long: 36.9839°N, 77.0072°W). Chesapeake is outlined in black.

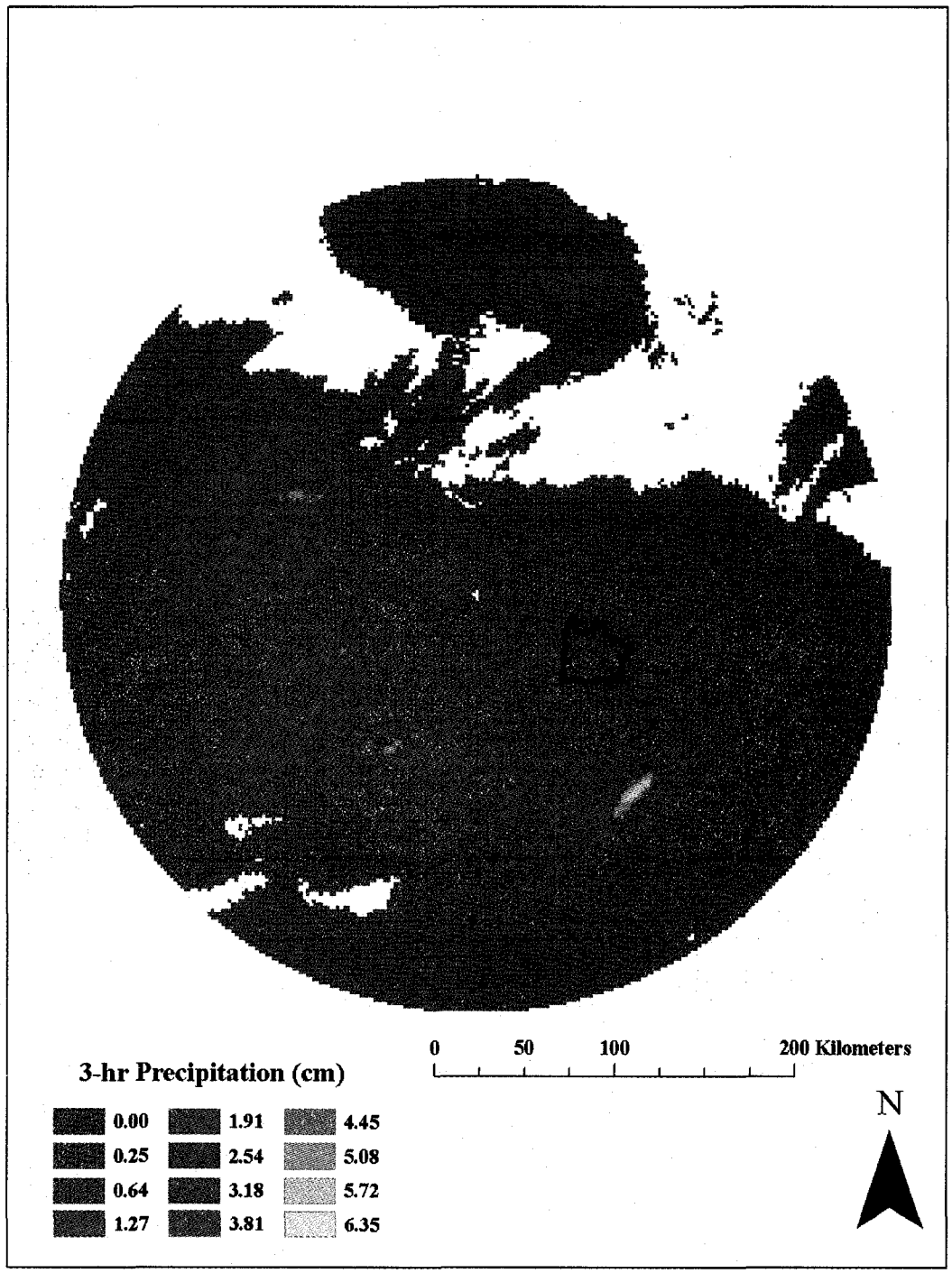

Figure 29. Sample of NEXRAD 3-hr precipitation accumulation data converted to ArcGrid format. (Data (14 May 2005 [0214-0514 EST]) were collected at KAKQ, Wakefield, Virginia (Lat/Long: 36.9839°N, 77.0072°W). Chesapeake is outlined in black.

of shapefiles used per day ranged from zero (no polygons extending into Chesapeake) to eight. Next, all 3-hr PA grids were reclassified using a model that reassigned "no-data" values a new value of zero (Figure 30). This step was needed because a no-data pixel value in any of the 3-hr PA grids excluded that pixel in the final product but zero provided a real value. Once converted and reclassified, all 3-hr PA grids were clipped to the extent of Chesapeake's boundary and resampled to 30m pixels. The clipped 3-hr PA grids were then added together to create WPA grids using overlay analysis in ArcGIS v.9.1, Spatial Analyst extension.

The final step in creating WPA grids was to normalize and rescale (0-100) precipitation values (X_{rp}) using Equation 7 (Figure 31). I was unable to find weekly or monthly historical minimum and maximum PA for any of the three nearby weather stations (i.e., KAKQ, KCPK, KORF [Norfolk International Airport]) or from the CMCC; only averages were reported. Thus, minimum (X_{min} = 0.0 in [0.0 cm]) and maximum (X_{max} = 10 in [25.4 cm]) WPA values for Chesapeake were based on information provided during a personal communication with Evan Stewart (Meteorologist, WVEC Television [March 2006]).

Weekly Abundance Maps

Spatially explicit weekly maps that predict abundance of *Cs. melanura* during eight different periods (Appendix I) were produced in a GIS (using ArcGIS v9.1). Periods were not selected randomly, but were chosen to represent the variation in AWAT and PA.

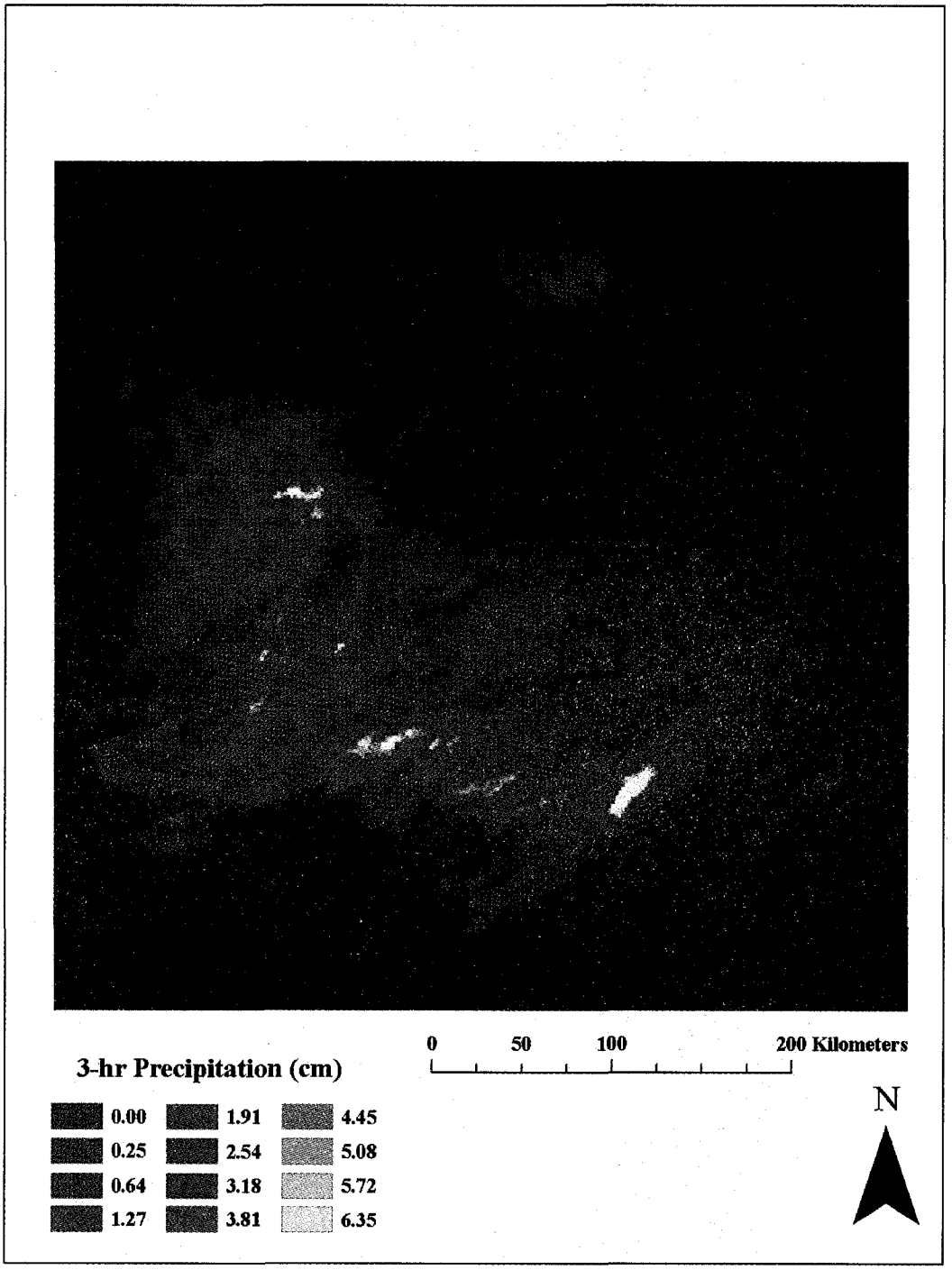

Figure 30. Sample of NEXRAD 3-hr precipitation accumulation reclassified (No data = 0) grid. Chesapeake is outlined in black. NAD-1983, State Plane, Virginia (South), FIPS-4502 Ft. Projection: Lambert Conformal, Conic (14 May 2005 [0214-0514 EST]).

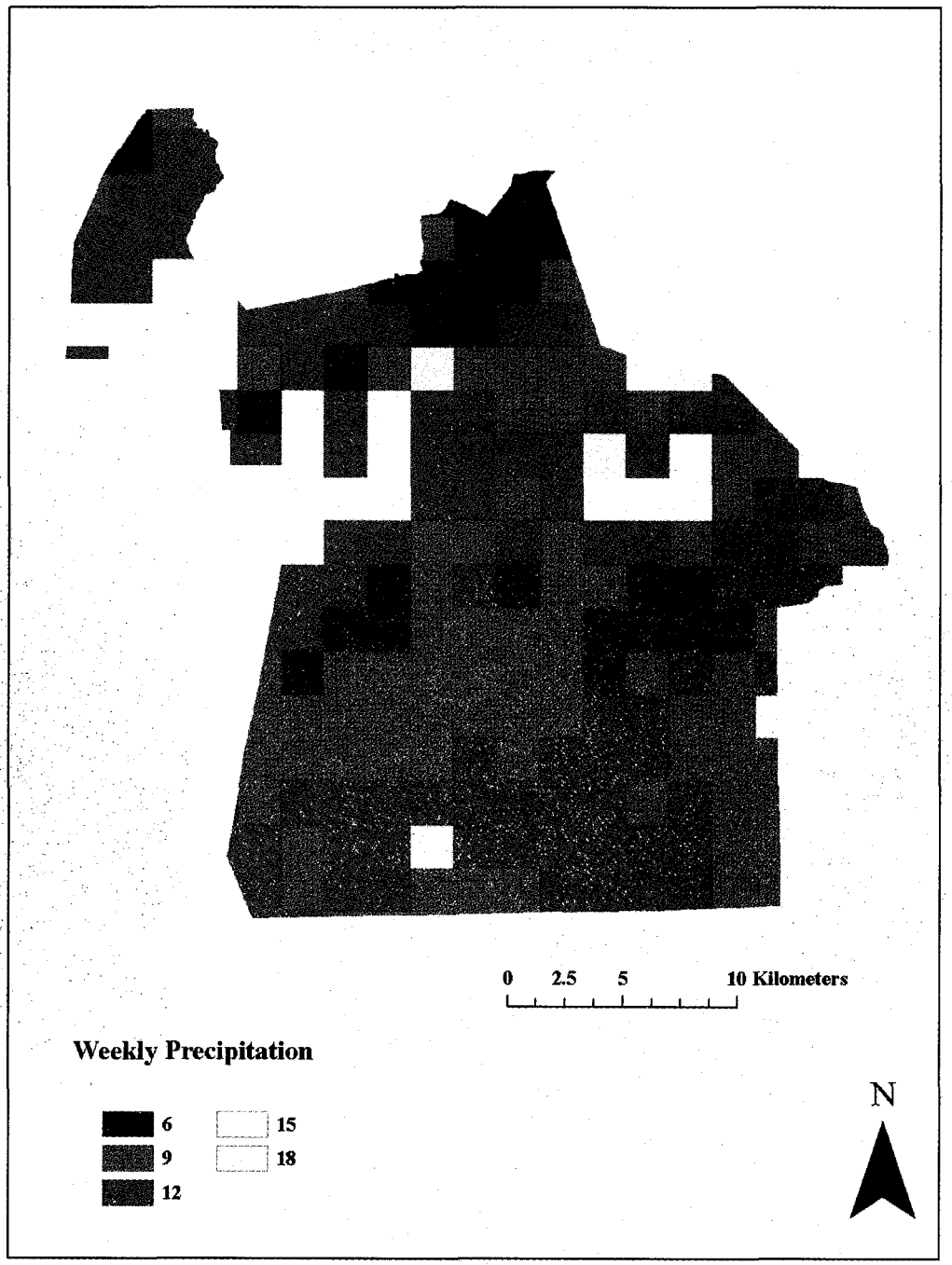

Figure 31. Final resampled NEXRAD-based precipitation accumulation grid. Pixel (30m x 30m) values represent precipitation accumulation for the week of May 14 – 20, 2006. Precipitation values were calculated using Equation 7 and weighted using the partial *R* value for precipitation (0.372) from the time-lag regression model (Table 20).

First, weekly maps representing the combined influence of calculated soil moisture (TMI), AWAT, and 2-week lag time PAs were generated on a pixel-by-pixel basis using an arithmetic overlay operation in ArcGIS v.9.1, Spatial Analyst extension with following equation:

Equation 8: $$WSC_{WR} = (TMI \times R_{TMI}) + (X_{rt} \times R_{AWAT}) + (X_{rp\text{-}2} \times R_{WPA}) \times 100$$

Where WSC_{WR} = the combined and weighted influences on *Cs. melanura* abundance for weighted TMI, AWAT, and WPA, TMI = the rescaled (0-100; Equation 5) TMI grid pixel values, R_{TMI} = the regression coefficient for the TMI, X_{rt} = the rescaled (0-100; Equation 6), constant-value, AWAT grid pixel values, R_{AWAT} = the partial regression coefficient for AWAT, $X_{rp\text{-}2}$ = the rescaled (0-100; Equation 7) WPA grid pixel values (for the 2-week lag-time model [Figure 32), and R_{WPA} = the partial regression coefficient for total WPA.

Final weekly abundance maps (grids) were created on a pixel-by-pixel basis with a spatial overlay operation using the following generalized equation:

Equation 9: $$Y_{AW} = HSI_{CM} \times WSC_{WR}$$

Where Y_{AW} = predicted weekly predicted adundance for *Cs. melanura* and HSI_{CM} = the rescaled pixel values (0-100) for habitat suitability determined in Chapter I (Figure 33) of this dissertation. Equations 8 and 9 are visually displayed in Figure 34. Following the overlay operation, final weekly abundance maps were reclassified into three equal intervals.

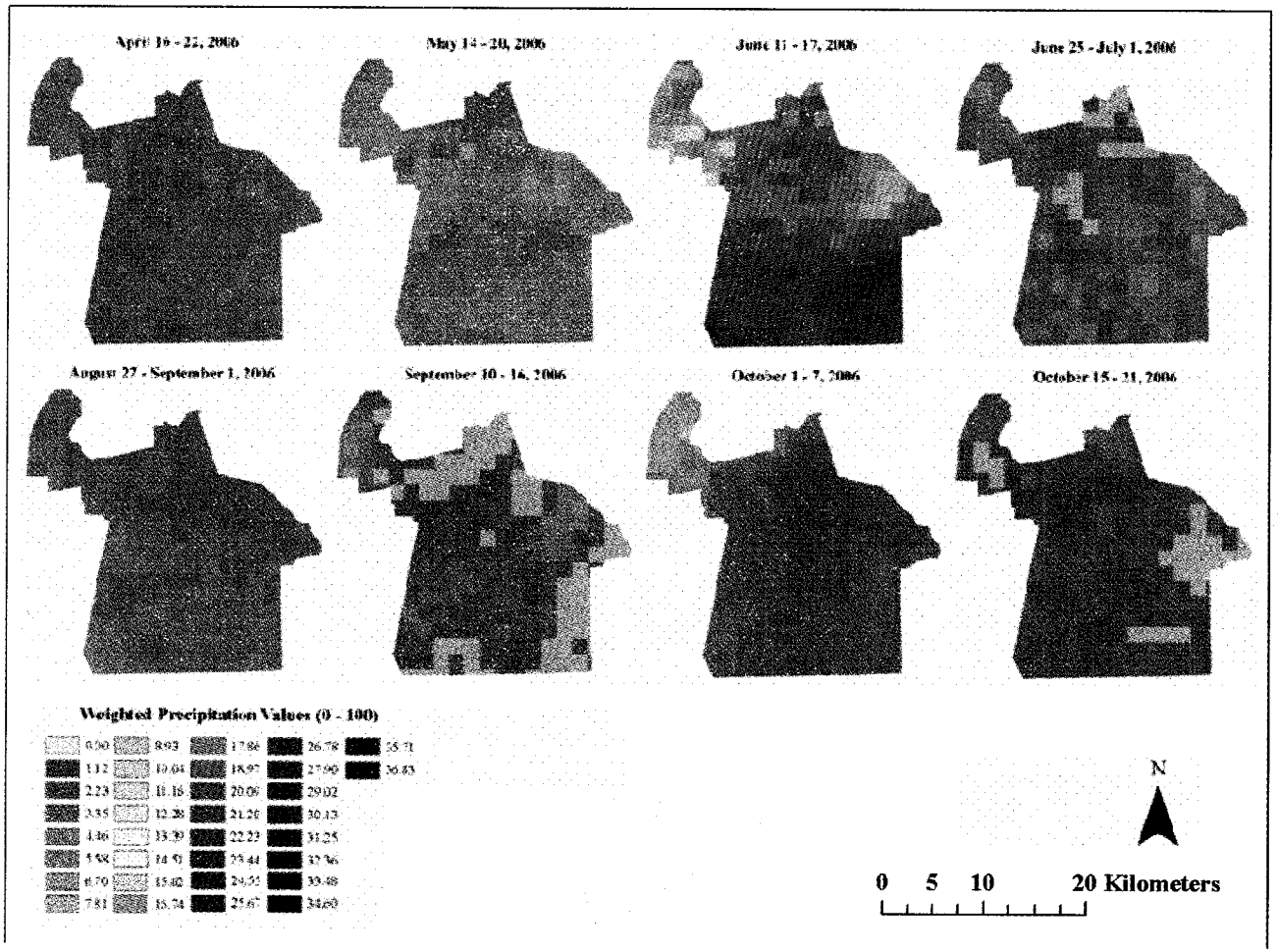

Figure 32. Pixel values for the eight final NEXRAD-based (weighted) weekly precipitation accumulation grids. Weeks specified in Appendix I. Pixel values were calculated using Equation 4 and weighted using the partial *R* value for precipitation (0.372) from the time-lag regression model (Table 20).

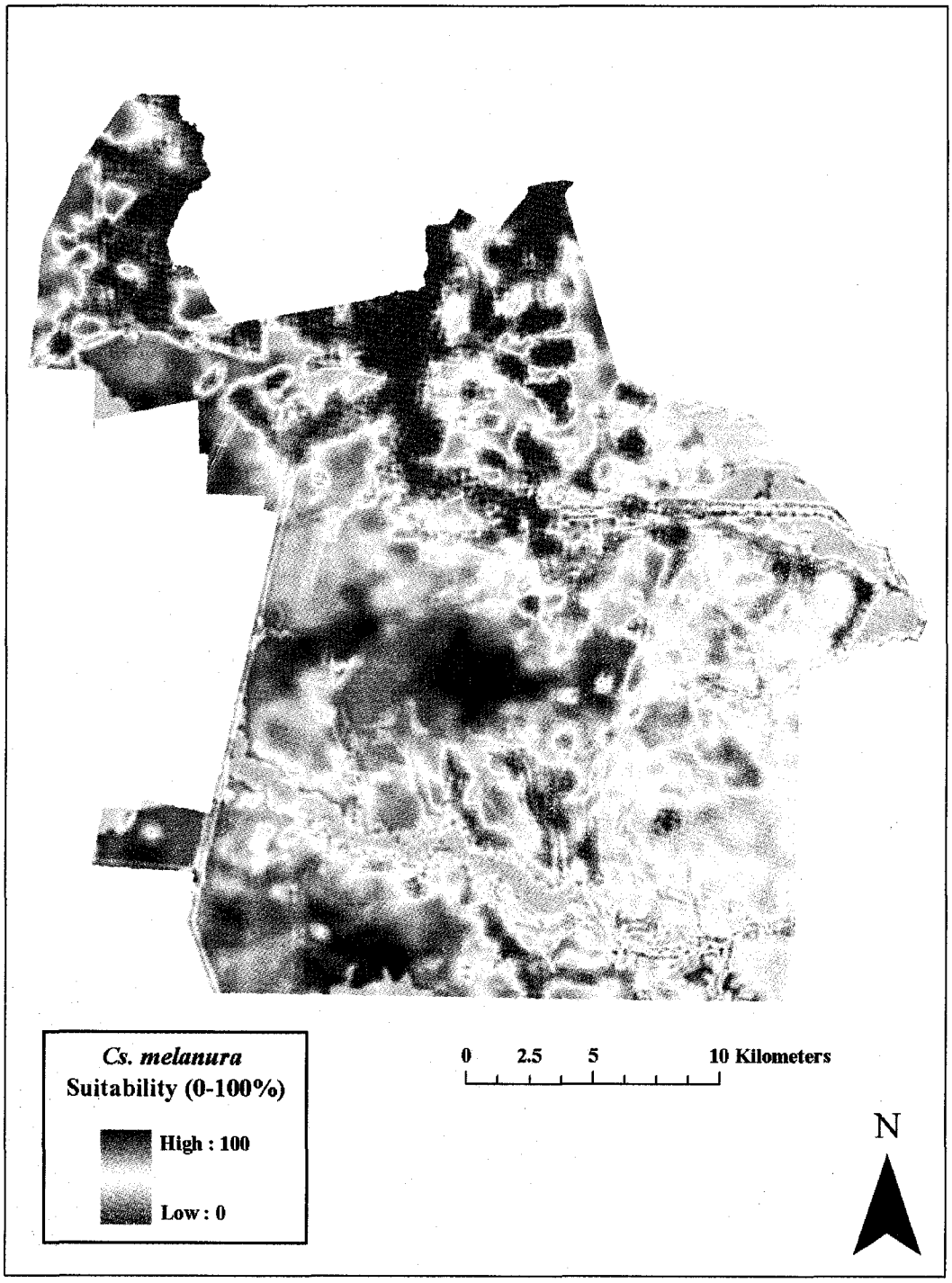

Figure 33. Rescaled (0-100) Habitat Suitability Index for *Cs. melanura* generated in Chapter II.

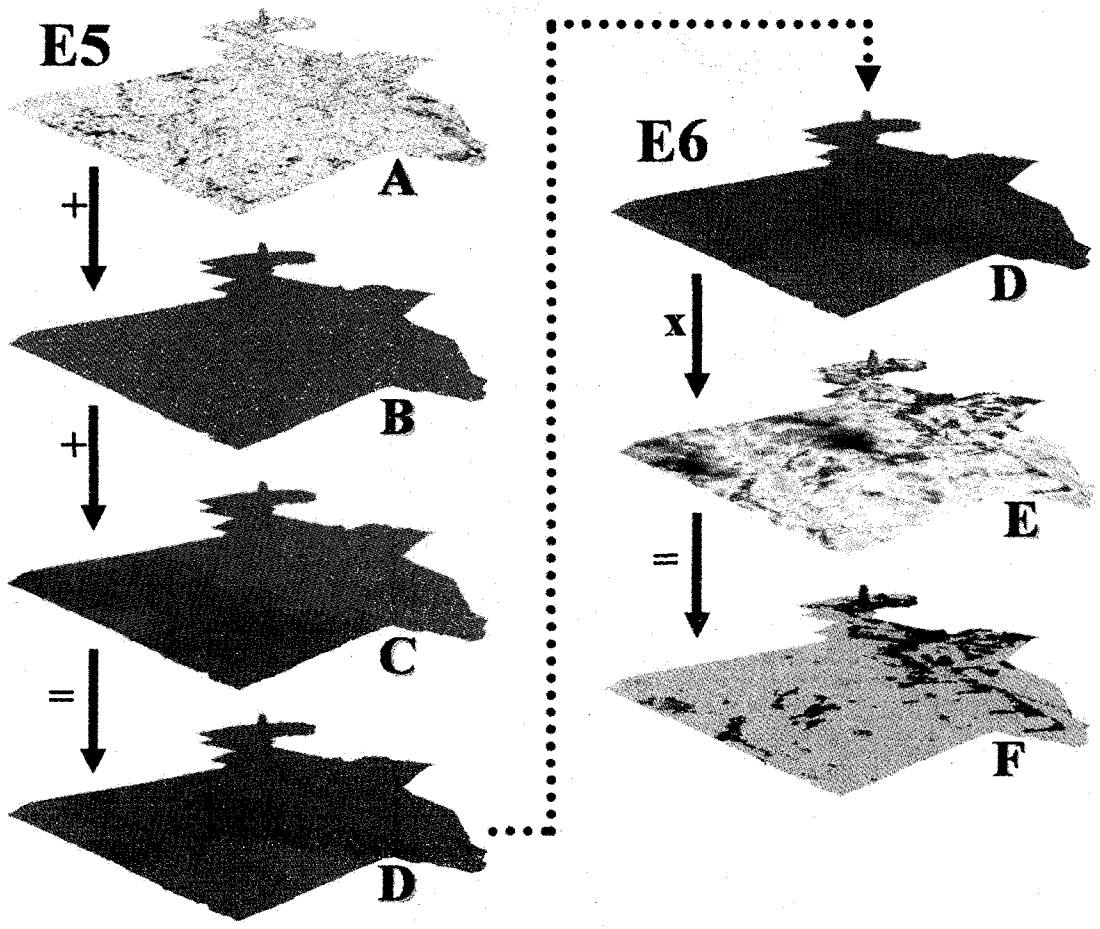

Figure 34. Summary of generic arithmetic operations, components, and products for Equations 8 and Equation 9: A) weighted topographic soil moisture index [TMI x R_{tm}], B) weighted [constant-value] average weekly temperature grid [X_{rt} x R_{ATW}], C) weighted weekly precipitation accumulation grid [$X_{rp\text{-}2}$ x R_{PAW}], D) the combined influences on *Cs. melanura* abundance for A – C [WSC_{WR}], E) the rescaled habitat suitability grid [HSI_{CM}] determined in Chapter I of this dissertation, and F) the final product [Y_{AW}], the weekly predicted adundance for *Cs. melanura*. Input grids used are for peroid 3 (Appendix I).

Results

Captures

Of the 46 permanent mosquito-trapping stations, 28 were located in or near (<200m) palustrine wetlands, the primary breeding habitat of *Cs. melanura*. This number increases to 38 traps at 400m, a distance well within the potential dispersal distance of *Cs. melanura*. Of the remaining trapping sites, six were located in or near (<200m) estuarine wetlands and two were in uplands; no traps were located in or near lacustrine or riverine wetlands. These locational assessments were made using System-Level National Wetland Inventory maps (USFWS, 2006).

In all, 275,726 female mosquitoes, representing the 29 CDC-listed EEE and WNV vector species (Appendix F), were captured by the CMCC in 2004. Of these, 171,071 (~62%) were *Cs. melanura* (Figure 35).

There was no significant difference in mean captures of *Cs. melanura* at trapping sites between 2003 and 2004 ($P = 0.325$, $F = 0.99$, $df = 60$ [Table 19]). In addition, captures of *Cs. melanura* at individual trapping sites common to both 2003 and 2004 were positively correlated ($R = 0.812$ [Table 19]). Results of these analyses indicate that both spatial and temporal similarities in capture patterns at trapping sites between the two years are sufficient to justify the analysis of 2004 capture data only.

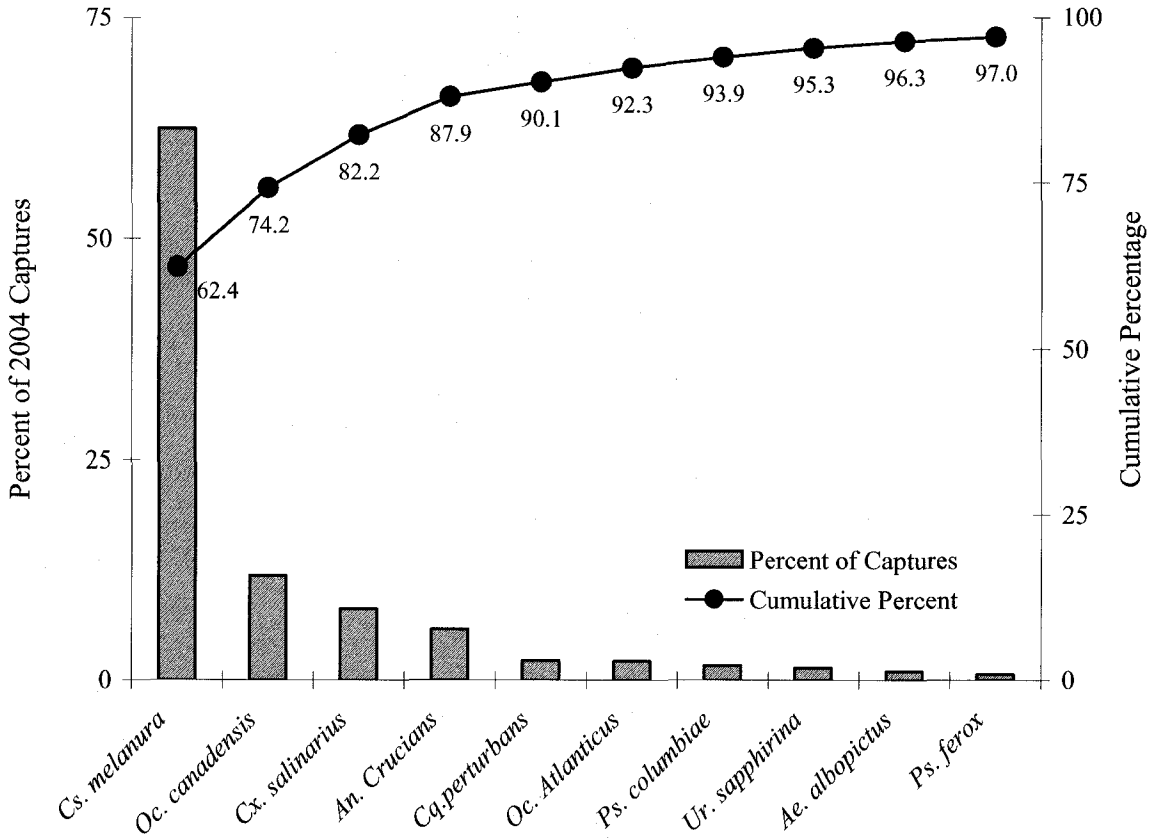

Figure 35. Summary of the cumulative numbers of the 10 most common mosquito species. The first Y-axis (left) represents the percent of total of captures of the 10 most frequently collected mosquito species by the CMCC from April through October, 2004. The second Y-axis (right) represents the cumulative percent of 2004 total captures as each species is added.

Table 19. Results the *a priori* single-factor ANOVA used to determine if there were differences in captures of *Cs. melanura*, by trapping site, between 2003 and 2004. Mean capture/TN and standard error are provided for each year. Pearson's correlation coefficient for captures/TN of *Cs. melanura* at individual trapping sites common to 2003 and 2004 is also provided.

ANOVA

Source	*df*	SS	MS	*F*	*P*
Groups	1	49,483	49,483	0.99	0.325
Trapping Sites	58	2,793,446	48,162		
Total	60	2,840,929			

2003 mean =	178.3
2003 Std Error =	46.7
2004 mean =	121.0
2004 Std Error =	32.1
Correlation Coefficient (*R*) =	0.812

Table 20. Summaries of multiple regression results for the six time-lag intervals. Values describe the relationships between captures of *Cs. melanura*[§] and the independent variables weekly precipitation accumulation (PA) and average weekly air temperatures (AWAT). Regression parameters (i.e., observations [week = 1], degrees of freedom [*df*]) and *P* values (significant values are underlined) regression equation coefficients and partial *R* values (i.e., Intercept, Precipitation, Temperature), and variance inflation factors (VIF) are provided.

	1-week lag	2-week lag	3-week lag	4-week lag	5-week lag	6-week lag
	0.519	0.585	0.529	0.390	0.358	0.433
R^2	0.269	0.342	0.280	0.152	0.128	0.188
RMSE	375.03	348.33	361.65	385.30	399.03	385.87
Observations	30	29	28	27	26	25
df	29	28	27	26	25	24
F	4.969	6.757	4.658	2.237	1.690	2.539
P	0.014	0.004	0.019	0.128	0.207	0.102
Intercept	-493.50	-422.51	-310.68	-289.87	-227.63	133.58
VIF	1.11	1.06	1.06	1.00	1.02	1.02
PA[†] (partial *R*)	-0.015	0.372	-0.366	-0.006	0.011	-0.292
PA[†] (equation)	-5.027	120.79	-123.29	-1.79	3.54	-99.69
AWAT[††] (partial *R*)	0.523	0.371	0.482	0.390	0.356	0.284
AWAT[††] (equation)	51.18	38.69	52.36	42.45	39.82	32.25

[§]Regressed against current average AWAT and lagged PA (1-week intervals)
[†]1-week intervals (lagged; see Table 18)
[††]1-week intervals (not lagged; see Table 18)

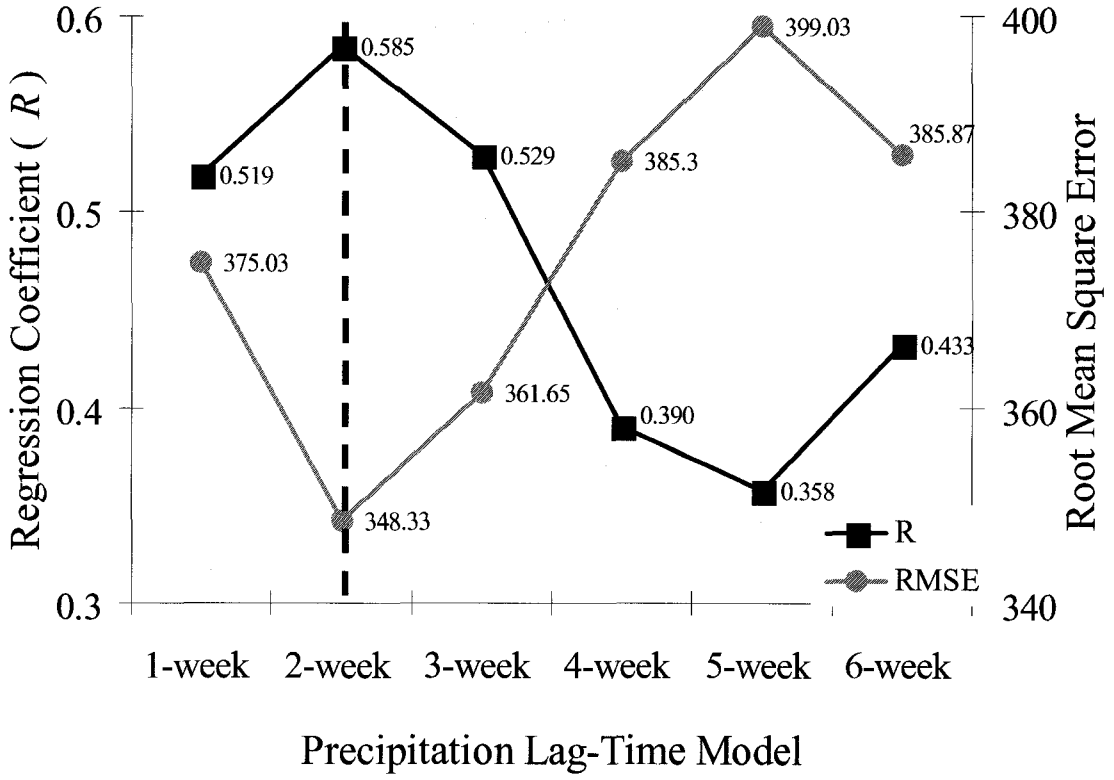

Figure 36. Summary of regression coefficients and root mean square error values for the precipitation time-lag model. The first X-axis (left) represents the regression coefficients (*R*) and the second X-axis (right) represents the root mean square error values for each the six *a priori* regression models used to test the hypothesis that fluctuations in weekly captures of *Cs. melanura* in 2004 were driven by average weekly air temperatures and recent precipitation accumulation (see Table 18).

*Weather Lag Time Analysis (*a priori*)*

Of the six time-lagged regressions that tested the hypothesis that weekly captures of *Cs. melanura* in 2004 were positively dependent on the collective properties associated with AWAT and recent PA, only three had significant ($P < 0.05$) relationships, i.e., the 1-, 2-, and 3-week precipitation lag time models (Table 20). The 2-week model had the highest regression coefficient ($R = 0.585$) and the lowest root mean squared error (RMSE = 348.33; Table 20 and Figure 36). The maximum variance inflation factor (VIF) for any

variable of the six regression models was 1.11, for the 1-week lag model. Consequently, I can assume no multicollinearity between the two independent variables. Fluctuations in *Cs. melanura* captures were best explained, with the least residual error (RMSE), by the 2-week precipitation lag-time model (Table 20; Figure 36). This suggests that the activities of *Cs. melanura* are, at least in part, related to by temperature and recent precipitation. Moreover, I should now be able to transfer these relationships to dynamic (weekly) abundance models that use spatially explicit weather data (i.e., NEXRAD 3-hr PA data).

Topographic Soil Moisture Index (TMI)

A significant positive relationship was observed between mean captures/TN of *Cs. melanura* and TMI values at trapping sites ($P = 0.0015$, $F = 11.689$, $df = 39$ [Table 21]). This result, similar to the previous time-lag analysis, supports the notion that *Cs. melanura* activities are related to environmental factors that tend to increase both humidity levels and the probability of surface wetness. If so, it is feasible to integrate this relationship with the spatially explicit weather data and the more static HSI from Chapter II to create a weekly abundance model for *Cs. melanura*.

Weekly Abundance Maps

The integration of weighted static grids, i.e., HSI_{CM}, TMI (Equation 8 [$R_{TMI} = 0.485$; Table 21]), with more dynamic weighted surfaces, i.e., AWAT (Equation 8 [$R_{PAW} = 0.372$; Table 20]) and PA (Equation 9 [$R_{ATW} = 0.371$; Table 20]) resulted in the creation of weekly *Cs. melanura* abundance maps (Equation 9) for, and based in part on, recent weather patterns. Only one of the eight weekly abundance maps (see Periods in Appendix

I) has predicted abundance of *Cs. melanura* exceeding 66% (moderate) of total potential abundance (Table 22; Figure 37).

Table 21. Regression results for the hypothesis that variation in captures of *Cs. melanura* among trapping sites is related to spatial variation in the calculated topographic soil moisture (TMI) values.

ANOVA

Source	*df*	SS	MS	*F*	*P*
Intercept	1	82,476.3	82,476.3	11.689	0.0015
Model	1	447,270.2	447,270.2		
Error	38	1,454,039	38,264.2		
Total	39	1,901,309	48,751.5		

Root Mean^2 Error =	195.61
R =	0.485
R^2 =	0.235
Y-intercept =	130.78
TMI coefficient =	64.07

Table 22. Summary of abundance values, including descriptive statistics, for the eight selected Periods. Refer to Figure 37 and Appendix I. Abundance: Low = 1-33%, Moderate = 34-66%, 67 = 100% of maximum potential weekly abundance for *Cs. melanura*.

Period[†]	1-33%[†]	34-66%[†]	67-100%[†]	Mean	Std Dev
A	96.68	3.32	0.00	34.10	5.91
B	67.88	32.12	0.00	43.60	15.41
C	21.55	77.66	0.79	59.16	14.04
D	61.02	38.98	0.00	45.86	16.09
E	85.72	14.28	0.00	33.71	11.55
F	93.05	6.95	0.00	35.29	8.39
G	97.49	2.51	0.00	33.83	5.16
H	99.85	0.15	0.00	33.05	1.29

[†]Value based on 768,696 (30m x 30m) pixels.

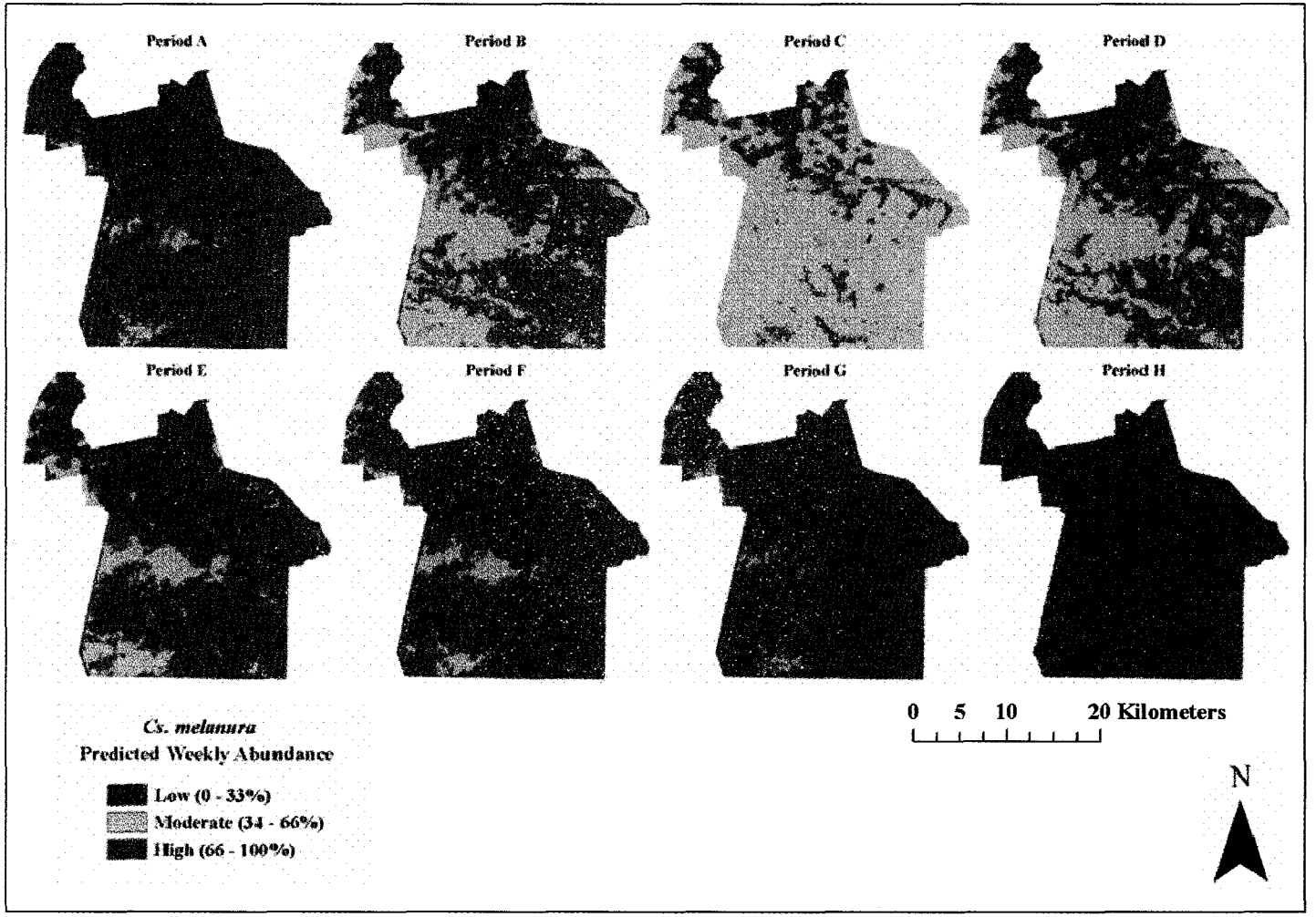

Figure 37. Final predicted weekly abundance grids for *Cs. melanura*. This includes Periods A-H (Appendix I) calculated using Equations 8 and 9. Classifications for low, moderate, and high predicted abundances are shown.

Discussion

Culiseta melanura is a common and widespread mosquito of the swamps of the eastern and central United States (Andreadis, 2002). Larvae generally develop in relatively cool subterranean habitats (Mahmood and Crans, 1998; Andreadis, 2002); however, they have been collected in discarded tires, man-made ditches, and temporary pools (Spielman, 1964; Wallis and Whitman, 1967; Pitts and Holbrook, 2000). Although not a human biter, and thus not generally the subject of service requests (2,411 in 2003; CMCC, 2004), its competence as the primary enzootic vector for EEE has made *Cs. melanura* the primary focus of the CMCC's adulticide efforts. In addition to adulticide, the CMCC began an early season (leaf-off) aerial larvacide program in 2004 to reduce the first broods of *Cs. melanura*, *Aedes vexans*, and *Ochlerotatus canadensis* (CMCC, 2004).

Culiseta melanura has a life history unique among species found in the region (*Cs. melanura* type; Crans, 2004). Like most *Culex* spp., it is multivoltine (> 1 brood/yr), but unlike *Culex*, which overwinters as an adult, *Cs. melanura* overwinters as larvae (Crans, 2004). The timing of adult emergence the following year is based on when eggs were laid, at what stage larvae overwintered, and water temperatures in larval habitats (Crans, 2004; Mahmood and Crans, 1998). Considering that soil temperatures are influenced by the temperature of precipitation (Hirobe et al., 1998), it is intuitive that warming rains will increase the temperatures of sub-surface water and surrounding soils associated with larval mosquito habitats, and thus increase rates of larval development. Rainfall also increases adult flight activity and host-seeking behavior (Shaman and Day, 2005); both would be reflected in increased captures at trapping sites—the dependent variable in my study's models.

Public health officials have long understood that climate drives the overall distribution of mosquito-borne diseases, but weather affects the timing and magnitude of outbreaks (Gill, 1920, Dobson and Carter, 1993, Epstein et al., 1998). Chesapeake lies within the Coastal Plain of the mid-Atlantic region where the most significant weather patterns are associated with storms. Between 1942 and 1984, nearly 1,350 powerful Atlantic storms have been recorded (Dolan et al., 1987). Many of these storms develop in the westerly wind belt of the middle-latitudes of the Atlantic Ocean, and therefore, are extratropical storms, or 'northeasters.' Another type of coastal storm forms over warm, tropical waters; these storms include hurricanes and the less powerful tropical storms (Dolan et al., 1988). Although these storms are rare compared to weaker storm systems, the energy and rainfall they deliver has a lasting influence on ecological processes, landscape configuration, and plant community structure (Young et al., 1995). Storms are often followed by a proliferation of mosquitoes, including *Cs. melanura* (Nasci and Moore, 1998), which can exploit additional breeding habitat resulting from heavy precipitation and subsequent increases in near-surface wetness and humidity that expand saturated lowlands (Shaman and Day, 2005).

Although mosquito abundance and the transmission of mosquito-borne pathogens are affected by hydrologic variability resulting from the spatial distribution of precipitation, and thus potential habitat, direct associations based on weather patterns alone are difficult to establish (Shaman and Day, 2005). The ability to map when, where, and how much precipitation occurs needs to be supplemented by the capability to model the settlement of water. Thus, the accuracy of surface wetness models is improved by incorporating topography and soil characteristics (Shaman and Day, 2005).

The TMI (after Beven, 1997) enabled me to model the distribution of areas in the landscape that are most prone to surface moisture. Because soil and vegetation characteristics were incorporated in the HSI for *Cs. melanura* (Chapter II), their reuse in my soil moisture index would be redundant. I was able to further improve the accuracy of the TMI by integrating the extensive drainage ditch network used in the hydrologic model by applying a stream-burning technique. This added both physical and ecological strength to the overall abundance models. Physically, the effect of ditches on Chesapeake's hydrology was captured and reflected in the TMI. Ecologically, it resulted in the formation of higher quality man-made mosquito habitat in otherwise inhospitable areas. Chesapeake was once largely covered by the forested wetlands of the Great Dismal Swamp, but much has been, and continues to be, ditched for farming and urban/suburban development. This network of ditches, now covering much of the city, was shown to be important habitat to *Cs. melanura* in Chesapeake (see Chapter II).

The positive relationship between extracted TMI values and *Cs. melanura* captures at trapping sites in my study was expected. This expectation was based to the proven efficacy of the soil moisture models of Beven (1997) and Iverson et al. (1997) and a well-documented dependence of mosquitoes on standing water.

Considering the meteorological and other affinities (described above), the positive relationships between *Cs. melanura* abundance and both warm temperatures and increased precipitation in my study was expected. This finding is further supported by Mahmood and Crans (1998), who found that the rate of larval development was temperature-dependent. My finding that *Cs. melanura* has a ~2-week delayed response to

precipitation accumulations is supported by Shaman et al. (2002), i.e., a 10-day lag was most effective in a similar model.

Fluctuations in *Cs. melanura* captures were best explained, with the least residual error, by the 2-week lag-time model (Table 20; Figure 36). This suggests that the activities of *Cs. melanura* are, at least in part, related to temperature and recent precipitation. With these affinities and response times statistically established, and further supported in the literature, their transference to weekly *Cs. melanura* abundance models that use the static habitat suitability index (from Chapter II), TMI and AWAT grids and spatially explicit precipitation data (i.e., NEXRAD 3-hr PA data) is justifiable.

Few studies have used NEXRAD data for modeling the habitat or abundance of organisms dependent on the distribution of surface water; most involve the movements of migratory birds (summarized in Diehl and Larkin, 2005). There are, however, many studies that use NEXRAD to model hydrology or to predict flooding or weather patterns (Bieringer and Ray, 1996; Bedient et al., 2000; Bedient et al., 2003; Whiteaker et al., 2006, among others). These latter applications of NEXRAD are similar to mine—the prediction of areas within the landscape most prone to surface wetness.

Besides being readily available and free, NEXRAD Level-III (WSR:88D) data can be downloaded in several commonly used spatial formats (e.g., ASCII, ArcView shapefile, GeoTIFF). The only real limitation to NEXRAD data is the 1-km pixel size. A smaller pixel would have allowed more fine-grained results in weekly abundance maps, but one kilometer is well within known flight ranges for *Cs. melanura* (Turell et al., 2005).

The primary benefit of the use of NEXRAD 3-hr PA data was the addition of a near real-time component to weekly abundance maps. The eight Periods (A-H; Appendix I; Figure 37) were not selected at random, but instead are intended to represent the range of temporal and spatial variation in predicted *Cs. melanura* abundance throughout the trapping season based on fluctuations in air temperature and precipitation accumulation. TMI and HSI values are static and do not change each week, but temperature and precipitation usually do. From these images (Figure 37), the effects of dynamic meteorological data on the distribution of *Cs. melanura* become evident. Two general and expected patterns arise. First, increases in predicted abundance tend to occur concentrically from core areas where HSI values are high (Figure 33). Second, and a function of the first pattern, as temperature and precipitation increases (Figure 32, Appendix I), areas of moderate predicted abundance became less disjunct (Figure 37). As expected, areas with high predicted abundance were, by far, the least common, and among the eight Periods, only occurred in small isolated pockets during Period C. Thus, areas with these elevated abundance values require both high temperatures and copious rainfall in order to develop.

Management Implications

Enzootic viral transmission cycles often are found in specific rural habitats where they can go largely undetected by most monitoring programs (Moore et al., 1993). This is especially true when vector species are not human biters, and thus are not frequently reported. When coupled with favorable weather and environmental conditions, viral amplification cycles can develop in *Cs. melanura* populations, and can increase in both

intensity and spatial distribution, leading to potential epizootic outbreaks (Moore et al., 1993). Thus, from a prevention and control standpoint, it is critical that mosquito control agencies such as the CMCC have the ability to rapidly track the spatial and temporal distributions of potential arboviral vectors such as *Cs. melanura*. My weekly abundance models (maps) provide this ability. Weekly maps can be prepared quickly using a series of sub-models I created in ArcGIS ModelBuilder. These sub-models perform arduous data preprocessing in streamlined and user-friendly menus. Most of the data needed are either free (e.g., NEXRAD, NHD, DEM, weather summaries) or generated by the agency itself (e.g., capture data). In addition, weekly maps are not hindered by biases associated with human population densities and residential complaints. They do, however, give the CMCC the ability to respond quickly to distributional changes of *Cs. melanura*, thus lowering transmission potential in nearby suburban and urban areas.

CHAPTER IV

SPATIALLY EXPLICIT PROTOCOLS FOR THE CONTROL OF *CULISETA MELANURA* (COQUILLETT) IN COASTAL-PLAIN HABITATS OF THE MID-ATLANTIC REGION

Introduction

Advances in Earth-observing sensors have resulted in the development of a wide variety of spatially explicit data applicable to the ecological study of disease vectors (Goetz et al., 2000). The development of GIS-based models of vector abundance and disease transmission using these data is now a common approach in arboviral research (Beck et al., 1994; Washino and Wood, 1994; Kaya et al., 2004; and others). As a result, surveillance, monitoring, and related public health policies associated with the study of arthropod-borne diseases (a.k.a., arboviruses) also have become more applied through the integration of epidemiological and spatial data (Clarke et al., 1996).

Although arboviruses have threatened public health in North America since Colonial times (Fischer and Schweigmann, 2004; Andersen, 2006), new diseases appear from time to time. One such mosquito-borne arbovirus in the mid-Atlantic region (MAR) is eastern equine encephalitis (EEE; Hassan et al., 2003). First isolated in North America in 1933 during simultaneous human outbreaks in Delaware, New Jersey and Virginia, EEE persists in the eastern North America, the Caribbean, and South and Central America (Weaver et al., 1999). Because of the relatively long history of association with North America, the epidemiology for EEE is well understood.

EEE foci are associated with freshwater swamps, the preferred habitat of the primary reservoir vector, *Culiseta melanura* (Weaver et al., 1999). Swamp-dwelling passerine birds are the dominant reservoir hosts (Komar et al., 1999). Once enzootic transmission is established, the virus becomes available to epizootic bridge vectors such as *Coquillettidia perturbans* and *Aedes vexans*, which readily feed on mammals as well as birds (Hassan et al., 2003).

The purpose of this chapter is to provide the reader and potential users with the necessary protocols for modeling the spatial and temporal abundance and distributions of mosquitoes, with emphasis on *Cs. melanura*, in a real-world coastal landscape of the MAR. Because most mosquito-control and public health agencies are unable to conduct exhaustive *in situ* monitoring and environmental data collection, they would benefit from the application of models capable of predicting the temporal and spatial distributions of mosquitoes at a landscape-scale (Shaman et al., 2002). My study produces such a potentially useful series of models.

The intended audience for this final chapter is primarily GIS analysts employed by mosquito-control and public health agencies. In addition, environmental managers and decision makers of these agencies with limited experience in spatial modeling could use these protocols to make decisions regarding mosquito monitoring and control practices.

In Chapter II of this dissertation, a set of scale-dependent habitat suitability indices (HSI) for mosquito species based on the "Hutchinsonian-niche concept" (Hutchinson, 1957) was constructed using spatially explicit habitat data (e.g., satellite imagery derivatives, soil surveys). This approach required the development of baseline classification models capable of identifying and ranking suitable habitat-based

environmental characteristics. These models, generated from inferential statistical models (i.e., multiple linear regression) and formatted for use in a GIS, are used to predict areas, or "patches," within the landscape in which mosquitoes are most likely to be abundant. Much attention was devoted to keeping the models streamlined, user-friendly, and not cost-prohibitive, while retaining the ability to process empirical data in real landscapes.

Chapter III augmented the semi-static HSI model generated in Chapter II with a dynamic GIS-based model using weather patterns and a topographic soil moisture index. This "dynamic" model is capable of predicting *where* and *when* adult *Cs. melanura* are likely to emerge in large numbers. The final products were weekly "predicted-abundance" maps that give mosquito-control agencies the ability to respond quickly to landscape-level changes in mosquito distributions using information from temperature and rainfall patterns.

Chapters II and III are designed for publication as separate entities. This chapter cogently summarizes the technical procedures of Chapters II and III together, with enough detail and background, for the recreation of a seamless series of models for predicting mosquito outbreaks. With the knowledge of how to apply these models (details to follow), mosquito-control agencies can pursue cost-reducing strategies that consider both spatial and temporal mosquito abundances at large spatial scales, e.g., the city of Chesapeake, an area of ~900km^2.

Because of similarities in climate and mosquito assemblages, this sequence of models should be effective throughout coastal-plain and lower-piedmont areas in the MAR. However, the potential for portability of these models to upper piedmont and montane regions of the MAR would need to be tested because of effects of elevation

from an ecological perspective. Higher elevations replicate higher latitudes and generally have different organismal assemblages. This is, in part, due to differences in climate (e.g., cooler temperatures, shorter active seasons) as well as differences in the mechanics of surface water distribution (e.g., soil type, slope, runoff and drainage potential). For example, *Cs. melanura* is found in lowland swamps throughout the MAR, but its range does not extend into the Appalachian range (Crans, www-rci.rutgers.edu).

In summary, this sequence of models should be useful to mosquito-control agencies because it consist of a series of robust components designed to use real-world data. First, the scale-appropriate HSI will establish a baseline model for mapping mosquito habitat. Secondly, the spatial integration of recent rainfall and temperature data will aid in locating, in near real time, which areas are the most likely to experience mosquito outbreaks in the coming days. This should lead to the development of environmentally sensitive strategies that will not only lower chemical and manpower costs by increasing the efficiency of control efforts, but also reduce transmission risks of mosquito-borne diseases such as EEE and West Nile virus (WNV). In addition, the software used for these models (i.e., ArcGIS) is the industry standard, and the data used (excluding capture data) are readily available and, in most cases free, making the use of these models by mosquito control agencies economical.

Methodologies

Study Area

These models were constructed with the cooperation of the Chesapeake Mosquito Control Commission (CMCC), Chesapeake, Virginia. Located in the Coastal Plain

physiographic region (Figure 1), the climate of Chesapeake is humid subtropical and similar to the rest of Virginia east of the Blue Ridge Mountains (Woodward and Hoffman, 1991). Monthly temperatures range from –1.8 (January) to 31.6 C (July) based on 30-yr averages (1971 – 2000; NCDC, 2002) collected at National Weather Service (NWS) Station KAKQ, Wakefield, Virginia located at Wakefield Municipal Airport (Lat/Long: 36.9839°N, 77.0072°W), about 50 km west of Chesapeake. Temperature extremes are ameliorated by proximity to the Chesapeake Bay and the Atlantic Ocean. Annual average precipitation is 114.4 cm (45.05 inches) based on 30-yr averages (1971 – 2000; NCDC, 2002). The growing season (frost-free days) for the region is 185 – 200 days (Palone and Todd, 1998).

Chesapeake was selected for study because: 1) the structure of the landscape is representative of the regional diversity of land use in the MAR, 2) although recently established (2003), the CMCC is using advanced mosquito-control technologies, and 3) of the occurrence, within the city, of ~30 mosquito species listed as potential vectors of EEE and WNV (Appendix A) by the Center for Disease Control (CDC). Suitable habitat for a broad range of mosquito species, including drainage ditches, tidal and freshwater creeks, and the Great Dismal Swamp with its canals and forested wetlands, is found throughout the Chesapeake. Thus, good mosquito habitat is often found near high densities of humans, creating a landscape conducive to the transmission of EEE, WNV, and other mosquito-borne diseases.

Chapter II (Overview)

In Chapter II, linear regression models were used to predict habitat suitability for mosquitoes in all areas within the landscape based on mosquito abundance (dependent variable [described in detail below]) at associated trap sites and habitat attributes (independent variables, Table 4). More specifically, each habitat attribute constituted a spatially continuous description of landscape pattern, such as hydrology, soil moisture properties, and digital satellite imagery enhancement (e.g., vegetation index), represented in raster format.

Dependent Variables

Mosquitoes were captured with CDC (CO_2-baited) light traps stationed at 46 permanent trapping sites throughout Chesapeake (Figure 1) from early April through early November, 2004. Only captures of females were used in analyses.

Model validation using capture data for alternate years (2003 and 2005) when mosquitoes were collected would have spatial redundancies because many trapping sites sampled in 2004 were also used in 2003 and 2005. In addition, the number of trapping sites in 2003 with sufficient trap nights (TNs) was smaller than 2004, and at the time analyses were run a complete set of 2005 capture data was not yet available. These problems are addressed below (see POLICY IMPLICATIONS: Sampling section). I conducted cross-year comparisons (2003-2004) to evaluate temporal patterns consisting of pair-wise *t*-test and correlation analysis of capture data for trapping sites common to both years (Zar, 1996). This analysis defined a statistically significant trend of similarity in captures between 2003 and 2004.

Information on geographic location (coordinates) and species-level capture data for individual trapping sites were stored in a GIS in ArcView point-shapefile format. Capture data were normalized to account for variation in trapping effort among the trapping sites by dividing total captures of each species collected at each site by the number of trap nights for that site. Normalization of capture data was needed to determine relative abundances of species at various locations. For example, if 1,000 individuals were captured at each of two trapping sites, and one of the sites was sampled twice as often as the other, it could be assumed that the relative abundance of that species at that site is half of the other, less sampled, site. Relative abundances are needed to determine the influence of independent variables across large spatial scales.

It was impractical to create predicted abundance models at the species level because of the large number (*ca.* 30) of mosquito species occurring in Chesapeake that are considered to be potential disease vectors. To reduce the number of models, only abundant species and species having high vector competence for EEE or WNV (N = 11; Table 1) were used. Vector competence is based on the susceptibility of mosquito species to dissemination of disease from a host, and transmission back to a host (Sardelis et al., 2001). As the most abundant species, *Cs. melanura* (70.3% of the species modeled) was modeled separately (CSMN; Table 1) because its large numbers compared to the other species would have been overpowering. Capture data for the other 10 species were combined into four separate groups based primarily on similarities in habitat requirements and life cycles, as follows (after Crans, 2004): 1) a single "competent-vector" group (ALSP) including captures of all modeled species except *Cs. melanura*, 2)

container-breeders (CONT), 3) swamp species (SWMP, excluding *Cs. melanura*), and 4) ephemeral pool species (EPHM; Tables 1 and 3).

Independent Variables

I used digital surrogates of habitat attributes as independent variables for these models because direct measurement of habitat attributes is not practicable at the landscape level (Goetz et al., 2000). Selection of attributes for inclusion is based, in part, on the ability to accurately represent, in digital format, critical niche dimensions of mosquitoes.

Many studies have linked the presence of disease vectors to spatial and temporal vegetation characteristics via spectrally derived vegetation indices (VI) that digitally represent various attributes of vegetative cover (e.g., vegetative moisture, biomass, photosynthetic activity; Goetz et al., 2000). Soil moisture properties and hydrologic features, well known to influence the suitability of mosquito habitats (Laird, 1988), were used.

I modeled vegetation attributes using Tasseled-Cap transformation (TC; Crist and Cicone, 1984). This VI was used in lieu of other, more commonly used VIs such as Normalized Difference Vegetation Index (a.k.a. NDVI), because its algorithms compute spectral information pertaining to soil and vegetation characteristics from all six Landsat bands, whereas most VIs use only red and near-infrared bands. It is important to note that algorithm coefficients are different for the different Landsat satellites (e.g., MSS, TM, ETM+) and they are easily calculated on ArcGIS ModelBuilder and Erdas Imagine software programs. Tasseled-Cap transformation reprojects data onto three orthogonal axes (components) that are known to correlate with suitable habitats of arbovirus vectors

(Beck et al., 2000): TC1 (brightness [soil characteristics]), TC2 (greenness [vegetation characteristics]), TC3 (wetness [soil and vegetation characteristics]).

Landsat-7 ETM+ was used because it is readily available, recognized by most applicable software packages (e.g., ESRI products, Erdas IMAGINE), and relatively inexpensive. Potential sources for Landsat imagery include: United States Geological Service (USGS) Earth Resources Observation and Science (EROS), NASA's Landsat Science Office, and the Virginia View program at Virginia Tech. The ETM+ image, dated 29 July 2002, represents the peak of the CMCC's mosquito trapping season.

Soil moisture variables were derived from SSURGO (Soil Survey Geographic) data that were exported in ArcView polygon shapefile format, free of charge, from the United States Department of Agriculture (USDA), Natural Resources Conservation Service's Soil Data Mart.

There are challenges associated with incorporating SSURGO spatial data into a GIS. Raster data are limited to a single value per pixel; however, SSURGO map units are made up of one or more named soil types (components), each with a distinguishing suite of properties. Thus, thematic representations of the soil properties of map units describing suitable mosquito habitat were created by pooling the properties (e.g., weighted averages, Table 7) of each component as a function of the percent of map unit composition. Pooling component properties enabled the creation of a continuous single-value-per-pixel raster surface for soil properties associated with mosquito breeding habitats (Laird, 1988).

A hydrologic features variable was constructed using two polygon shapefiles: the National Hydrology Dataset ([NHD, 2002] USGS) and a digitized map of the canals and ditches of Chesapeake provided by the CMCC. These shapefiles were overlaid to create a

single polygon shapefile, and then converted to a binary grid of Chesapeake water bodies (i.e., water = 1, not water = 0).

The impact of factors influencing landscape-level patterns, processes, and functions is scale-dependent (Turner, 1989). I accounted for this issue by creating a series of grids for each habitat-attribute raster by aggregating pixel data to increasingly larger scales (1 x 1 through 21 x 21, 30-m/side pixels, odd numbers only [Table 5, Figure 2]). ArcGIS ModelBuilder was used to generate this multi-stepped model that: 1) created a new set of raster layers for each independent variable, one for each of the 11 scales, and 2) extracted values from these new rasters that correspond to locations for each of the 46 trapping sites into a new shapefile (Figure 38).

Data for TC and soil property derivatives were aggregated using a moving-window function that replaced raw attribute values with the focal neighborhood mean of all pixels within their respective spatial scales. A similar function was used to generate focal neighborhood sums for quantifying the spatial density in binary data layers (e.g., water = 1, not water = 0).

Model Analyses

I needed to determine that the 11 spatial scales were statistically autocorrelated (interdependent), and that the interdependencies exceeded the maximum aggregation resolution (Table 5) in order to treat differing spatial scales as the same independent variable. To justify potential multiple-scale models, I performed a preliminary analysis to determine the range, or "on the ground" distance, of spatial autocorrelation associated with each independent variable (Table 10).

I used Pearson's correlation analysis (captures vs. extracted raster [point] values) to determine the scale at which each mosquito species group responded most strongly for each independent variable (Figure 39). These results were used to reduce the number of scales per variable for all possible regressions (APR) to one, thereby determining the pool of independent variables, including the scale of representation most important to each species group. Final selection of independent variables from this pool, for each species group, was based on a combination of high R^2-values and low root mean^2 errors in APRs.

Multiple (linear) regression models were used to quantify habitat suitability, pixel-by-pixel, based on the most parsimonious set of independent variables as determined by APR models. A habitat suitability map for each species group was produced in a GIS (using ArcGIS v9.1) using linear regression equations to perform arithmetic overlay operations. Standardized raster-formatted data layers for each independent variable (described above) were weighted using the associated partial regression coefficients (b), and overlaid using the generalized equation below (Equation 2). Following the overlay operation, final maps were ranked for suitability, i.e., percent predicted mosquito abundance (Y).

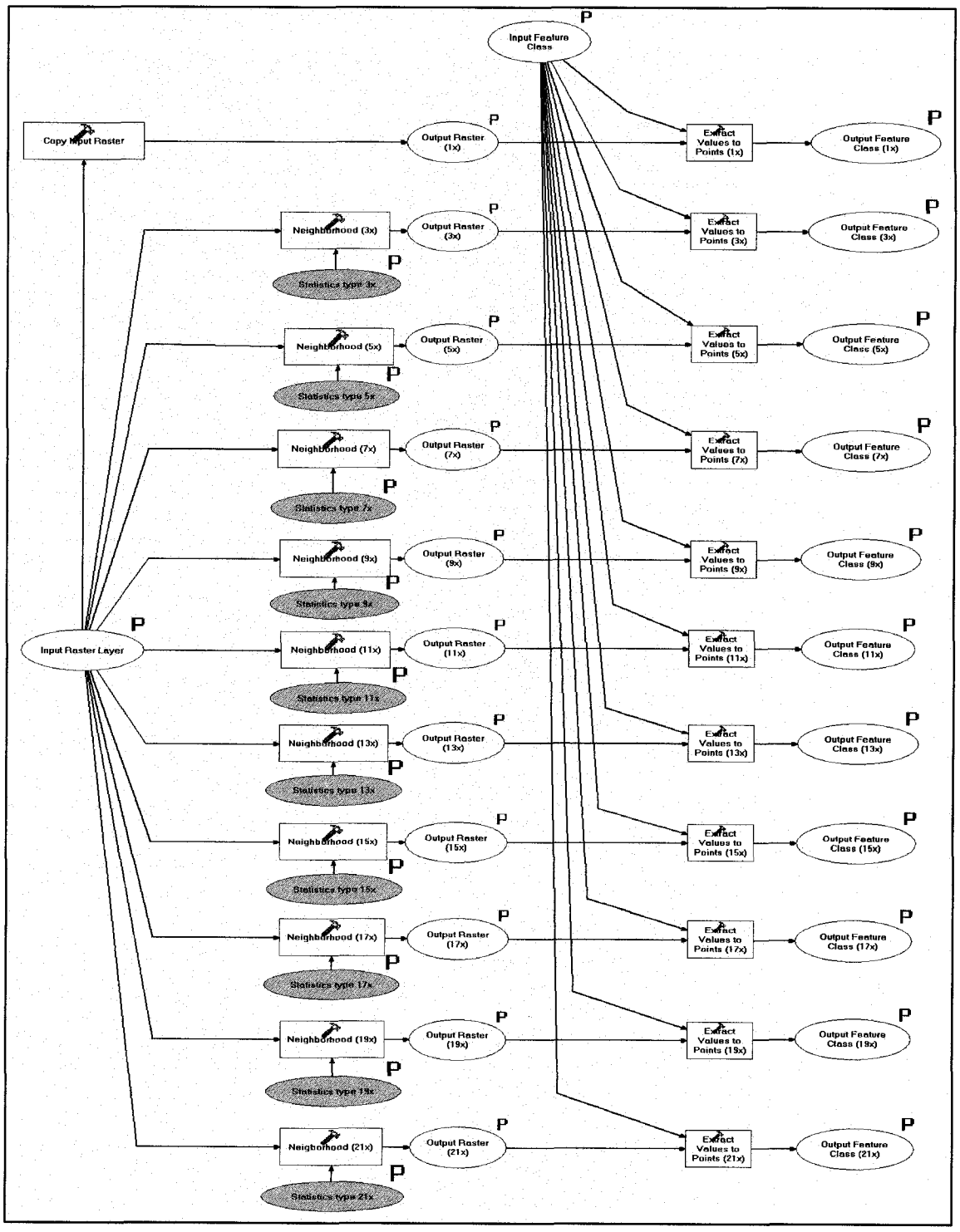

Figure 38. ArcGIS Modelbuilder model used to extract values from independent variable rasters coincident with the 46 trapping sites. Final outputs are a set of point shapefiles, with the aggregated values from rasters at each of the spatial scales specified in Table 5.

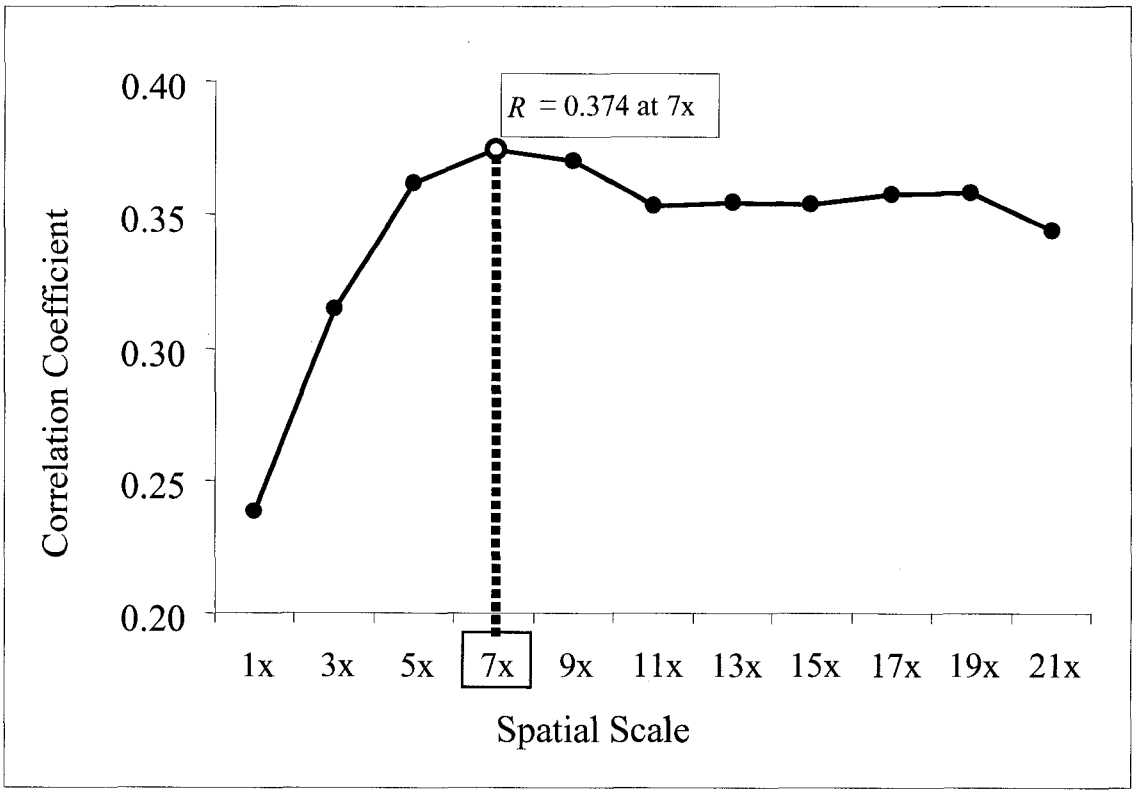

Figure 39. An example of a plot used to determine the most influential scale for each independent variable. This shows a plot of Pearson's correlation coefficients (*R*, Y-axis) between mosquito captures (ALSP group) and Tasseled-Cap brightness (TC1) for each of the 11 spatial scales (X-axis, [7x = seven pixels/side; see Table 5]). The highest *R*-value was for 7x (7.29 ha).

Chapter III (Overview)

It is well understood that spatial and temporal fluctuations in mosquito abundance are influenced by weather patterns (Rogers, 1967; Shaman et al., 2002; Reiter, 2001; Tong and Hu, 2001; USDA, 2004; and others). Rainfall increases soil moisture, near-surface humidity, and in turn, the diversity and abundance of habitats available to breeding mosquitoes. These increases intensify both flight activity and host-seeking behavior (Shaman and Day, 2005). Moreover, the distribution and accumulation of rainwater within natural watersheds at both macro- and micro-scales are closely tied to topography

(Yeh et al., 1998; Bernhardsen, 2002; Garbrecht and Martz, 2000; Shaman et al., 2002). Researchers have long used topographic indices to predict relative soil moisture and potential surface wetness (Beven and Kirkby, 1979; Urban et al., 2000).

Chapter III addressed the spatial and temporal distribution, within the City of Chesapeake, Virginia, of the primary enzootic vector of EEE, the bird-feeding mosquito *Cs. melanura* (Nasci and Edman, 1984; Crans et al., 1994). *Culiseta melanura* is a common and widespread mosquito of the swamps of the eastern and central United States (Andreadis, 2002). Larvae generally develop in relatively cool subterranean habitats (Mahmood and Crans, 1998; Andreadis, 2002); however, they have also been collected in discarded tires, man-made ditches, and temporary pools (Spielman, 1964; Wallis and Whitman, 1967; Pitts and Holbrook, 2000). Although not a human biter, and thus not generally the subject of service requests (2,411 in 2003; CMCC, 2004), its competence as the primary enzootic vector for EEE has made *Cs. melanura* the primary focus of the CMCC's adulticide and larvacide programs (CMCC, 2004).

The objective of Chapter III was to augment the semi-static HSI model for *Cs. melanura* (generated in Chapter II; Figure 31) with a dynamic GIS-based model incorporating recent weather patterns and a soil moisture index based on topographic derivatives to predict mosquito abundance. This "dynamic" model is capable of predicting not only *where*, but also *when*, adult *Cs. melanura* are likely to occur in large numbers. To achieve this predictability, I used recent spatially explicit meteorological data (NEXRAD: ***NEX***t-generation [Doppler] ***RAD***ar, National Oceanic and Atmospheric Administration [NOAA], NWS) to create weekly "accumulated precipitation" grids that were overlaid onto weekly temperature grids and a topographic soil moisture index (TMI)

to map areas with high probabilities of surface and subsurface wetness. Thus, knowing current rainfall amounts and distributions, I was able to map which areas of suitable breeding habitat, from Chapter II, are most likely to experience outbreaks of adult mosquitoes.

Dependent Variable

Only captures of *Cs. melanura* (2004) were used in analyses in this chapter. As in Chapter II, capture data were normalized to account for variation in trapping effort among trapping sites. Cross-year comparisons for this single-species model for 2003 and 2004 consisted of ANOVA (between years) and correlation analysis (among sites) of *Cs. melanura* capture data for the trapping sites common to both years (Zar, 1996). Again, these analyses defined a statistically significant trend of similarity in captures between 2003 and 2004, relieving the need to conduct parallel analyses for both years.

Independent Variables

A series of multiple linear regression models was used to test the *a priori* hypothesis that fluctuations in weekly captures of *Cs. melanura* were functions of current average weekly air temperature (AWAT) and recent precipitation accumulation (PA). Six time-sequential regression analyses were run ($\alpha = 0.05$); in each successive regression, weekly captures of *Cs. melanura* were regressed against AWAT for the same 1-week PA period for successively earlier weekly intervals (see Table 7). Weekly intervals of the three datasets (i.e., captures, AWAT, PA) used in these regressions were calculated for 32 weeks (4 April – 10 October, 2004). Temperature and precipitation data for the City of

Chesapeake were provided by the CMCC. Similar temperature datasets are widely available. Fluctuations in *Cs. melanura* captures were best explained, with the least residual error, by the 2-week lag-time model. This suggests that the activities of *Cs. melanura* are, at least in part, related to temperature and recent precipitation.

Soil moisture characteristics (SSURGO Soil Surveys # va550, va800, va810: USDA, Natural Resources Conservation Service [NRCS] Soil Data Mart.) were inherent in the *Cs. melanura* HSI created in Chapter II. As such, the use of soil characteristics in the soil moisture index would likely result in statistical redundancies. Therefore, I used a complementary TMI (after Beven, 1997) to circumvent these issues in lieu of Iverson et al.'s (1997) integrated soil moisture index that directly incorporates soil moisture derivatives. Because the TMI uses only topographic derivatives (i.e., digital elevation model [DEM], hydrologic model, slope surface) my model has the theoretical equivalent of a soil moisture index with both soil and topographic properties.

The components of the TMI, a digital elevation model (DEM), a hydrologic model, and a slope surface for the City of Chesapeake, were constructed in ArcGIS Spatial Analyst extension. Equation 4, after Beven (1997) was used to create the TMI surface model.

TMI values that spatially coincided with the locations of trapping sites were extracted from the TMI grid to create a soil moisture point shapefile. This procedure was similar to the one used in Chapter II for extracting pixel values at trapping sites from aggregated habitat attribute grids. Extracted TMI values were used as the independent variable in an *a priori* linear regression model testing the hypothesis that variation in captures of *Cs. melanura* among trapping sites (dependent variable) is related to spatial

variation in the calculated TMI values (Zar, 1996). The significant positive relationship between captures/TN of *Cs. melanura* and TMI values at trapping sites ($P < 0.05$) justified the incorporation of this relationship into weekly abundance models for *Cs. melanura*.

Neither the *Cs. melanura* HSI (from Chapter II) nor the TMI described above are prone to temporal changes because the factors involved in their creation are relatively static (e.g., topography, soil characteristics, vegetation patterns). The primary role of weekly weather data grids described below was to provide a dynamic and environmentally based aspect to the abundance models created in this study.

Integration of temperature and precipitation data into a single output is problematic because they are represented by different data types (intervals for temperature and ratio for precipitation) and relative scales. Consequently, both datasets were normalized and rescaled using Equation 6 (temperature) and Equation 7 (precipitation).

Spatially explicit temperature data for Chesapeake were not available; as a result AWAT grids used in these models had a constant citywide value. AWAT values in 2006 for Chesapeake were calculated using Equation 6 and transferred to constant-value AWAT grids using Quality Controlled Local Climatological Data from the National Climatic Data Center (QCLCD: NCDC) collected at the NWS Station at KCPK (Lat/Long: 36.6639°N, 76.3306°W). Historical minimum and maximum AWAT values (March – October) were based on 30-yr monthly records from 1971-2000 (NCDC, 2002) collected at station KAKQ, in Wakefield, Virginia.

NEXRAD Level-III (WSR:88D), 3-hr precipitation accumulation data (NOAA, NCDC) were used to create spatially explicit, georeferenced weekly precipitation accumulation (WPA) grids. These data were downloaded at no cost (http://www.ncdc.noaa.gov/nexradinv) in ArcView shapefile format using the NEXRAD Data Exporter (BETA v.1.3.3). The NEXRAD data source closest to Chesapeake is KAKQ (a.k.a., National Doppler Radar Site, Norfolk/Richmond).

NEXRAD 3-hr PA shapefiles were preprocessed into WPA grids using a series of models created in ArcGIS v.9.1, Modelbuilder, making the creation of WPA grids streamlined and highly repeatable.

WPA grids were created in ArcGrid format by batch-conversion of 3-hr PA shapefiles for a given day (Figures 29 and 40; 1km x 1km pixels) using ArcGIS ModelBuilder. Only shapefiles with coverage (polygons) within Chesapeake were used; thus, the number of shapefiles used per day ranged from zero (no polygons extending into Chesapeake) to eight. Next, all 3-hr PA grids were reclassified using a model created in ArcGIS ModelBuilder (Figure 41) that reassigned "no-data" values a new value of zero. This step was needed because a no-data pixel value in any of the 3-hr PA grids excluded that pixel in the final product but zero provided a real value. Once converted and reclassified, all 3-hr PA grids were clipped to the extent of Chesapeake's boundary and resampled to 30m pixels. Clipped 3-hr PA grids were overlaid (additive) to create WPA grids in ArcGIS v.9.1, Spatial Analyst extension.

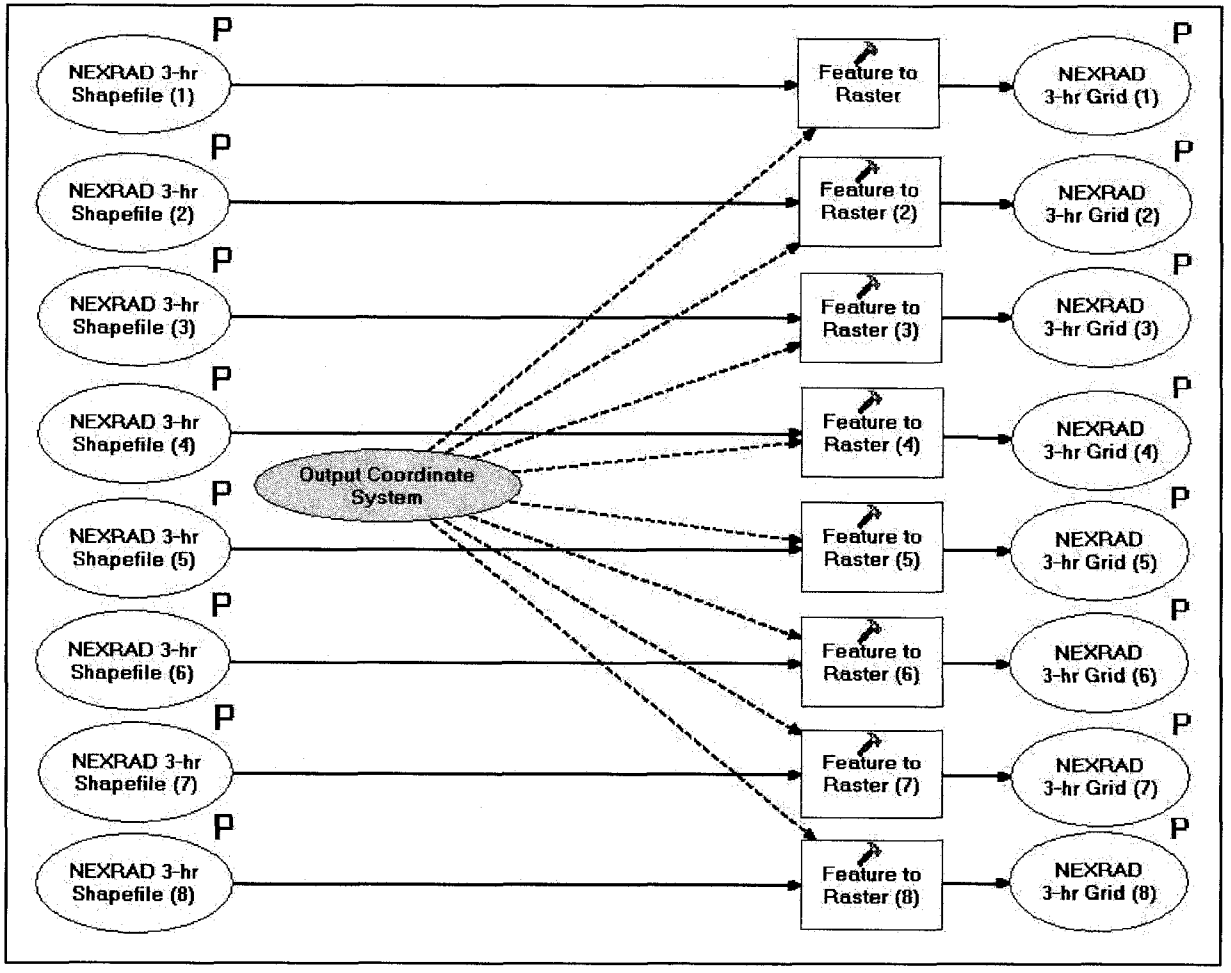

Figure 40. ArcGIS Modelbuilder model used to convert raw NEXRAD (Level-III [WSR:88D]) 3-hr precipitation accumulation from ArcView shapefile format to ArcGrid format. This model was designed to convert the maximum possible daily files ($N = 8$); other models for converting fewer (2-7) were also constrcted, but not provided.

The final step in creating WPA grids was to normalize and rescale (0-100) precipitation values using Equation 7 (Figure 31). I was unable to find weekly or monthly historical minimum and maximum PA for any of the three nearby weather stations (i.e., KAKQ, KCPK [Chesapeake Regional Airport], KORF [Norfolk International Airport]) or from the CMCC; only averages were reported. Thus, minimum and maximum weekly precipitation accumulation values for Chesapeake were based on information provided during a personal communication with Evan Stewart (Meteorologist, WVEC Television [March 2006]).

Weekly Abundance Maps

Weekly predicted abundance maps for *Cs. melanura* representing the combined influence of calculated soil moisture (TMI), AWAT, and 2-week lag time PAs were generated on a pixel-by-pixel basis using an arithmetic overlay operation in ArcGIS v.9.1, Spatial Analyst extension using Equation 8. Final weekly abundance maps (grids) were created on a pixel-by-pixel basis with a spatial overlay operation using the Equation 9. Final weekly abundance maps were reclassified into areas having low, moderate, and high predicted abundance (Figure 37).

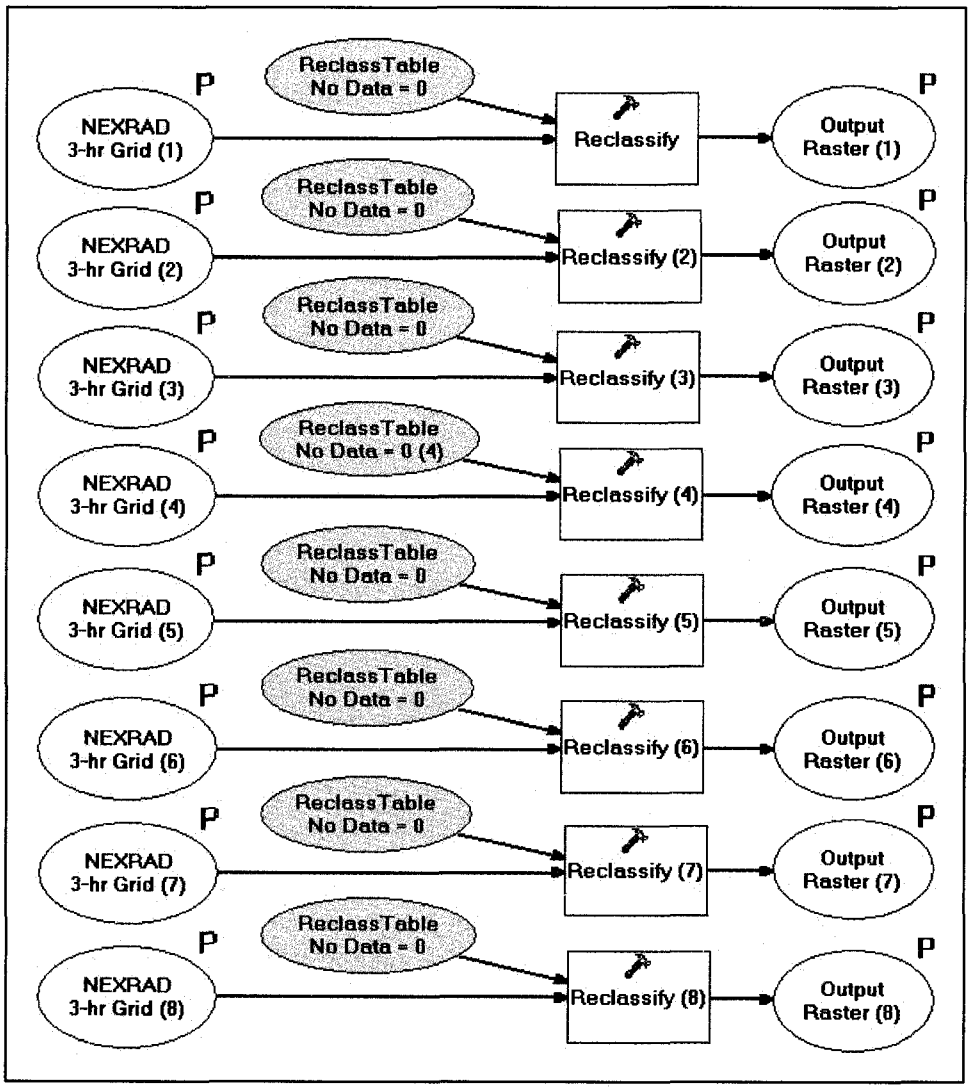

Figure 41. ArcGIS Modelbuilder model used to reclassify 3-hr precipitation accumulation grids by reassigning all "no-data" values in each grid a new value of zero. This model was designed to convert the maximum possible daily files ($N = 8$); other models for converting fewer (2-7) were also constructed, but not provided.

Policy Implications

Preprocessing and Experimental Design

The majority of work associated with the construction of multi-layered spatially explicit models is associated with the preprocessing of data. Through trial and error, I have created a set of preprocessing models, in ArcGIS ModelBuilder (Spatial Analyst extension), which greatly reduce the data preparation time required to carry out these analyses (see Figures 38, 40, and 41). Although these models do not account for all preprocessing steps, the presented examples should provide potential users with a basic blueprint for data formatting and preparation. Time-saving preprocessing steps are most useful for producing weekly abundance maps because these maps are temporally repetitive and need to be prepared quickly.

The statistical tests used in Chapters II and III (e.g., linear regression, *Chi*-square, ANOVA) were primarily selected for applicability to the hypothesis and for the type of data presented. However, because these models were intended to be as user-friendly as possible, the availability of these tests among commonly accessible statistical packages (e.g., SPSS, NCSS, SigmaStat, and others) that require little or no computer language skills to use was also an important consideration.

Sampling

The sampling design and data collection techniques for mosquito captures used in these studies were developed by the CMCC, and thus, not specifically tailored for integration into spatial models. Consequently, I am providing a short discussion, including recommendations, of modifications in sampling design and data collection that could be

used to improve the accuracy and precision of habitat suitability and predicted abundance models such as those summarized in this chapter. These modifications include issues with selection of representative habitats to census, number and distribution of trapping sites, and data collection techniques.

Of the 46 permanent mosquito-trapping sites used in these models, 28 were in close proximity (<200m) to palustrine (forested) wetlands. This number increases to 38 sites at 400m. Of the remaining trapping sites, six were placed in or near (<200m) estuarine wetlands and two were in uplands; no trapping sites were placed in or near lacustrine (lake/reservoir) or riverine wetlands. This propensity to establish trapping sites in forested wetlands was due to the habitat affinities of *Cs. melanura*, the target species of the CMCC monitoring and control efforts, and resulted in potentially insufficient censusing of habitat types important to many other disease-vector and nuisance species (Turell et al., 2001; Crans, 2004; Turell et al., 2005). I suggest that habitat types be censused using a stratified scheme that represents the range of habitats of all mosquito species of interest. Such a scheme would enhance model sensitivity towards less common but perhaps critical mosquito habitats, while at the same time reduce the overemphasis of habitats commonly used by many mosquito species.

As specified above, the number of trapping sites used for analysis in both Chapter II and Chapter III was 46. This sample size is sufficient for single-year analyses, but my models were designed to provide iterative results for use in trend analysis for long-term control and surveillance programs. Considering this, 46 trapping sites limits the amount of spatial variation in mosquito captures, and extracted independent variables, which can be introduced, thus limiting the types of viable statistical tests and model validation

methods that can be used. The best-case scenario would be to have many more trapping sites, each censused regularly throughout the trapping season. This not only would increase the long-term value of the collected data, but it also would increase the power of statistical analyses used for surveillance purposes (White, 2001). Increasing the number of trapping sites would also allow users to reserve data in order to perform within-year model validation. Further, more trapping sites could potentially reduce habitat-type sampling issues: 1) by allowing for more replicates (trapping sites) in rare, but critical, habitat types, and 2) by enabling users to alter the stratification scheme of habitat-type censusing in response to species-specific (or species-group) outbreaks.

Trapping Technique

Females are most easily attracted to traps when they are either seeking a blood meal or searching for a place to lay their eggs; two common trap types used are CO_2-baited and gravid traps. Gravid traps attract females to an oviposition medium in lieu of a blood meal attractant (CO_2). Some mosquito species (e.g., *Culex* spp., *Ochlerotatus triseriatus*) are more accurately represented using gravid traps than CO_2-baited light traps (CDC, 2003; USACE, 2005). The CMCC made limited use of gravid traps in 2004, and these data were not made available for this study. Godsey et al. (2005) reported ~3.4 times the number of captures of *Culex* spp. in gravid traps than in light traps baited with dry ice. White et al. (2003) had similar results during a study in north-central Ohio. In my study, *Cx. erraticus*, *Cx. pipiens*, and *Cx. restuans* collectively represented only 0.89% of all captures (Appendix A). Without gravid-trap data for comparison, I cannot conclude with confidence that capture numbers for these species, and others caught more readily in

gravid traps, are either accurate or inaccurate representations. I recommend a combination of CO_2-baited light and gravid traps, because they have been shown to be complementary and likely to produce better assessments of mosquito communities at trapping sites than either technique alone (CDC, 2003).

Future Policy Implications

In addition to the models presented here, there are several augmenting factors that could be easily processed into spatial format, including: larval monitoring and control data, bird surveillance (e.g., dead birds, sentinel bird flocks), and human demographics. Except for larval monitoring and control, these datasets would be more closely associated with reducing the risks of disease transmission than with efforts to control nuisance mosquito species.

Larval Monitoring

As with my models, Shaman et al. (2002) used captures of adults to predict emergence of adults from modeled larval habitats. They concluded that larval monitoring data, which they did not have, would have enhanced the predictive power of their models. Many mosquito control and surveillance programs have only recently begun to collect larval data. For example, the CMCC, the source of capture data for my study, began an early season (leaf-off) aerial larvacide program in 2004 to reduce the first broods of *Cs. melanura*, *Aedes vexans*, and *Ochlerotatus canadensis* (CMCC, 2004). At the time of my analyses, these data were unusable. However, pre- and post-larvicide monitoring data from both treatment and control sites could be used not only to quantify the effects of

control efforts, but also to increase power of my models to assess habitat suitability and predict mosquito abundance. Mosquitoes need surface water for larval development. This makes potential geographic positions of breeding and larval development predictable, thus suggesting prudent locations to interrupt viral epidemiologic cycles of mosquito-borne diseases using spatial modeling.

Avian Surveillance

Both EEE and WNV use birds as primary reservoir hosts (Hassan et al., 2003; Komar et al., 2003). The 1999 human outbreak of WNV in New York was coincident with sizeable die-offs of birds, especially American Crows (*Corvus brachyrhynchos* [Rappole et al., 2000]). Mostashari et al. (2003) reported a strong spatial correlation between the occurrence of dead birds and WNV activity. They suggested that data on dead birds could be integrated into disease surveillance programs to provide an early warning system of viral activity in both mosquitoes and birds. This would be especially critical when reports of dead birds coincide spatially with outbreaks of known vector species such as *Cs. melanura*. This program would require general public involvement for these data to be productive and reliable. Consequently a standardized and uncomplicated system for reporting dead birds must be developed. With accurate locational information, this reporting system could easily be adapted into spatially explicit models.

Sentinel birds have long been used to monitor arbovirus activity (Moore et al., 2003). The CMCC has an established sentinel bird (chickens) program for detecting EEE and WNV presence and activity (CMCC 2004). Similar to dead bird reports, sentinel bird data can be used as early warning system of viral activity and to quantify transmission

rates (Komar, 2001). Because the geographic location of sentinel flocks is usually known, data are especially suited for integration into spatial models.

Vulnerable Human Populations

Children and the elderly are at a higher risk for debilitating complications resulting from viral encephalitis (Whitley and Kimberlin, 1999; Peterson and Marfin, 2002). Because of these elevated risks, it is critical that these two demographic groups be considered when monitoring arboviral activity. Nursing homes and retirement communities, schools and playgrounds, theme parks, and other places where either children or the elderly congregate could be incorporated into a GIS and used in an overlay analysis with predicted abundance maps. This would enable mosquito control agencies to take preventive actions when mosquito outbreaks arise.

In summary, the predictive value of my models can be enhanced by the integration of one or more of the data layers described above. Larval monitoring and control data would likely be the most costly but also the most useful. The incorporation of facilities for elderly and children into a GIS would have one-time costs, with minimal revision, compared to programs for collecting information on dead birds or sentinel flocks. Expenses for all enhancements can be justified as part of an effective public-health program for a municipality.

Scientific Implications

Integrated Pest Management

The use of digital satellite data in GIS is becoming a valuable and commonly used approach in the study of vector ecology and disease transmission (Clarke et al., 1996; Kitron, 1998). Surveillance, monitoring, and subsequent health policies associated with the study of vector-borne emerging infectious diseases are becoming more streamlined and functional through the integration of spatial, ecological, and epidemiological data (Clarke et al., 1996; Dister et al., 1997; Boone et al., 2000; Glass et al., 2000; Srivastava et al., 2001).

The ability to assess habitat suitability and predict spatial and temporal abundances of mosquitoes with accurate landscape-level data is paramount in the development of effective, efficient, and environmentally sound mosquito control measures. The models described herein, derived from spatially explicit empirical data, are useful for both locating good mosquito habitat and for predicting species abundances within real landscapes. The use of data collected by remote-sensing techniques enabled the integration and analysis, within the framework of a GIS, of large and diverse data sets to an areal extent not feasible by *in situ* data collection. Furthermore, the data used in these models were either provided (e.g., captures data, Chesapeake hydrology [canals and ditches]), downloaded at no cost (i.e., NHD, SSURGO, NEXRAD) or relatively inexpensive (i.e., Landsat ETM+, QCLCD).

These models are relatively objective, making them equally effective in densely population areas and isolated areas. This quality is essential because enzootic viral transmission cycles are often centered in rural habitats, and thus go undetected by most

monitoring and surveillance protocols (Moore et al., 1993). This is especially true when vector species are not human biters, such as *Cs. melanura*, and, as a consequence, are not reported frequently as a nuisance in service calls. Coupled with favorable weather and environmental conditions, viral amplification cycles can rapidly increase in magnitude and distribution, leading to potential epizootic outbreaks (Moore et al., 1993). Therefore, from the standpoint of prevention and control, it is critical that mosquito control agencies have the ability to quickly track changes in the distributions of arboviral vectors such as *Cs. melanura*, in addition to nuisance species. Changes in predicted mosquito distributions can be overlaid (in a GIS) with adulticide truck routes, thus enabling mosquito control agencies to apply insecticides in a more effective, timely, economical, and environmentally sensitive manner. These changes could also be incorporated into an integrated management plan that includes not only surveillance and chemical control, but also source reduction (e.g., habitat modification and elimination [ditch maintenance, containers]), biological control (e.g., predator introduction [mosquito fish, *Gambusia holbrooki*]), and agency personnel and public education. Collectively, these efforts would reduce sources of public health and disease transmission risks, while minimizing the negative impacts on control measures on people and the environment (Kent, 1989).

Population and Vector Ecology

The basic tenets of population regulation (e.g., rates of birth, death, immigration, and emigration) and metapopulation regulation (e.g., dispersal, asynchrony) are relative, but in theory are relevant regardless of species or assemblage of species. Furthermore, principles borrowed from metapopulation theory to govern the preservation of threatened

and endangered species and the conservation of economically important species can be reversed to eradicate or control nuisance species (Earn et al., 1998). It is now axiomatic that spatial and temporal factors influencing dispersion and colonization of organisms play vital roles in the dynamics of populations and metapopulations. Bascompte and Rodríguez-Trelles (1998) constructed a mathematical model to describe such regulation and the spread of infectious disease, and included parallels in terminology between the two concepts: colonization $\approx$ transmission, extinction $\approx$ eradication, habitat destruction $\approx$ host vaccination. Therefore, viral transmission in its strictest sense is a form of dispersal, and to be viable a virus must successfully disperse and colonize within the landscape inhabited by both vector and host.

My models were based on the collective influence of spatially explicit habitat characteristics. These types of influences drive the spatial distributions of organisms, but were largely ignored before the publication of Levins' (1969) metapopulation theory. Notable exceptions are Huffaker (1958) and Andrewartha and Birch (1954). More recently, the role of spatial structure has emerged as a pivotal influence on the spatial and temporal distributions and abundances of organisms (e.g., Lindenmayer and Lacy, 1995; Lindenmayer and Possingham, 1996; Bender et al., 2003; Tischendorf et al., 2003) and has become a major motivation for much current research, including mine. Traditional models tended to oversimplify the mechanics of population regulation, and thus generally provide limited insight in real-world situations (Hanski 1994). In most cases, spatially influential factors were only implicitly addressed (Levins, 1969; Lande, 1987; Keeling, 2002). Population- and community-level studies generally do not explicitly incorporate the influence of spatial factors because hierarchical theory traditionally introduces

environmental factors at ecosystem and landscape levels of ecology. Distributional dynamics becomes even more convoluted if spatial heterogeneity of landscape characteristics is considered. Thus, spatially explicit landscape components, important and often continuous in variation, must be considered if ecologically integrated pest management techniques, such as those to control arthropod vectors, are to be effective.

As the use of GIS in applied natural sciences becomes more extensive, so does the knowledge to use this new set of tools in a manner that emphasizes the analysis of spatially explicit environmental data (Johnson 1993). As a result, much recent research represents the hybridization of traditional spatially implicit with spatially explicit models (Hokit et al., 2001; Bender et al., 2003; Tischendorf et al., 2003; Baguette, 2004; among others).

CHAPTER V

GENERAL SUMMARY

The first recorded North American outbreak of West Nile virus in New York (1999) initiated an unprecedented surge in research pertaining to the control and prevention of mosquito-borne disease. Much of the subsequent research was directed toward the development of environmentally sensitive integrated pest management programs. Most of these studies were conducted at relatively small spatial scales using *in situ* data collection methods, and thus were not practical for most municipality-run mosquito control agencies with large jurisdictions. I have addressed this problem by creating a series of GIS-based models designed to rank habitat suitability and predict the spatial and temporal abundances of mosquitoes in real-world landscapes of the mid-Atlantic region.

Chapter II

My habitat suitability indices (HSI) used species-group models based on similarities in mosquito life histories, habitat affinities, and vector competence. By using species groups in lieu of single-species models, I was able to reduce my analyses to a more manageable number of regression models.

I did not incorporate land cover/use data (USGS: NLCD) in my HSI regression models for three reasons: 1) an unacceptably low level of accuracy in the NLCD Level II classification that that would have decreased overall model reliability, 2) not all Level II classes were represented at trap-site locations, making the ranking of city-wide habitat

suitability problematic due to potential disproportions and omissions of land use/cover classes in subsequent analyses, and 3) NLCD data are categorical and would have required analysis independent from the main regression model. The latter is the least problematic of the three.

I expected positive relationships between predicted habitat suitability for mosquitoes and properties associated with increased soil moisture content (potential flooding/ponding) and vegetative vigor; however, this was not the case for my study. In fact, captures for all species groups were showed negative associations with at least one of independent variables derived from soil data and at least one of the three Tasseled-Cap variables. Although unexpected, many of these associations were explainable and supported by the literature. It is, however, noteworthy that all R values > 0.500 represented positive influence on habitat suitability.

For example, the negative relationships between mosquito captures for many species groups and Tasseled-Cap wetness (TC3) are likely to be indirectly related to the positive relationships with canopy cover (TC2), which is considered to carry more explanatory power than TC3. In other words, spectral reflectance values are largely a function of the uppermost layer in the scene, and thus increased summer foliage decreases the ability to detect the underlying soil wetness (TC3).

Another factor influencing the spatial distribution of mosquitoes in my study was the extensive network of ditches and canals that has been constructed throughout Chesapeake, especially in the southern regions of the city. Although this network has effectively transformed wetlands into uplands, the ditches that remain are excellent mosquito breeding sites in otherwise less suitable habitat. This was most evident for *Cs.*

melanura, and the EPHM and SWMP groups. This influence was quantified by the positive responses of most species groups to the independent variable HYDSUM, which accounted for the spatial distribution of ditches and canals.

Culiseta melanura responded best to independent variables at broad spatial scales. Visual overlay of suitable habitat and the National Wetland Inventory maps supported this pattern, where large and contiguous areas of suitable habitat for *Cs. melanura* dominate. The other species groups all had smaller and more localized areas of suitable habitat; this pattern was also seen in the regression models. It would be difficult to sort through possible explanations for the variations species-group responses to spatial scales, but predictability of mosquito abundance in my regression models was increased by the incorporation of differing spatial scales.

Chapter III

This chapter addressed the spatial and temporal distributions of *Culiseta melanura*, the primary enzootic vector of EEE in the mid-Atlantic region. The weekly-predicted abundance model created in this chapter was designed to augment the semi-static HSI model for *Cs. melanura* generated in Chapter II. This was done by combining a time-tested topographic soil moisture index (TMI), based on topographic derivatives calculated from a digital elevation model (DEM), and digital weather data, and then integrating these results with the HSI from Chapter II.

Because the distribution and accumulation of precipitation in watersheds are intimately tied to topography, the TMI I used allowed me to determine which areas in the landscape are most prone to flooding or ponding. I was able to increase the accuracy of

the TMI by integrating Chesapeake's extensive drainage ditch network to modify the DEM used in the hydrologic model using the stream-burning technique. This technique captured the physical effects the ditch network added the hydrology in Chesapeake.

The positive relationship between *Cs. melanura* captures TMI values at trapping sites in my study was expected. This expectation was based on the proven efficacy of this soil moisture model and a well-documented dependence of mosquitoes on the distribution of surface water.

Considering the known dependence of mosquitoes on meteorological patterns, the positive relationships between *Cs. melanura* abundance and both warm temperatures and increased precipitation in my study was expected. Additionally, my finding that *Cs. melanura* has a ~2-week delayed response to precipitation accumulations is supported by other studies using spatially based models similar to mine. With these affinities and response times statistically established, and further supported in the literature, their transference to weather-driven weekly *Cs. melanura* abundance models was justifiable.

To my knowledge, my use of NEXRAD precipitation data is unique among epidemiological and entomological studies. I was able to incorporate a near real-time component to weekly abundance maps using NEXRAD precipitation accumulation data. Thus, from a prevention and control standpoint, it is critical that mosquito control agencies such as the CMCC have the ability to rapidly track the spatial and temporal distributions of potential arboviral vectors such as *Cs. melanura*.

Chapter IV

This chapter was different from Chapters II and III because it does not present new research. Instead, the purpose of this chapter was to provide potential users with the necessary protocols needed to apply the models created in the previous two chapters. This chapter emphasizes the spatial and temporal modeling of abundance and distributions for *Cs. melanura*, in a real-world coastal landscape of the MAR. The intended audience for this final chapter was GIS analysts employed by mosquito-control and public health agencies and environmental managers and decision makers of these agencies with limited experience in spatial modeling. In addition to reviewing the methods I used in selection and implementation of independent variables, I provided an overview for the ArcGIS models (created in ModelBuilder, Spatial Analyst extension) I used to reduce the effort needed for data preprocessing.

This chapter also addressed possible improvements on sampling design and trapping technique. In addition, I provided supplementary sections on future policy implications as well as scientific implications of Chapters II and III. Future policy implications discussed were the implementation of ancillary datasets such as larval mosquito and avian surveillance, and vulnerable human demographics. Scientific implications included a discussion on the usefulness of my research to development of an environmentally sensitive integrated pest management program and the significance of this research regarding vector and population ecology.

REFERENCES

Anderson G. 2006. State mosquito control policies: preventing emerging diseases. National Conference of State Legislatures, Nashville, TN.

Anderson J.R., Hardy E.E., Roach J.T., and Witmer R. 1976. A land-use and land-cover classification system for use with remote sensor data. USGS Profession Paper 964.

Andreadis T.G. 2002. Epizootiology of *Hyalinocysta chapmani* (Microsporidia: Theleohaniidae) infections in the field populations of *Culiseta melanura* (Diptera: Culicidae) and *Orthocyclops modestus* (Copepoda: Cyclopidae); a three-year investigation. Journal of Invertebrate Pathology 81: 14-121.

Andrewartha H.G. and Birch L.C. 1954. The Distribution and Abundance of Animals. Chicago University Press, Illinois.

Baguette M. 2004. The classical metapopulation theory and the real, natural world: a critical appraisal. Basic and Applied Ecology 5: 13-224.

Barrera R., Torres N., Freier J.E., Navarro J.C., Garcia C.M., Salas R., Vasques C. and Weaver S.C. 2001. Characterization of enzootic foci of Venezuelan equine encephalitis virus in western Venezuela. Vector-Borne and Zoonotic Diseases 1: 19-230.

Bascompte J. and Rodríguez-Trelles F. 1998. Eradication thresholds in epidemiology, conservation biology and genetics. Journal of Theoretical Biology 192: 415-418.

Baylis M., Bouayoune H., Touti J. and Hasnaoui E.H. 1998. Use of climatic data and satellite imagery to model the abundance of *Culicoides imicola*, the vector of African horse sickness virus, in Morocco. Medical and Veterinary Entomology 12: 255-266.

Beasley W.B.C., Davis C.T., H. Guzman, Vanlandingham D.L., Amelia P.A., da Rosa T., Parsons R.E., Higgs S., Tesh R.B. and Barrett A.D.T. 2003. Limited evolution of West Nile virus has occurred during its southwesterly spread in the United States. Virology 309: 190-195.

Beck L.R., Lobitz B.M. and Wood B.L. 2000. Remote sensing and human health: new sensors and new opportunities. Emerging Infectious Diseases 6: 217-226.

Beck L.R., Rodríguez M.H., Dister S.W., Rodríguez A.D., Rejmánková E., Ulloa A., Meza R.A., Roberts D.R., Paris J.F., Spanner M., Washino R.K., Hacker C. and Legters L.J. 1994. Remote sensing as a landscape epidemiological tool to identify villages at high risk for malaria transmission. American Journal of Tropical Medicine and Hygiene 51: 271-280.

Bedient P.B., Holder A., Benavides J.A. and Vieux B.E. 2000. NEXRAD radar for flood prediction in Houston. Journal of Hydrologic Engineering 5: 269-277.

Bedient P.B., Hoblit B.C., Gladwell D.C. and Vieux B.E. 2003. Radar-based flood warning system applied to tropical storm Allison. Journal of Hydrologic Engineering 8:308-318.

Bellows A.S., Mitchell J.C. and Pagels J.F. 2001. Macrohabitat and microhabitat affinities of small mammals in a fragmented landscape on the upper Coastal Plain of Virginia. American Midland Naturalist 146: 345-360.

Bender D.J., Tischendorf L. and Fahrig L. 2003. Using patch isolation metrics to predict animal movement in binary landscapes. Landscape Ecology 18: 17-39.

Beringer D.B. and Ball J.D. 2004. The effects of NEXRAD graphical data resolution and direct weather viewing on pilots' judgments of weather severity and their willingness to continue a flight. Final Report: DOT/FAA/AM-04/5, U.S. Dept. of Transportation, Federal Aviation Administration. Office of Areospace Medicine, Washington, D.C.

Bernhardsen T. 2002. Geographic Information Systems: an Introduction, 3rd ed. John Wiley and Sons, Inc. New York.

Beven K.J. 1997. Topmodel: a critique. Hydrologic Processes 11: 1069-1085.

Beven K.J. and Kirkby M.J. 1979. A physical-based variable contributing area model of basin hydrology. Hydrology Science Bulletin 24: 43-69.

Bieringer P., and Ray P.S. 1996. A comparison of tornado lead times with and without NEXRAD Doppler radar. Weather and Forecasting 11: 47-52.

Boone J.D., McGwire K.C., Otteson E.W., DeBaca R.S., Kuhn E.A., Villard P., Brussard P.F. and St. Jeor S.C. 2000. Remote sensing and geographic information systems: charting Sin Nombre virus infections in deer mice. Emerging Infectious Diseases 6: 248-258.

Botterweg P.F. 1982. Dispersal and flight behaviour of the spruce bark beetle *Ips typographus* in relation to sex, size and fat content. *Zeitschrift für Agnewandte* Entomologic 94: 466- 489.

Calisher C.H. 2004. Eastern equine encephalitis virus: still with us, still interesting. In: ACVP and ASVCP (eds.), 55th Annual Meeting of the American College of Veterinary Pathologists (ACVP) and 39th Annual Meeting of the American Society of Clinical Pathology (ASVCP), 2004 - Orlando, FL, USA. Ithaca: International Veterinary Information Service (www.ivis.org), Document No. P1238.1104. pp. 1-2.

Campbell J.B. 2002. Introduction to Remote Sensing, 3rd ed. Guilford Press, New York.

Carpenter S.J. and W.J. LaCasse. 1955. Mosquitoes of North America, North of Mexico. University of California Press, Berkeley, CA.

CDC. 1992. Eastern equine encephalitis virus associated with *Aedes albopictus*—Florida.1991. Morbidity and Mortality Weekly Report 41: 115-121.

CDC. 2003. Epidemic/epizootic West Nile virus in the United States: guidelines for surveillance, prevention, and control—3rd ed. Centers for Disease Control and Prevention, National Center for Infectious Diseases, Division of Vector-Borne Infectious Diseases, Fort Collins, Colorado.

Clarke K.C., McLafferty S.L. and Tempalski B.J. 1996. On epidemiology and geographic information systems: a review and discussion of future directions. Emerging Infectious Diseases 2: 85-92.

CMCC. 2004. Chesapeake Mosquito Control Commission: 2004 Annual Report. Chesapeake, VA.

Congalton R.G. and Green K. 1998. Assessing the Accuracy of Remotely Sensed Data: Principles and Practices. Lewis Publishers, Boca Raton, FL.

Cowardin L.M., Carter V., Golet F.C. and LaRoe E.T. 1979. Classification of Wetlands and Deepwater Habitats of the United States. U.S. Department of the Interior, Fish and Wildlife Service, Northern Prairie Wildlife Research Center, Jamestown, ND, publication 0421. Washington, D.C.

Crans W.J., Caccamise D.F. and McNelly J.R. 1994. Eastern equine encephalomyelitis virus in relation to the avian community of a central cedar swamp. Journal of Medical Entomology 31: 711-728.

Crans W.J. 2004. A classification system for mosquito life cycles: life cycle types for mosquitoes of the northeastern United States. Journal of Vector Ecology 29: 1-10.

Crist E.P. and Cicone R.C. 1984. Application of the Tasseled Cap concept to simulate thematic mapper data. Photogrammetric Engineering and Remote Sensing 50: 343-352.

Cupp E.W., Klinger K., Hassan H.K., Viguers L.M. and Unnasch T.R. 2003. Transmission of eastern equine encephalomyelitis virus in central Alabama. American Journal of Tropical Medicine and Hygiene 68: 495-500.

Dauphin G., Zientara S., Zeller H. and Murgue B. 2004. West Nile: worldwide current situation in animals and humans. Comparative Immunology, Microbiology, and Infectious Diseases 27: 343-355.

Devine P.A. 2003. West Nile virus infection. Primary Care Update Ob/Gyns 10: 191-195.

Diehl R.H. and Larkin R.P. 2005. Introduction to WSR-88D (NEXRAD) for ornithological research. In: C.J. Ralph and T.D. Rich (eds.), Bird Conservation Implementation and Integration in the Americas: Proceedings of the Third Annual Partners in Flight Conference. Technical Report PSW-GTR-191, Albany, CA. pp. 876-888.

Dirnböck T., Hobbs R.J., Lambeck R.J. and Caccetta P.A. 2002. Vegetation distribution in relation to topographically driven processes in southwestern Australia. Applied Vegetation Science 5: 147-158.

Dister S.W., Fish D., Bros S., Frank D.H. and Wood B.L. 1997. Landscape characterization of peridomestic risk for Lyme disease using satellite imagery. American Journal of Tropical Medicine and Hygiene 57: 687-692.

Dobson A. and Carper R. 1993. Biodiversity. Lancet 342: 1096-1099.

Dolan R., Hayden B., Bosserman K. and Lisle L. 1987. Frequency and magnitude data on coastal storms. Journal of Coastal Research 3: 245-247.

Dolan R., Lins H. and Hayden B. 1988. Mid-Atlantic coastal storms. Journal of Coastal Research 4:417-433.

Duelli P., Zahradnik P., M. Knizek and Kalinova B. 1997. Migration in spruce bark beetles (*Ips typographus* L.) and the efficiency of pheromone traps. Journal of Applied Entomology 121: 297-303.

Earn D.J.D., Rohani P. and Grenfell B.T. 1998. Persistence, chaos and synchrony in ecology and epidemiology. Proceedings of the Royal Society of London 265: 7-10.

Epstein P.R., Diaz H.F., Elias S., Grabherr G., Graham N.E., Martens W.J.M., Mosley-Thompson E. and Susskind J. 1998. Biological and physical signs of climate change: focus on mosquito-borne diseases. Bulletin of the American Meteorological Society 79: 409-417.

Estrada-Peña A. 1999. Geostatistics as predictive tools to estimate *Ixodes ricinus* (Acari: Ixodidae) habitat suitability in the Western Palearctic from AVHRR satellite imagery. Experimental and Applied Acarology 23: 337-349.

Fischer S. and Schweigmann N. 2004. *Culex* mosquitoes in temporary urban rain pools: seasonal dynamics and relation to environmental variables. Journal of Vector Ecology 29:365-373.

Garbrecht J. and Martz L.W. 2000. Digital elevation model issues in water resources modeling. In: D. Maidment and D. Djokic (eds.), Hydrologic and Hydraulic Modeling Support with Geographic Information Systems. ESRI Press, Redlands, CA. pp. 1-27.

Gauch H. G. and Whittaker R.H. 1972. Comparison of ordination techniques. Ecology 53: 868-875.

Gill C.A. 1920. The role of meteorology and malaria. Indian Journal of Medical Research 8: 633-693.

Gjullin C.M., Yates W.W. and Stage H.H. 1950. Studies on *Aedes vexans* (Meig.) and *Aedes sticticus* (Meig.), flood-water mosquitoes, in the lower Columbia River Valley. Annals of the Entomological Society of America 43: 262-275.

Glass G.E., Schwartz B.S., III, Morgan J.M., Johnson D.T., Noy P.M. and Israel E. 1995. Environmental risk factors for Lyme disease identified with geographic information systems. American Journal of Public Health 85: 944-948.

Glass G.E., Cheek J.E., Patz J.A., Shields T.M., Doyle T.J., Thoroughman D.A., Hunt D.A., Enscore R.E., Gage K.L., Irland C., Peters C.J. and Bryan R. 2000. Using remotely sensed data to identify areas at risk for hantavirus pulmonary syndrome. Emerging Infectious Diseases 6: 238-247.

Godsey M.S., Jr., Nasci R., Savage H.M., Aspen S., King R., Powers A.M., Burkhalter K., Colton L., Charnstzky D., Lasater S., Taylor V. and Palmisano C.T. 2005. West Nile virus—infected mosquitoes, Louisiana, 2002. Emerging Infectious Diseases 11: 1399-1404.

Goetz S.J., Prince S.D. and Small J. 2000. Advances in satellite remote sensing of environmental and epidemiological applications. Advances in Parasitology 47: 289-307.

Goldfield D.R. 1873. Disease and urban image: yellow fever in Norfolk, 1855. Virginia Cavalcade, 23: 34-41.

Guerra M., Walker E, Jones C., Paskewitz S., Cortinas M.R., Stancil A., Beck L., Bobo M. and Kitron U. 2002. Predicting the risk of Lyme disease: habitat suitability for *Ixodes scapularis* in the north central United States. Emerging Infectious Disease 8: 289-297.

Hanski I. 1994. A practical model of metapopulation dynamics. Journal of Animal Ecology 63: 151-162.

Hassan H.K., Cupp E.W., Hill G.E., Katholi C.R., Klinger K. and Unnasch T.R. 2003. Avian host preference by vectors of eastern equine encephalomyelitis virus. American Journal of Tropical Medicine and Hygiene 69: 641-647.

Hay S.I., Snow R.W. and Rogers D.J. 1998. From predicting mosquito habitat to malaria seasons using remotely sensed data: practice, problems, and perspectives. Parasitology Today 14: 306-313.

Hayes R.O., Maxwell E.L., Mitchell C.L. and Woodzick T.L. 1985. Detection, identification, and classification of mosquito larval habitats using remote sensing scanners in earth-orbiting satellites. Bulletin of the World Health Organization 63: 361-374.

Hershner C.H. 1999. Tulloch ditching. Technical Report 99-4, Center for Coastal Marine Management, Virginia Institute of Marine Science, Gloucester, VA.

Higgs S., Snow K. and Gould E.A. 2004. The potential for West Nile virus to establish outside its natural range: a consideration of potential mosquito vectors in the United Kingdom. Transactions of the Royal Society of Tropical Medicine and Hygiene 98: 82-87.

Hirobe M., Tokuchi N. and Iwatsubo G. 1998. Topographic differences in soil N transformation patterns along a forest slope. In: K. Sassa (ed.), Environmental Forest Science. Kluwer Academic Publishers, Norwell, MA. pp. 26-48.

Hopkins J.D. 2002. Developing a Community Mosquito Abatement Program. University of Arkansas, Division of Agriculture, Cooperative extension Service, FSA7060-PD-9-02N.

Horsfall W.R. 1955. Mosquitoes: their Bionomics and Relation to Disease. Ronald Press. New York, NY.

Howard L.O., Dyar H.G. and Knab F. 1912. The Mosquitoes of North Central America and the West Indies. Publication 159, Carnegie, Institute, Washington, D.C.

Huang C., B. Wylie, C. Homer, L. Yang and G. Zylstra. 2002. Derivation of a Tasseled Cap transformation based on Landsat 7 at-satellite reflectance: International Journal of Remote Sensing 23: 1741-1748.

Huffaker C.B. 1958. Experimental studies of predation: dispersal factors and predator-prey oscillation. Hilgardia 27: 343-383.

Hutchinson G.E. 1957. Concluding Remarks. Population Studies: animal ecology and demography. Cold Spring Harbor Symposia on Quantitative Biology 22: 415-427.

Iverson L.R., Dale M.E., Scott C.T. and Prasad A. 1997. A GIS-derived integrated moisture index to predict forest composition and productivity of Ohio forests (U.S.A.). Landscape Ecology 12: 331-348.

Johnson C.M., Johnson L.B., Richards C. and Beasley V. 2002. Predicting the occurrence of amphibians: an assessment of multiple-scale models. In: J.M. Scott, P.J. Heglund, M.L. Morrison, J.B. Haufler, M.G. Raphael, W.A. Wall, and F.B. Samson (eds.), Predicting Species Occurrences: Issues of Accuracy and Scale. Island Press, Washington, D.C. pp. 157-170.

Johnson D.H. 2002. The role of hypothesis testing in wildlife science. The Journal of Wildlife Management 66: 273-276.

Johnson L. B. 1993. Ecological analysis using geographical information systems. In: S. B. McLaren and J. K. Braun (eds.), GIS Applications in Mammalogy. Special Publication of the Oklahoma Museum of Natural History, Norman, Oklahoma—in collaboration with—the Carnegie Museum of Natural History, Pittsburgh, PA. pp. 27-38.

Kaya S., Sokal J. and Pultz T.J. 2004. Monitoring environmental indicators of vector-borne disease from space: a new opportunity for RADARSAT-2. Canadian Journal of Remote Sensing 3: 560-565.

Keating J., Macintyre K., Mbogo C.M., Githure J.I. and Beier J.C. 2004. Characterization of potential larval habitats for *Anopheles* mosquitoes in relation to urban land-use in Malindi, Kenya. International Journal of Heath Geographics 3: 9-21.

Keeling M.J. 2002. Using individual-based simulations to test the Levins metapopulation paradigm. Journal of Animal Ecology 71: 270-279.

Kent R. (moderator). 1989. Proceeding of the 76th annual meeting of the New Jersey Mosquito Control Association, Inc. New Jersey Department of Environmental Protection, Trenton, NJ.

Kilpatrick A.M., Kramer L.D., Campbell S.R., Alletne E.O., Dobson A.P. and Daszak P. 2005. West Nile virus risk assessment and the bridge vector paradigm. Emerging Infectious Diseases 11: 425-429.

Kitron U. 1998. Landscape ecology and epidemiology of vector-borne diseases: tools for spatial analysis. Journal of Medical Entomology 35: 435-445.

Komar N. 2001. West Nile surveillance using sentinel birds. Annals of the New York Academy of Sciences 951: 58-73.

Komar N., Dohm D.J., Turell M.J. and Spielman A. 1999. Eastern equine encephalitis in birds: relative competence of European Starlings (*Sturnus vulgaris*). American Journal of Tropical Medicine and Hygiene 60: 387-391.

Laird M. 1988. The Natural History of Larval Mosquito Habitats. Academic Press Inc., San Diego, CA.

Lande R. 1987. Extinction thresholds in demographic models of territorial populations. American Naturalist 130: 624-635.

Lathrop R.G., Cole M.B. and Showalter R.D. 2000. Quantifying the habitat structure and spatial pattern of New Jersey (U.S.A.) salt marshes under different management regimes. Wetlands Ecology and Management 8: 163-172.

Levin S.A. 1992. The problem of pattern and scale in ecology. Ecology 73: 1943-1967.

Levins R. 1969. Some demographic and genetic consequences of environmental heterogeneity for biological control. Bulletin of the Entomological Society of America 15: 237-240.

Li V. 2004. Simple mathematical models for interacting wild and transgenic mosquito populations. Biomathematical Sciences 189: 39-59.

Liew C. and Curtis C.F. 2004. Horizontal and vertical dispersal of dengue vector mosquitoes, *Aedes aegypti* and *Aedes albopictus*, in Singapore. Medical and Veterinary Entomology 18: 351–360.

Lindenmayer D.B., and Lacy R.C. 1995. Metapopulation viability of Leadbeater's possum, *Gymnobelideus leadbeateri*, in fragmented old-growth forests. Ecological Applications 5: 164-182.

Lindenmayer D.B. and Possingham H.P. 1996. Modelling the inter-relationships between habitat patchiness, dispersal capability and metapopulation persistence of the endangered species, Leadbeater's possum, in south-eastern Australia. Landscape Ecology 11: 79-105.

Linthicum K.J., Anyamba A., Tucker C.J., Kelly P.W., Myers M.F. and Peters C.J. 1999. Climate and satellite indicators to forest Rift Valley fever epidemics in malaria. Science 285: 397-400.

Ludwig J. A. and Reynolds J. F. 1988. Statistical Ecology—a Primer on Methods and Computing. John Wiley and Sons, New York.

Mahmood F. and Crans W.J. 1998. Effect of temperature on the development of *Culiseta melanura* (Diptera: Culicidae) and its impact on the amplification of eastern equine encephalomyelitis virus in birds. Journal of Medical Entomology 35: 1007-1012.

Makar R.S. and Stowell C.P. 2004. West Nile virus: and emerging infection in transfusion medicine. Clinical Microbiology Newsletter, 26(9).

Manel S., Dias J.M., Buckton S.T. and Ormerod S.J. 1999. Alternative methods for predicting species distribution: an illustration with Himalayan river birds. Journal of Applied Ecology 36: 734-747.

Matthews G., Matthews R. and Landis W. 1994. Nonmetric clustering: new approaches for ecological data. Proceedings of the 10th Conference on Artificial Intelligence for Applications, San Antonio, TX.

Maurer B.A. 1999. Untangling Ecological Complexity. The University of Chicago Press, Chicago, IL.

McCune B. 1997. Influence of noisy environmental data on canonical correspondence analysis.Ecology 78: 2617-2623.

McLean R.G., Ubico S.R., Docherty D.E., Hansen W.R., Sileo L. and McNamara T.S. 2001. West Nile transmission and ecology in birds. Annals of the New York Academy of Sciences 951: 54-57.

Meisch M.V. 1994. The dark ricefield mosquito *Psorophora columbiae*. Wing Beats 5:8.

Moore C.G., McLean R.G., Mitchell C.J., Nasci R.S., Tsai T.F., Calisher C.F., Marfin A. A., Moore P.S. and Gubler D.J. 1993. Guidelines for arbovirus surveillance programs in the United States. Division of Vector-Borne Infectious Diseases, National Center for Infectious Diseases, CDC, Fort Collins, CO.

Mostashari F., Kulldorff M., Hartman J.J., Miller J.R. and Kulasekera V. 2003. Dead bird clusters as an early warning system for West Nile activity. Emerging Infectious Diseases 9: 641-646.

Nasci R.S. and Edman J.D. 1984. *Culiseta melanura* (Diptera: Culicidae): population structure and nectar feeding in a freshwater swamp and surrounding areas of southeastern Massachusetts, USA. Journal of Medical Entomology 21: 567-572.

Nasci R.S. and Moore C.G. 1998. Vector-borne disease surveillance and natural disasters. Emerging Infectious Diseases 4: 333-334.

NCDC 2002. Climatography of the United States, No. 81. Monthly station normals of temperature, precipitation, and heating and cooling degree days 1971-2000, No. 44, Virginia. NOAA, National Environmental Satellite, Data and Information Service, Asheville, NC.

Nihel, N, Hashida Y., Kobayashi M. and Ishii A. 2002. Analysis of malaria endemic areas on the Indochina Peninsula using remote sensing. Japanese Journal of Infectious Disease 55: 160-166.

NRCS 1995. Soil Survey Geographic Database: Data Use Information. Misc. Publication #1527. United States Department of Agriculture, National Soil Service Center, Fort Worth, TX.

Oaks R.Q., Jr. and Whitehead D.R. 1979. Geologic setting and origin the Dismal Swamp, southeastern Virginia and northeastern North Carolina. In: P.W. Kirk, Jr. (ed.), The Great Dismal Swamp. The University Press of Virginia, Charlottesville, VA. pp. 1-24.

O'Malley C.M. 1990. *Aedes vexans* (Meigen): An old foe. Proceedings of the New Jersey Mosquito Control Association. pp. 90-95.

O'Loughlin E.M. 1981. Saturation regions in catchments and their relations to soil and topographic properties. Journal of Hydrology 53: 229-246.

O'Loughlin E.M. 1986. Prediction of surface saturation zones in natural catchments by topographic analysis. Water Resources Research WRERAO 22: 794-804.

Overgaard H.J., Ekbom B., Suwonkerd W. and Takagi M. 2003. Effect of landscape structure on anopheline mosquito density and diversity in northern Thailand: implications for malaria transmission and control. Landscape Ecology 18: 605-619.

Palone R.S. and Todd A.H. (eds). 1997. Chesapeake Bay riparian handbook: a guide to establishing and maintaining riparian forest buffers. USDA, Forest Service. NA-TP-02- 97.

Patz J.A. 1998. Predicting key malaria transmission factors, biting and entomological inoculation rates, using modelled soil moisture in Kenya. Tropical Medicine and International Health 3: 818-827.

Peterson M.D. and Marfin A.A. 2002. West Nile virus: a primer for the clinician. Annals of Internal Medicine 137: 173-179.

Pitts C.W. and Holbrook G.L. 2000. Mosquito biology and control. The Pennsylvania State University, Agricultural Research and Cooperative Extension, Report: 20M7/00ps 38272. University Park, PA.

Pope K., Masuoka P., Rejmankova E., Grieco J., Johnson S. and Roberts D. 2005. Mosquito habitats, land use, and malaria risk in Belize from satellite imagery. Ecological Applications 15: 1223-1232.

Pope K., Rejmankova E., Savage H.M., Arredondo-Jimenez J.I., Rodriguez M.H. and Roberts D. 1994. Remote sensing of tropical wetlands for malaria control in Chiapas, Mexico. Ecological Applications 4: 81-90.

Rappole J.H., Derrickson S.R. and Hubálek Z. 2000. Migratory birds and the spread of West Nile virus in the western hemisphere. Emerging Infectious Diseases 6: 319-328.

Reiter P. 2001. Climate change and mosquito-borne disease. Environmental Health Perspectives 109:141-161.

Rey J.R., Nishimura N., Wagner B., Braks M.A.H, O'Connell S.M. and Loundibos L.P. 2006. Habitat segregation of mosquito arbovirus vectors in south Florida. Journal of Medical Entomology 43: 1134-1141.

Rogers A.J. 1967. Emphasis on control of adult mosquitoes in Florida. In: T.D. Peck (ed.), Proceedings and Papers of the 35th Annual Conference of the California Mosquito Control Association, Inc. and the 23rd Annual Meeting of the American Mosquito Control Association. pp. 29-31.

Rogers D. 1977. Study of a natural population of *Glossina fuscipes fuscipes* Newstead and a model of fly movement. The Journal of Animal Ecology 46: 309-330.

Rouse J.W., Haas R.H., Schell J.A. and Deering D.W. 1974. Monitoring vegetation systems in the Great Plains with ERTS. Proceedings, 8th Annual ERTS Symposium 1: 48-62.

Sardelis M.R., Turell M.J., Dohm D.J. and O'Guinn M.L. 2001. Vector competence of selected North American *Culex* and *Coquillettidia* mosquitoes for West Nile virus. Emerging Infectious Diseases 7: 1018-1022.

Saunders W. 2000. Preparation of DEMs for land use in environmental modeling analysis. In: D. Maidment and D. Djokic (eds.), Hydrologic and Hydraulic Modeling Support, Environmental SystemsResearch Institute, Inc., Redlands, CA. pp. 29-31.

Shaman J., Stieglitz M., Stark C., Le Blancq S. and Cane M. 2002. Using a dynamic hydrology model to predict mosquito abundances in flood and swamp water. Emerging Infectious Diseases 8: 6-13.

Shaman J. and Day J.J. 2005. Achieving operational hydrologic monitoring of mosquitoborne disease. Emerging Infectious Diseases 11: 1343-1350.

Shaler N.S. 1890. General account of the fresh-water morasses of the United States, with a description of the Dismal Swamp district of Virginia and North Carolina. U.S. Geological Survey Annual Report 10: 255-339.

Shuchman R.A., Malinas N.P. and Edson R. 2002. The role of remote sensing and GIS for impact modeling and risk assessment of vector-borne diseases. The 5th International Conference on the use of Geoinfromation Technologies for Territorial Development Management, Republic of Crimea, Ukraine.

Spielman A. 1964. Swamp mosquito, *Culiseta melanura*: occurrence in an urban habitat. Science 143: 361-362.

Srivastava A., Nagpal B.N., Saxena R. and Subbarao S.K. 2001. Predictive habitat modelling for forest malaria vector species *An. dirus* in India—A GIS-based approach. Current Science 80: 1129-1134.

Slaff M. 1990. The biology of *Culex salinarius*. Proceedings of the New Jersey Mosquito Control Association. pp 71-72.

Store R. and Jokimäki J. 2003. A GIS-based multi-scale approach to habitat suitability modeling. Ecological Modelling 169: 1-15.

Swem, E.G. (ed). 1922. Description of the Dismal Swamp and a Proposal to Drain the Swamp, by William Byrd of Westover Heartman's Historical Series No. 38. Gift Publication, Metuchen, NJ.

Tate C.M., Howerth E.W., Stallknecht D.E., Allison A.B., Fischer J.R. and Meade D.G. 2005. Eastern equine encephalitis in a free-ranging white-tailed deer (*Odocoileus virginianus*). Journal of Wildlife Diseases 41: 241-245.

Tischendorf L., Bender D.J. and Fahrig L. 2003. Evaluation of patch isolation metrics in mosaic landscapes for specialist vs. generalist species. Landscape Ecology 18: 41-50.

Todd S.W. and Hoffer R.M. 1998. Responses of spectral indices to variations in vegetation cover and soil background. Photogrammetric Engineering and Remote Sensing 64: 915-921.

Tong S. and Hu W. 2001. Climate variation and incidence of Ross River virus in Cairns, Australia: a time-series analysis. Environmental Health Perspectives 109: 1271-1273.

Turell M.J., O'Guinn M.L., Dohm D.J. and Jones J.W. 2001. Vector competence of North American mosquitoes (Diptera: Culicidae) for West Nile virus. Journal of Medical Entomology 38: 130-134.

Turell M.J., Dohm D.J., Sardalis M.R., O'Guinn M.L., Andreadis T.G. and Blow J.A. 2005. An update on the potential of North American mosquitoes (Diptera: Culicidae) to transmit West Nile virus. Journal of Medical Entomology 42: 58-62.

Turner M.G. 1989. Landscape ecology: the effect of pattern on process. Annual Review of Ecology, and Systematics 20: 171-197.

Urban D.L., Miller C., Halpin P.N. and Stephenson N.L. 2000. Forest gradient responses in Sierran landscapes: the physical template. Landscape Ecology 15: 603-620.

USACE 2005. Integrated Pest Management (IPM) Plan, Craney Island Dredged Material Management Area, mosquito surveillance and control (Draft). U.S. Army Corps of Engineers, Norfolk District. POC: Keith Lockwood, Operations Branch.

USDA 2004. Epidemiology and ecology of eastern equine encephalomyelitis. Animal and Plant Health Inspection Service (AHPIS)/Veterinary Services, Center for Epidemiology and Animal Health, Center for Emerging Issues.

USFWS 2006. National Wetland Inventory Maps, NWIDBA.CONUS_wet_poly: U.S. Department of the Interior, Fish and Wildlife Service, Branch of Habitat Assessment, Washington, D.C.

Vaidyanathan R., Edman J.D., Cooper L.A. and Scott T.W. 1997. Vector competence of mosquitoes (Diptera: Culicidae) from Massachusetts for a sympatric isolate of eastern equine encephalomyelitis virus. Journal of Medical Entomology 34: 346-52.

Vainio J. and Cutts F. 1998. Yellow Fever. World Health Organization, Report: WHO/EPI/GEN/98.11.

VDH 2004. Virginia arbovirus surveillance and response plan, 2004. Virginia Department of Health, Office of Epidemiology, Richmond, VA.

Walker N. 1992. The eastern treehole mosquito, *Aedes triseriatus*. Wing Beats 3:17.

Wallis R.C. and Whitman L. 1967. *Culiseta melanura* (Coquillett) breeding in artificial containers. Journal of Medical Entomology 4: 273-274.

Washino R.K. and Wood B.L. 1994. Application of remote sensing to arthropod vector surveillance and control. American Journal of Tropical Medicine and Hygiene 5: 134-144.

Weaver S.C., Powers A.M., Brault A.C. and Barrett A.D. 1999. Molecular epidemiological studies of veterinary arboviral encephalitides. The Veterinary Journal 157: 123-138.

White B.J., Andrew D.R., Mans N.Z., Ohajuruka O.A. and Garvin M.C. 2003. West Nile virus in mosquitoes of northern Ohio, 2003. American Journal of Tropical Medicine and Hygiene 75: 346-349.

White D.J. 2001. Vector Surveillance for West Nile virus. Annals of the New York Academy of Sciences 951: 74-83.

Whiteaker T.L., Robayo O., Maidmont D.R. and Obenour D. From a NEXRAD rainfall map to flood inundation map. Journal of Hydrologic Engineering 11: 37-45.

Whitley R.J. and Kimberlin D.W. 1999.Viral encephalitis. Pediatrics in Review 20: 192-198.

Wiens J.A., 1976. Population responses to patchy environments. Annual Review of Ecology and Systematics 7: 81-120.

Wonham M.J., de-Camino-Beck T. and Lewis M.A. 2004. An epidemiological model for West Nile virus: invasion analysis and control applications. Proceedings of the Royal Society of London 271: 501-507.

Woodward S.L. and Hoffman R.L. 1991. The nature of Virginia. In: K. Terwilliger (coordinator), Virginia's Endangered Species. McDonald and Woodward Publishing, Blacksburg, VA. pp. 23-48.

Wrigley N. 1985. Categorical Data Analysis for Geographers and Environmental Scientists, 1st ed. Longman, Inc., New York.

Yeh P.J.-F. and Eltahir E.A.B. 1998. Stochastic analysis of the relationship between topography and the spatial distribution of soil moisture. Water Resources Research 34: 1251-1263.

Young D.R., Shao G. and Brinson M.M. 1995. Spatial and temporal growth dynamics of barrier island shrub thickets. American Journal of Botany 82:638-645.

Zar J.H. 1999. Biostatistical Analysis, 4th ed. Prentice-Hall Inc., Upper Saddle, NJ.

Zolubas P. and Byers J.A. 1995. Recapture of dispersing bark beetles, *Ips typographus* L. (Col., Scolytidae) in pheromone-baited traps: regression models. Journal of Applied Entomology 19: 285-289.

Zumr V. 1992. Dispersal of the spruce bark beetle *Ips typographus* (L.)(Col., Scolytidae) in spruce woods. Journal of Applied Entomology 114: 348-352.

APPENDIX A

Mosquito species captured in Chesapeake in 2004 listed by the CDC as potential vectors of West Nile virus. Listed = species (*N*=29) has been found associated with WNV positive pools (1999-2004 [99-04]). (Source = http://www.cdc.gov/ncidod/dvbid/).

Species	99	00	01	02	03	04	Total	All Yrs	% Captures[†]
Ae. aegypti				X	X	X	3		0.0040
Ae. albopictus		X	X	X	X	X	5		1.0318
Ae. vexans	X	X	X	X	X	X	6	X	0.6361
An. barberi			X	X			2		0.0026
An. crucians/bradleyi			X	X	X	X	4		5.7084
An. punctipennis		X	X	X	X	X	5		0.2726
An. quadrimaculatus			X	X	X	X	4		0.6679
Cq.perturbans			X	X	X	X	4		2.2013
Cx. erraticus				X	X	X	3		0.3135
Cx. pipiens	X	X	X	X	X	X	6	X	0.0248
Cx. restuans	X	X	X	X	X	X	6	X	0.5404
Cx. salinarius	X	X	X	X	X	X	6	X	8.0346
Cx. territans					X		1		0.0537
Cs. melanura		X	X	X	X	X	5		62.5022
Oc. atlanticus/tormentor			X			X	2		2.1268
Oc. canadensis		X	X	X	X	X	5		11.7967
Oc. cantator		X	X	X			3		0.0015
Oc. grossbecki					X		1		0.0007
Oc. infirmatus					X		1		0.1892
Oc. sollicitans			X	X		X	3		0.0022
Oc. sticticus					X	X	2		0.0007
Oc. taeniorhynchus			X	X	X		3		0.0033
Oc. triseriatus		X	X	X	X	X	5		0.1239
Or. signifera			X	X			2		0.0117
Ps. ciliata				X			1		0.0343
Ps. columbiae			X	X	X	X	4		1.6463
Ps. ferox		X			X	X	3		0.6916
Ps. howardii					X	X	2		0.0069
Ur. sapphirina			X	X	X	X	4		1.3716

[†] Percent of 2004 total CDC light trap captures for CDC listed WNV vectors species.

APPENDIX B

Maximum Pearson's correlation coefficients between species group captures and independent variables Maximum Pearson's correlation coefficients (*R*; [+ or -]) for species group captures (Table 1) and the nine independent variables at all 11 spatial scales (Tables 4, 5, and 7) are provided. Only scales with at least one maximum *R*-value for a species group are shown.

Variable_Scale	CONT	SWMP	EPHM	ALSP	CSMN
TC1_07x		0.269		0.374	
TC1_17x			0.456		
TC1_21x	0.208				-0.368
TC2_07x				-0.260	
TC2_09x		-0.239			
TC2_21x	-0.436		0.289		0.308
TC3_01x	-0.219				
TC3_07x				-0.364	
TC3_09x		-0.269			
TC3_21x			-0.424		0.285
HYDSM_03x		0.204	-0.111		
HYDSM_05x				0.178	
HYDSM_11x	-0.161				
HYDSM_15x					0.301
DRAIN_01x		-0.221		-0.246	
DRAIN_05x			0.116		
DRAIN_11x	-0.420				
DRAIN_17x					0.510
HYDPC_01x		-0.209		-0.239	
HYDPC_11x	-0.409				
HYDPC_15x			0.085		
HYDPC_17x					0.493
RUNOF_11x	-0.287				
RUNOF_17x		0.074		0.086	0.291
RUNOF_19x			0.259		
AWS25_01x		-0.261			
AWS25_07x					0.184
AWS25_09x				-0.304	
AWS25_11x	-0.340				
AWS25_21x			-0.086		
WTDAJ_01x	0.506		-0.089		
WTDAJ_11x					0.086
WTDAJ_21x		-0.161		-0.185	

APPENDIX C

Summary R^2-values for the multiple regression validation trials. Chi-square results (H_o: R^2-values different than expected [original R^2-values]) are also provided. Chi-square (X^2) table value ($df = 14$) is 23.68.

Trial	ALSP	CONT	SWMP	EPHM	CSMN
1	0.2703	0.4938	0.0945	0.7431	0.3619
2	0.1751	0.2246	0.4674	0.6284	0.2305
3	0.2183	0.5420	0.5318	0.6878	0.271
4	0.3173	0.7046	0.2293	0.5577	0.1726
5	0.3314	0.4656	0.1467	0.3884	0.2061
6	0.2996	0.4370	0.1635	0.7269	0.175
7	0.4493	0.4752	0.2911	0.2240	0.1636
8	0.2611	0.5751	0.2109	0.4589	0.2482
9	0.2275	0.4485	0.3776	0.1755	0.2341
10	0.2768	0.7246	0.4025	0.6912	0.2664
11	0.6811	0.5300	0.0731	0.6528	0.2224
12	0.2556	0.7331	0.1594	0.3230	0.3741
13	0.2147	0.1821	0.6617	0.3012	0.1744
14	0.0094	0.3245	0.2767	0.4696	0.1755
15	0.2710	0.5233	0.4955	0.4835	0.2823
Calc X^2	0.9702	0.8765	2.8144	3.4327	1.1126
Reject Ho:	No	No	No	No	No

APPENDIX D

Summary of root mean squared error (RMSE) values for the multiple regression validation trials. Chi-square results (H_0: RMSE different than expected [original RMSE]) are also provided. Chi-square (X^2) table value ($df = 14$) is 23.68.

Trial	ALSP	CONT	SWMP	EPHM	CSMN
1	0.246	0.718	0.105	0.172	0.288
2	0.317	0.719	0.146	0.159	0.377
3	0.326	0.362	0.170	0.300	0.243
4	0.259	0.969	0.307	0.083	0.168
5	0.304	0.629	0.172	0.276	0.300
6	0.312	0.733	0.205	0.314	0.339
7	0.306	0.488	0.138	0.135	0.295
8	0.331	0.748	0.301	0.251	0.404
9	0.153	0.885	0.395	0.241	0.380
10	0.179	0.715	0.365	0.198	0.348
11	0.304	0.945	0.578	0.174	0.284
12	0.318	0.768	0.914	0.492	0.336
13	0.292	0.407	0.336	0.790	0.411
14	0.566	0.546	0.235	0.134	0.254
15	0.167	0.601	0.396	0.107	0.351
Calc X^2	1.395	1.947	4.314	3.774	2.079
Reject Ho:	No	No	No	No	No

APPENDIX E

Summary of ANOVA *P*-values for multiple regression validation trials. Percent of trials for each group where P<0.05 is provided.

Trial	ALSP	CONT	SWMP	EPHM	CSMN
1	0.011	< 0.001	0.019	0.012	0.009
2	0.041	< 0.001	0.008	0.044	< 0.001
3	0.005	< 0.001	0.028	0.036	< 0.001
4	0.004	0.001	0.036	< 0.001	< 0.001
5	0.019	< 0.001	0.037	0.021	< 0.001
6	< 0.001	< 0.001	0.042	< 0.001	0.001
7	< 0.001	< 0.001	< 0.001	< 0.001	< 0.001
8	0.022	< 0.001	0.018	0.011	< 0.001
9	0.017	< 0.001	0.016	0.034	0.017
10	0.003	< 0.001	0.006	< 0.001	< 0.001
11	0.034	0.041	0.005	0.005	< 0.001
12	< 0.001	< 0.001	0.046	0.001	< 0.001
13	0.045	< 0.001	0.141	0.011	< 0.001
14	0.058	< 0.001	0.012	< 0.001	< 0.001
15	0.011	< 0.001	0.037	< 0.001	< 0.001
Significant	93%	100%	93%	100%	100%

APPENDIX F

Summary of trapping site locations (coordinates) and captures/TN of *Cs. melanura* for trapping sites. Coordinate system = NAD-1983, State Plane, Virginia (South), FIPS-4502 Ft. Projection: Lambert Conformal, Conic.

Trapping Site	N (ft)	W (ft)	2003 Captures	2004 Captures
CMCC001	12,086,918.629	3,476,087.15305	32.3	46.3
CMCC002	12,082,227.020	3,464,139.80785	136.2	80.7
CMCC003	12083,057.464	3,459,067.79218	342.6	112.5
CMCC004	12,089,077.304	3,446,305.39807	1061.6	440.5
CMCC005	12,125,131.998	3,439,902.57844	67.9	85.0
CMCC006	12,102,169.495	3,441,143.39272	916.6	560.2
CMCC007	12,102,330.848	3,437,515.74478	318.0	653.1
CMCC008	12,090,413.597	3,451,005.36669	318.2	258.4
CMCC009	12,108,036.219	3,432,282.66795	414.0	385.6
CMCC010	12,124,339.084	3,410,119.01067	212.9	45.8
CMCC011	12,139,884.295	3,428,709.12494	8.2	4.3
CMCC012	12,137,761.413	3,405,680.10726	54.7	63.0
CMCC013	12,157,404.855	3,428,205.45082	129.0	36.5
CMCC014	12,148,320.732	3,460,745.16183	8.0	2.0
CMCC015	12,166,259.580	3,436,666.74093	187.9	56.0
CMCC016	12,184,121.686	3,413,202.39415	149.6	19.2
CMCC017	12,131,776.881	3,436,353.44805	24.7	35.1
CMCC018	12,133,341.149	3,461,708.81035	7.2	11.0
CMCC019	12,131,205.590	3,453,960.44954	21.6	13.9
CMCC020	12,140,526.085	3,453,161.35048	18.6	2.8
CMCC021	12,139,243.655	3,387,068.07544	38.0	27.3
CMCC022	12,108,615.955	3,404,511.98697	361.1	301.1
CMCC023	12,123,669.410	3,385,119.05031	61.7	72.1
CMCC025	12,144,490.252	3,379,225.85188	12.4	11.9
CMCC026	12,116,562.161	3,394,552.21924	318.2	231.9
CMCC027	12,135,664.656	3,385,000.33172	33.5	29.2
CMCC028	12,170,255.141	3,380,341.06414	19.7	10.8
CMCC029	12,176,588.870	3,405,368.02009	56.1	27.0
CMCC032	12,146,608.236	3,461,994.58339	0.5	1.4
CMCC036	12,123,816.809	3,447,266.35314	16.5	35.0

APPENDIX G

Summary of weekly datasets for *Cs. melanura* captures/TN, total accumulated precipitation, and average weekly air temperature for 2004.Summary of weekly ($N = 32$) datasets for *Cs. melanura* captures/TN, total accumulated precipitation (PA), and average weekly air temperature (AWAT) for April through October, 2004, for the City of Chesapeake, Virginia. Data provided by the CMCC.

Week	Raw *Cs. melanura* Captures	PA (inches)	AWAT (C)
1	0	0.54	10
2	0	1.02	12
3	8	1.56	14
4	534	0.20	23
5	283	0.86	17
6	284	3.44	18
7	831	2.37	24
8	1,862	2.42	24
9	1,346	1.12	25
10	652	0.71	23
11	631	1.55	23
12	129	0.15	26
13	994	1.19	24
14	543	0.37	24
15	786	2.78	27
16	881	0.93	27
17	1,000	3.72	25
18	912	1.46	27
19	249	3.76	25
20	593	4.19	24
21	660	2.14	25
22	547	2.97	24
23	669	1.05	25
24	945	0.61	25
25	842	2.22	23
26	323	0.00	20
27	363	0.64	22
28	206	4.14	17
29	85	0.70	16
30	1,218	0.82	16
31	299	0.10	14
32	323	0.00	20

APPENDIX H

Summary of average weekly air temperature (AWAT) from April 1 – November 4, 2006. AWAT = average (observed) weekly air temperature C (QCLCD: NCDC [KCPK]). AWAT (constant-value) grid scores were calculated using Equation 6. Final weighted AWAT grid scores[†] (FAGWS) are components of Equation 8.

Month	Week ending	AWAT	AWAT Grid Score	FAGWS
April	8	15.34	42.62	15.86
April	15	15.48	43.10	16.03
April	22	16.67	47.14	17.54
April	29	16.55	46.74	17.39
May	6[††]	17.18	48.88	18.18
May	13	17.03	48.37	17.99
May	20	17.99	51.63	19.21
May	27	20.94	61.66	22.94
June	3[††]	23.88	71.65	26.65
June	10	21.42	63.29	23.54
June	17	21.29	62.85	23.38
June	24	26.02	78.93	29.36
July	1[††]	25.19	76.10	28.31
July	8	25.08	75.73	28.17
July	15[††]	26.56	80.76	30.04
July	22	27.52	84.02	31.26
July	29	25.49	77.12	28.69
August	5	30.72	94.90	35.30
August	12	24.93	75.22	27.98
August	19	24.83	74.88	27.86
August	26	25.73	77.94	28.99
September	2	25.00	75.46	28.07
September	9	22.46	66.83	24.86
September	16[††]	20.78	61.11	22.73
September	23	21.03	61.96	23.05
September	30[††]	19.20	55.74	20.74
October	7	19.17	55.64	20.70
October	14	17.19	48.91	18.20
October	21[††]	16.13	45.31	16.86
October	28	10.74	26.99	10.04
November	4[††]	11.58	29.95	11.11

[†](Raw AWAT grid value) x (regression coefficient [$R = 0.371$, Table 20]).

[††]Data used in eight sample period dynamic models (2-week delay).

APPENDIX I

Eight weekly periods for average weekly air temperature (AWAT) and weekly precipitation accumulation (WPA). Periods were selected to represent the variation in AWAT and WPA (Figure 32). See corresponding weekly abundance maps (Figure 37).

Period	AWAT (degrees C)	PA (Average [cm])
A	30 April – 6 May (17.18)	16 – 22 April (2.11)
B	28 May – 3 June (23.88)	14 – 20 May (3.96)
C	25 June – 1 July (25.19)	11 – 17 June (21.54)
D	9 – 15 July (26.56)	25 June – 1 July (2.44)
E	10 – 16 September (20.78)	27 August – 2 September (3.01)
F	24 – 30 September (19.20)	10 – 16 September (2.37)
G	15 – 21 October (16.13)	1 – 7 October (1.57)
H	29 October – 4 November (11.58)	15 – 21 October (1.60)

VITA

Alan Scott Bellows was born in Wahiawa, Hawaii on December 13, 1960, the son of Barbara Ann and Ronald Lawrence Bellows. After completing high school at W.T. Woodson High School, Fairfax, Virginia in 1979, he attended Newport News Shipbuilding Apprentice School, Newport News, Virginia, from 1981-1986 where he graduated as Journeyman foundry worker. He continued working at Newport News Shipbuilding until 1993. In the fall of 1993, he entered Christopher Newport University, Newport News, Virginia, where he earned a Bachelor of Science degree (Biology) in 1996. From 1996-1998, he attended Virginia Commonwealth University in Richmond, Virginia, where he earned a Master of Science degree (Biology). He entered Old Dominion University, Norfolk, Virginia, in the fall of 2001, where he earned his Doctor of Philosophy degree in Ecological Sciences in the fall of 2007. He is currently working as a wildlife ecologist at a privately owned environmental consulting company in Virginia Beach, Virginia.